# INFORMATION TO USERS

This manuscript has been reproduced from the microfilm master. UMI films the text directly from the original or copy submitted. Thus, some thesis and dissertation copies are in typewriter face, while others may be from any type of computer printer.

**The quality of this reproduction is dependent upon the quality of the copy submitted.** Broken or indistinct print, colored or poor quality illustrations and photographs, print bleedthrough, substandard margins, and improper alignment can adversely affect reproduction.

In the unlikely event that the author did not send UMI a complete manuscript and there are missing pages, these will be noted. Also, if unauthorized copyright material had to be removed, a note will indicate the deletion.

Oversize materials (e.g., maps, drawings, charts) are reproduced by sectioning the original, beginning at the upper left-hand corner and continuing from left to right in equal sections with small overlaps.

Photographs included in the original manuscript have been reproduced xerographically in this copy. Higher quality 6" x 9" black and white photographic prints are available for any photographs or illustrations appearing in this copy for an additional charge. Contact UMI directly to order.

ProQuest Information and Learning
300 North Zeeb Road, Ann Arbor, MI 48106-1346 USA
800-521-0600

UMI®

UNIVERSITY OF OKLAHOMA

GRADUATE COLLEGE

# CRYSTALLINE AND AMORPHOUS PHASES IN POLYMER ELECTROLYTES AND MODEL SYSTEMS

A Dissertation

SUBMITTED TO THE GRADUATE FACULTY

in partial fulfillment of the requirements for the

degree of

Doctor of Philosophy

By

Christopher Peter Rhodes

Norman, Oklahoma

2001

**CRYSTALLINE AND AMORPHOUS PHASES IN**

**POLYMER ELECTROLYTES AND MODEL SYSTEMS**

A DISSERTATION APPROVED FOR

THE DEPARTMENT OF CHEMISTRY AND BIOCHEMISTRY

BY

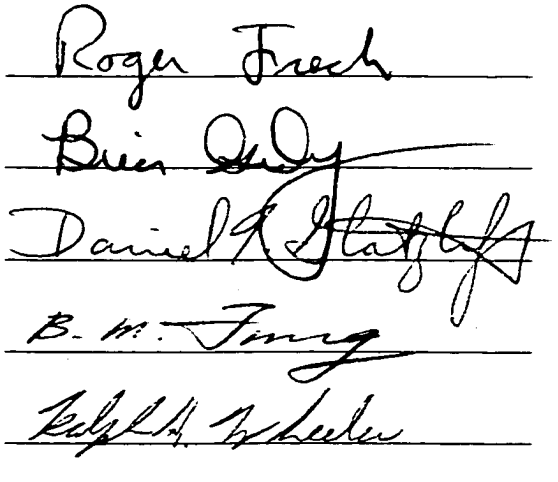

## Acknowledgements

**Roger Frech,** I am grateful to you for your patience and encouragement and for providing me with numerous opportunities. I enjoyed working with you and sharing the "Ahha, so that's how it works" moments. Thanks for sharing the joy in science. I did my best to warn you about Lone Star. Hat's off to you, my friend. I wish you and your family all the best. Let it be said that the best is yet to come.

**Ralph Wheeler**, thank you for your help and encouragement. It has been a pleasure to work with you and get to know you as a scientist and as a person. **Brian Grady**, thanks for the opportunity to work at SSRL. Maybe you can stay at the Hilton someday. Thanks for the encouragement and support. It was fun. **Dan Glatzhofer**, thanks for serving on my committee and for your commitment to good science. Let no one forget, I was the first to see your operational battery at midnight. **Bing Fung**, I appreciate your tenacity and thanks for your advice and serving on my committee. **John Furneaux**, thanks for your instrumental expertise and your enthusiasm for science. I learned lots and laughter is good medicine. **Peter Bruce, Bruno Scrosati, Steve Greenbaum** and **Jin Kee Hyun,** thanks for useful and interesting collaborations which helped to stretch me in new directions. **Scott Boesch** and **Haitao Dong,** it was great to work with you both and may the force be with you. Scott, will you still be in Norman when we read this in twenty years?

**Shawna York**, thanks for your friendship over the past few years. Looking back, we have been through lots, and it is good bring out the best in each other. Somehow we made it this far! **Barry Klassen, Xulong Zhang** and **Renee Cole,** I appreciate all the assistance in the lab and with my research projects. You were good models, and I hope to contribute to others as much as you have to me. **Varuni Seneviratne, Fred McKenna, Rebecca**

**Sanders, Chris Burba, Matt Petrowsky,** and **Nathalie Rocher,** thanks for your friendship and support, and listening to many hours of my presentations. Science and people are made better by sharing. **Masood Khan,** thanks for your assistance with the x-ray analysis and your attention to detail. **Jean Keil**, thanks for helping with all the paperwork and all the jellybeans. **Emilio** and **Sharon**, thanks for the many good meals at Pepes. For support and financial assistance, I am thankful to the **University of Oklahoma Department of Chemistry and Biochemistry** and to the **Oklahoma Center for the Advancement of Science and Technology**.

Thanks to the continued love and support of my mother and father, **Carolyn** and **Peter Rhodes** who have encouraged me to find a profession I enjoyed. Thanks to my sister **Sylvia** and my brother **Carl**. You are my family and my support. Thanks to **Lee** and **Lorinda Grey** and **their family**, for their many prayers and thoughts for me. Thanks to my grandpa **Carl Butler** and **his family**, who helped me to open doors that will never be shut. **Melvin, Lans, Edmond, John, June, Verna, Bradley**, and **your families**, you all are my family and will be with me wherever I go. Thanks to all my **brothers and sisters in Christ.** Thanks to the support and prayers of my family and all my extended family. Thanks to **God** and **His Son** for hearing and answering my prayers.

## Table of Contents

## Abstract

Polymer electrolytes represent a relatively new class of ionic conductors with potential applications in rechargeable batteries and other electrochemical devices. The most investigated systems consist of poly(ethylene oxide), PEO, with dissolved salts. Ionic transport in these systems is highly coupled to the relaxation processes of the polymer backbone and has been determined to occur predominantly in the amorphous phase for a number of polymer-salt systems. The microscopic mechanism of ionic transport in these systems is not well understood, but certainly involves the breaking and reforming of cation-ether oxygen bonds and changes in the local conformation. The characterization of ion-ion and ion-polymer interactions furthers our molecular level understanding of ionic conductivity in these systems.

The characterization of crystalline phases of polymer-salt complexes and model systems provides particular insight into local structure in these systems. Crystalline phases of systems with the general formula $CH_3(OCH_2CH_2)_nOCH_3$:MX, where n=1-4 and MX=$LiCF_3SO_3$ or $NaCF_3SO_3$, have been isolated and characterized. The comparison of these structures provides insight into changes in coordination and conformation with chain length. In a number of the crystalline structures, the local coordination environment of the cation and the torsional angle sequences of the bonds in the ethylene oxide units are remarkably similar to those present in the high molecular weight crystalline compounds. The comparison of spectra of the glyme -salt crystalline compounds to glyme-salt solutions shows that both similar and different local structures are present in solution compared to the crystalline phase.

A symmetry-based vibrational analysis is used to interpret bands in crystalline polymer-salt compounds. Vibrational spectroscopic data of crystalline polymer:salt complexes reveal the presence of dynamic coupling of the triflate anion modes which is characteristic of a highly ordered crystalline matrix. The comparison of x-ray, vibrational spectroscopic, and DSC data of the crystalline and amorphous phases reveals structural similarities and differences between the phases. Analysis of Raman and x-ray data of PEO-$LiCF_3SO_3$ films suggests that the amorphous phase contains local structures which resemble the structure present in crystalline $P(EO)_3$:$LiCF_3SO_3$. It is proposed that within the "amorphous" phase of the polymer-salt systems there exist salt-rich regions whose local structures resemble the crystalline compound. These local structures have implications for ionic transport, since ions at the domain boundaries of salt-rich regions or clusters may make a significant contribution to the ionic conductivity.

# Preface

This thesis comprises the present summary and work from the following publications which are referred to in the text by their Roman numerals and included in the Appendix.

I. Cation-anion and cation-polymer interactions in $(PEO)_nNaCF_3SO_3$ (n=1-80). C. P. Rhodes and R. Frech, *Solid State Ionics* **121**, 91 (1999).

II. A Symmetry-based Analysis of Raman and Infrared Spectra of the compounds (Poly(ethylene oxide))$_3LiCF_3SO_3$ and (Poly(ethylene oxide))$NaCF_3SO_3$. C. P. Rhodes and R. Frech., *Solid State Ionics* **136-137**, 1131 (2000).

III. Vibrational analysis of the polymer electrolyte $P(EO)_6$:$LiAsF_6$. C. P. Rhodes and R. Frech., *Macromolecules* **34**, 1365 (2001).

IV. Local Structures in Crystalline and Amorphous Phases of Diglyme-$LiCF_3SO_3$ and Poly(ethylene oxide)-$LiCF_3SO_3$ Systems: Implications for the Mechanism of Ionic Transport. C. P. Rhodes and R. Frech, *Macromolecules* **34**, 2660 (2001).

V. Structural investigation of crystalline and solution phases of monoglyme:lithium triflate systems, C. P. Rhodes, M. Khan, M. Ruff and R. Frech, *submitted to J. Phys. Chem.*

VI. Crystalline phases of poly(ethylene oxide) oligomers and sodium triflate: changes in coordination and conformation with chain length, C. P. Rhodes, M. Khan and R. Frech, *submitted to J. Phys. Chem.*

# Chapter 1. Introduction

The improvement of energy storage and conversion technologies is of significant interest for our modern society. A variety of factors including economics, increased convenience, and environmental concerns are driving the development of new materials. Two of the major applications for energy storage and conversion technologies are electric vehicles and portable electronic devices. The development of electric and fuel cell powered cars is motivated by the need for low and zero emission vehicles. Electric vehicles based on current technologies do not meet targeted cost or performance goals. Improved power sources are needed for portable electronic devices including cell phones and laptop computers as these devices find increased use in our everyday lives.

A key component of electrochemical devices is the solid electrolyte, which conducts electricity by the motion of ions. A new class of ionic conductors, polymer electrolytes, was discovered by Wright and co-workers *(1)*, and subsequently these materials were proposed as solid electrolytes for electrochemical systems by Armand et. al. *(2)*. The current research challenge in polymer electrolytes is to develop a system that has a high ionic conductivity, a high cation transference number, interfacial and electrochemical stability, and desirable mechanical properties at ambient conditions. Despite considerable research the microscopic mechanism of ionic conductivity in polymer electrolytes remains not well understood. For a number of polymer-salt systems, the ionic conductivity has been found to occur predominately in the amorphous phase of polymer electrolytes and be strongly coupled to the segmental motion of the polymer host *(3-6)*. A few polymer-salt systems have shown higher ionic conductivities for the crystalline phase compared to the amorphous phase *(7)*. The structure of the ionically conducting phase and the relationship between microscopic

structure and ionic transport have not been well determined. Furthering our understanding of ion-ion and ion-polymer interactions in the ionically conducting phase underlies our understanding of the microscopic mechanism of ionic transport in polymer electrolytes and is necessary for the rational synthesis of new systems.

The objective of my research was to investigate structure in poly(ethylene oxide)-salt systems with particular emphasis on the microscopic structure of the ionically-conducting phase. One strategy was to investigate the structure of crystalline phases. Local structures present in the amorphous phase may resemble the local structures present in the crystalline phases. A second strategy was to examine low molecular weight model systems. These model systems allow the investigation of the dependence of chain length on local structure and provide insight into structure in the amorphous phase of polymer electrolytes. An additional goal of my research efforts was to further the correlations between spectra and structure in these systems.

# Chapter 2. Polymer Electrolytes

## 2.1 General concepts

Polymer electrolytes are formed when a salt is dissolved in a solid coordinating polymer. Solid polymer electrolytes (SPE) differ from polyelectrolytes, where one of the ions is covalently bound to the polymer, and gel-electrolytes, where small organic molecules are contained within the polymer matrix. Within the field of solid state electrochemistry, polymer electrolytes are a relatively new class of ionic conductors, and their ionic transport mechanism is different than that of other solid electrolytes such as inorganic crystals and glasses. Polymer electrolytes were first investigated by Fenton, Parker and Wright who discovered that crystalline complexes formed from alkali metal salts and poly(ethylene oxide) have significant ionic conductivities *(1)*. Subsequently, Armand et al. recognized the potential applications of these new materials in electrochemical devices *(2)*. Over the past twenty years, polymer electrolytes have been intensively studied and are the subject of numerous books, book sections and review articles *(8-15)*.

One of the most studied applications for polymer electrolytes is rechargeable batteries. A schematic diagram of a rechargeable battery is presented in Figure 2.1. Within a battery, the electrolyte serves to physically separate the electrodes and transport cations (e.g. lithium or other ions) between the electrodes during charge and discharge cycles. A number of properties of SPE make them of interest for battery applications. The flexibility of SPE allows them to maintain contact with the electrodes as they change in volume during charge and discharge cycles. The flexibility of SPE also allows them to be engineered to any shape and be easily fabricated and processed. Because of their rigidity, SPE can be formed as very thin films, which increases the overall energy density of the battery. Polymer electrolytes

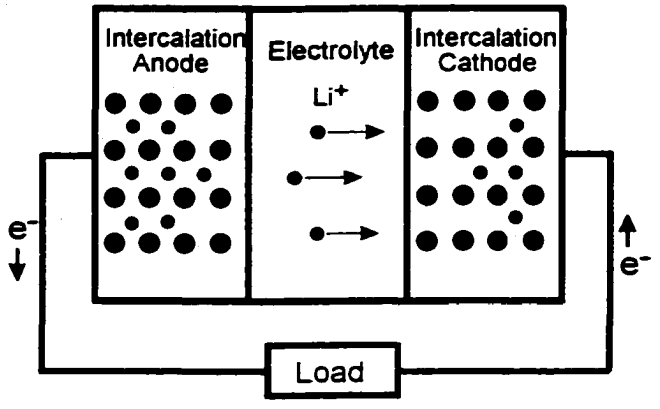


*Figure 2.1. Schematic of a rechargeable "rocking chair" lithium battery during discharge cycle.*

offer advantages in safety compared to liquid electrolytes, which are volatile and prone to leakage. Also, liquid electrolytes can cointercalate into the electrodes and react with the electrode material. Rechargeable batteries that use solid polymer electrolytes can be made to be lighter, thinner, and safer.

## 2.2 Thermodynamics of dissolution

The dissolution of a salt in a solvent, either liquid or solid, is described thermodynamically by the change in the Gibbs free energy $\Delta G$ at constant temperature and pressure. $\Delta G$ is a function of the change in enthalpy ($\Delta H$), the change in the entropy ($\Delta S$) and the temperature,

$$\Delta G = \Delta H - T\Delta S. \qquad (2.1)$$

The dissolution is a spontaneous process if $\Delta G$ of the system is negative, with the sign and magnitude of $\Delta G$ determined by the individual terms. The system in the initial state is composed of a polymer solvent and ions within a crystalline matrix, and in the final state the ions are fully dissolved by the polymer solvent. The disordering of the ions from the

crystalline lattice to the polymer solution is a positive contribution to the entropy of dissolution. The strong specific interactions of the ions with the polymer affect the energies of specific polymer conformations, and this effect is a negative contribution to the entropy of dissolution. The chain stiffening caused by the interactions of the ions with the polymer reduces the segmental motion of the polymer and is observed experimentally by an increase in the glass transition temperature $T_g$ with increasing salt content *(16)*. Due to the competing terms, the entropy change of the system can be positive or negative. The effect of $\Delta S$ on $\Delta G$ is a function of temperature, and at higher temperatures, the $-T\Delta S$ term will dominate the equation. With increasing temperature salt precipitation is observed in a number of systems, which indicates that the overall entropy of dissolution is negative in those systems *(17)*.

The enthalpy change of dissolution is the enthalpy after dissolution minus the enthalpy before dissolution. The factors which affect the overall enthalpy of dissolution are (a) the lattice energy of the salt, (b) the strength of association of the groups on the polymer chains, (c) the formation of coordinate bonds of the polymer and the cation, and (d) electrostatic interactions between the dissolved ions. In practice, it is apparent that the major factors which determine whether a salt will dissolve in a polymer are the lattice energy of the salt and the solvation of the cations by the polymer chains *(18)*. The primary interaction of the polymer is with the cation, and the anion is only weakly solvated by the polymer.

The thermodynamic description provides a basis for understanding which salts dissolve in which polymers. We consider the salts first. The choice of cation for the polymer-salt electrolyte largely depends on the electrode materials, since the function of the electrolyte is to transport the ions between the electrodes. Lithium and sodium are the most investigated cations for intercalation electrodes because of their high charge to mass ratios, however other metals including $K^{-}$, $Ca^{2-}$, $Mg^{2-}$ have also been investigated *(19-26)*. Here we

consider predominately $Li^+$ and $Na^+$ salts. Anions have been chosen which minimize interactions between the anion and the cation within the polymer-salt solution since strong interactions can impede ionic transport. Studies of ion pairing in liquid electrolytes have shown that ion pairing is minimized by choosing a solvent that has a high electron donating ability and an anion that is large and easily polarizable *(27)*. The interactions of the ions in the solution are a legacy of the interactions of the ions in the lattice *(18)*. Salts with low lattice energies are desirable, and an upper limit of 720 J/mol has been suggested *(28)*. Some anions which have been investigated are $I^-$, $ClO_4^-$, $SCN^-$, $CF_3SO_3^-$, $(CF_3SO_2)_2N^-$, $(CF_3SO_2)_3C^-$, $AsF_6^-$, $PF_6^-$, and $SbF_6^-$.

In order for a polymer to dissolve a salt, there must be electron-donating groups on the polymer chain capable of coordinating the cation of the salt. The polymer acts as a nucleophilic ligand (Lewis base) and the cation acts as an electrophile (Lewis acid). The most investigated groups are polymers containing oxygen, however polymers containing nitrogen and sulfur have also been investigated. The strength of the interaction between the polymer groups and the cation can be described by the donor number/acceptor number *(29, 30)* or the hard/soft acid base theory *(31, 32)*. The most investigated polymer hosts are polyethers, since the ether oxygens are excellent coordinating groups for a variety of cations. The prototypical polymer host is polyethylene oxide $(-CH_2-CH_2-O-)_n$ abbreviated PEO. The comparison of salts dissolved in ethers with different numbers of ethoxy units, namely $\{CH_2-O\}_n$, $\{CH_2-CH_2-O\}_n$ and $\{CH_2-CH_2-CH_2-O\}_n$, provides an interesting comparison since the repeat units have the same coordinating units. Polyethers with $\{CH_2-O\}_n$ or $\{CH_2-CH_2-CH_2-O\}_n$ repeat units are weaker solvents than PEO *(2, 33)*. PEO has an intermolecular spacing that is appropriate to maximize solvation of the cation. The chain can wrap around the cation making coordination sites available without significant strain of the

polymer. The situation is similar to that present in macrocycles such as crown ethers. If the uncoordinated polymer chain is in a conformation which is already suitable for the cation, then the entropy loss due to coordination is minimized *(18)*. The ethylene oxide unit is an important monomeric unit for polymer electrolyte systems as evidenced by the investigation of a variety of polymer architectures which incorporate the ethylene oxide moiety including comb polymers *(34)*, copolymer systems *(35, 36)*, and systems using ethylene oxide units in side chains *(37)*.

## 2.3 Phase equilibria

Polymer electrolytes based on PEO with dissolved salts are in general multiphase systems. Knowledge of the phases present, their relative amounts, their structures, their interfaces and the dynamic equilibrium between phases is crucial to understanding the properties of polymer electrolytes. Phase diagrams have been determined using a variety of techniques including DSC, XRD, DTA, NMR, optical microscopy and conductivity. The phase diagrams of numerous PEO-salt systems have been reported *(38-42)*. The phase diagrams for the binary systems PEO-$LiCF_3SO_3$ and PEO-$NaCF_3SO_3$ are presented in Figure 2.2. A eutectic or quasieutectic point is characteristic of the phase behavior of these systems. For a given system, the phases and their relative percentages generally depend on a number of factors including temperature, salt concentration, molecular weight of the polymer *(43)*, thermal history *(44)*, time *(45)*, and preparation method *(46)*. For polymeric hosts with high molecular weights, the attainment of thermodynamic equilibrium below the eutectic temperature is limited by the slow kinetics of crystallization due to the chain entanglements. Consequently the systems generally form a metastable solids, and for this

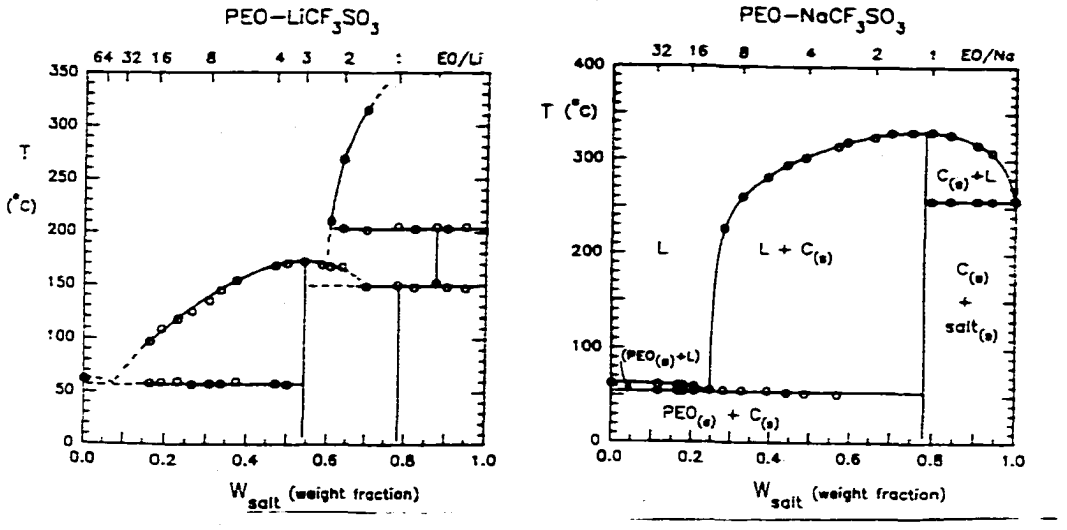


*Figure 2. 2 Phase diagram of PEO-$LiCF_3SO_3$ (left) (40) and phase diagram of PEO-$NaCF_3SO_3$ (right) (41).*

reason it has been suggested that these are psuedo phase diagrams. Various techniques have been used to determine the morphology of polymer electrolytes *(28)*.

Below the melting temperature of PEO, three phases are generally present in PEO-salt systems: a pure crystalline PEO phase, a crystalline polymer-salt phase, and an amorphous phase. A visual representation of these phases is presented in Figure 2.3. The structures of each of these phases will be discussed in Chapter 5. Crystalline PEO has a melting point of 65°C, and the amorphous phase of pure PEO has glass transition temperature of approximately -60°C *(8)*. The morphology and growth rates of the spherulitic PEO crystals have been studied by a number of techniques *(47, 48)*. Studies of the crystallization of pure PEO reveal the importance of molecular weight on the relative crystallinity and the morphology of the crystals *(49, 50)*. The second type of crystalline phases are crystalline complexes of PEO with salts, forming crystalline polymer-salt

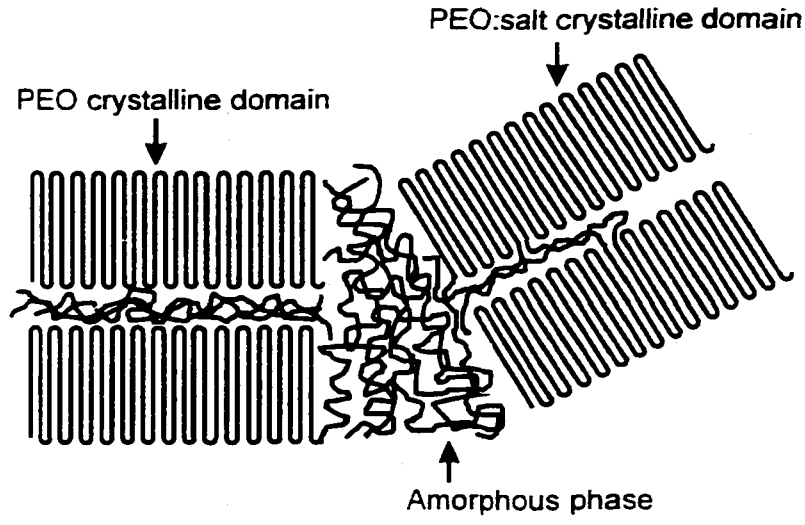


*Figure 2.3. Visual representation of phases present in PEO-salt systems at room temperature and moderate salt concentrations.*

compounds. PEO forms crystalline complexes with a variety of different cations and anions, and a thorough presentation of complexes of PEO with various metal salts is presented elsewhere *(51)*. The polymer salt complexes form with a variety of different stiochiometries, generally with ether oxygen to cation ratios of 6:1 to 1:1. The structures of PEO-salt complexes are discussed in section 5.1. The amorphous phase is of primary interest since the ionic conductivity for a number of systems has been found to occur predominantly in the amorphous phase, regardless of the coexistence of crystalline phases *(3, 4)*. The temperature-dependent conductivities of PEO:$NH_4SCN$ shown in Figure 2.4 allow the ionic conduction of the crystalline and amorphous phases for this system to be compared *(38)*. PEO-salt systems generally show a hysteresis effect as conductivity is measured as a function of temperature due to the slow kinetics of crystallization. The ionic conductivity of the system during the heating cycle, where the sample is semicrystalline, is much different than the ionic conductivity during the cooling cycle, where the sample is fully amorphous due to

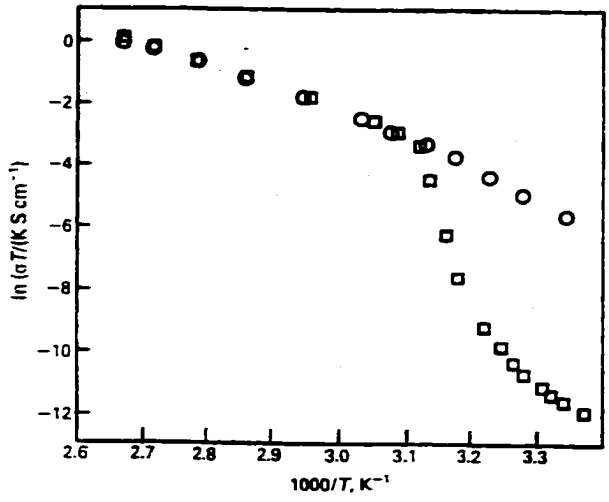


*Figure 2.4. Hysteresis effect on the conductivity of $P(EO)_8$:$NH_4SCN$ shown by data for the heating cycle(□), where the sample was initially a semicrystalline sample, and the cooling cycle(○), where the sample was quenched into an amorphous phase (38).*

quenching. The data clearly shows the higher conduction of the amorphous phase compared to a semicrystalline phase of this system. The finding that ionic conduction occurs in the amorphous phase has been particularly important and has directed future research efforts towards increasing the fraction of the amorphous phase and obtaining completely amorphous polymer electrolytes. The higher ionic conductivity of the amorphous phase compared to the crystalline phase does not apply to all polymer systems. A recent study demonstrated that in some systems, the crystalline phase has a higher ionic conductivity than the amorphous phase *(7)*.

## 2.4 Structure

The properties of polymer electrolytes are a result of their microscopic structure and dynamics. Determining the microscopic structure and relationship of structure to ionic

transport provides the basis for improving material properties. A variety of experimental techniques have been applied to study the structure of polymer electrolytes: vibrational spectroscopy, x-ray diffraction (XRD), neutron scattering, nuclear magnetic resonance (NMR), x-ray absorption spectroscopy, differential scanning calorimetry, microscopy, x-ray photoelectron spectroscopy, and EXAFS *(8, 9, 52-59)*. Two particularly important aspects of local structure are the interactions of ions with other ions and the interaction of ions with the polymer.

Ionic association, i.e. direct ion-ion interactions, is a widespread phenomena in polymer electrolytes and has been observed by various techniques, including vibrational spectroscopy *(60, 61)*, molecular dynamics simulations *(62-67)*, and transference number measurements *(68-70)*. Ionic association is a function of the effective coulombic forces between ions, which is affected by the choice of cation, anion and the value of the dielectric constant of the medium, which is a polymer solvent in this case. For poly(ethylene oxide) the dielectric constant is between 5 and 8, and this low value of the dielectric constant generally results in significant ionic association. The result of ionic association is the presence of different ionic species that can be classified generally as "free" ions, contact ion pairs and aggregates. "Free" ions are cations or anions in which the first solvation shell is composed entirely of solvent molecules. "Free" ions are equivalent to solvent separated ion pairs, and the two cannot be distinguished spectroscopically. Following the notation suggested by Bruce and Gray for a for a salt MX composed of $M^+$ cations and $X^-$ anions, these can be written as $[MX]_s^0$ where the subscript s denotes a solvent separated ion pair *(18)*. Ionic association can result in the formation of contact ion pairs, written as $[MX]^0$, which denotes direct cation-anion interaction. Ionic association can also result in the formation of ionic aggregate species which can take the form of $[M_2X]^+$, $[MX_2]^-$ and other larger aggregates. It is

important to remember that these charged species do not exist as distinct, isolated species since local charge balance must be maintained, and therefore in the immediate vicinity of a charged entity, like a "free" ion or a charged aggregate, is a counter ion. The nature of these species is highly dependent on the polymer-salt system and is also a function of molecular weight, salt concentration and temperature *(71)*. The contribution of free ions, ion pairs and aggregates to the ionic conductivity has been the source of much debate and research and will be further considered in section 5.3. Vibrational spectroscopy has been particularly useful to probe ionic association in polymer electrolytes *(60, 72, 73)*. The vibrational frequencies for modes of a number of anion, particularly $CF_3SO_3^-$ and $ClO_4^-$ anions, are sensitive to the coordination to one or more cations, and the frequencies have been used to infer coordination environments of the anion *(61, 74-76)*. The modes of the triflate anion have been studied in a variety of solvents *(77, 78)*.

The interaction of the cation with the host polymer is an important aspect of structure in polymer electrolytes. In polymer-salt systems, the cation is coordinated by electron-donating groups on the polymer. The overall cation coordination number depends a number of factors including the choice of cation but ranges from four to ten *(79, 80)*, with typical coordination numbers of 4-5 for lithium in polyethers *(81)*. Ionic transport has been shown to be intimately related to the relaxation processes of the polymer, particularly the segmental motion or β–relaxation *(82)*. These polymer relaxation processes necessarily involve changes in the conformation of the polymer and breaking and reforming of cation-polymer bonds as the cation is transported through the polymer matrix. Vibrational spectroscopy has been used to study the conformation in pure PEO *(83-93)*, and changes in polymer conformation due to cation complexation *(79, 94-96)*. NMR studies of polymer electrolytes reveal that the interaction of the salt with the polymer strongly reduces the chain

mobility *(97)*, and the addition of salt was found to increase the energy barriers to segmental motion *(98)*. NMR studies of PEO-$LiCF_3SO_3$ have shown that the nature of ion-polymer interaction in the amorphous phase is similar to the interaction in the crystalline polymer:salt phase *(59)*. Insights into ion-polymer interactions have been provided by studies of crystalline polymer-salt complexes (described in Chapter 5) and by model systems of glymes with dissolved salts (described in Chapter 4).

## 2.5 Ionic transport

### 2.5.1 Transport properties

From the perspective of applications, one of the most important properties of polymer electrolytes is their ability to transport ions. The ionic transport is described by the ionic conductivity $\sigma$, transference numbers $T$, transport numbers, $t$, and diffusion coefficients D. For a binary polymer-salt solution, three transport properties are needed to describe the system *(99)*. A variety of techniques are used to measure transport properties in polymer electrolytes *(100, 101)*.

The focus of much of the experimental and theoretical is focused on the ionic conductivity $\sigma(T)$. Ionic conductivities for a number of PEO-MX systems have been reported *(102)*, and typical conductivities for PEO-salt systems are $10^{-3} - 10^{-4}$ S cm$^{-1}$ at 100°C and $10^{-6} - 10^{-8}$ S cm$^{-1}$ at room temperature ($\sigma(T)$ will be discussed in section 2.5.2). Below the critical entanglement limit, ionic conductivity is a function of the molecular weight of the polymer. The critical chain entanglement limit of PEO which was determined by viscoelastic measurements occurs at a molecular weight of 3200 *(11)*. Below this limit, the molecular weight dependence of cationic transport is related to the diffusion of the polymer chains and is described by the Rouse-Zimm model *(103, 104)*. Above this limit, the motion of the

entangled polymer chains is described by the reptation model of de Gennes *(105)*. Above the critical chain entanglement limit, the molecular weight of the polymer has been shown to have no significant effect on the cation mobility *(11)*. NMR studies have shown that the addition of salt does not affect the critical entanglement limit of the polymer *(56, 98)*.

The ionic conductivity results from the contribution of all mobile charge carriers. For a dilute system, the ionic conductivity $\sigma$ can be described by the Kohlrausch summation

$$\sigma(T,P) = \sum_i n_i q_i \mu_i \qquad (2.1)$$

where $n_i$, $q_i$, and $\mu_i$ refer to the concentration of charge carriers, the charge, and the mobility of the $i$th species respectively. The carrier number $n$ includes all charged species including single cations, single anions and larger ionic clusters and is a complicated function of concentration, temperature and pressure. In an infinitely dilute system, the conductivity can be described by the Nernst-Einstein relationship

$$\sigma = nF^2(D_+ + D_-)/RT \qquad (2.2)$$

where $n$, $F$, $D_+$, $D_-$, $R$, and $T$ refer to the concentration of charge carriers, Faraday's constant, the diffusion coefficient of the cation, the diffusion coefficient of the anion, the gas constant, and the temperature respectively. Both of these equations provide important insights into ionic conduction but fail to quantitatively describe the experimental conductivity in concentrated electrolytes *(106)*. Pulse-field gradient NMR studies of poly(propylene oxide)-$LiCF_3SO_3$ complexes revealed that that ion-ion interactions strongly reduce the ionic mobility *(107)*. The comparison of experimental conductivities to theoretical conductivities calculated from the Nernst-Einstein relation show that significant discrepancies exist *(108-110)*. An assumption of the Nernst -Einstein relation is the complete dissociation of the ions, which is invalid at high salt concentrations where significant ion

pairing and clustering occurs. Interionic interactions complicate the interpretation of $\kappa$, $D$ and $\mu$ since an ion or charged species cannot be regarded independent of other ions. At typical salt concentrations, polymer electrolytes are not ideal solutions. Methods have been developed for determining transport properties of polymer electrolytes which are based on concentrated solution theory and do not require assumptions concerning the ideality of the solution *(68, 70, 111)*. Concepts of concentrated solution theory like friction coefficients for ion-ion and ion-solvent interactions have been recently investigated *(112, 113)*.

The measurement and interpretation of transport and transference numbers in polymer electrolytes has been a source of debate within the field *(111)*. Various techniques have been used to measure the transference numbers *(17, 114-116)*, and often the results for a single system disagree *(117-119)*. The basis of these discrepancies are related to the various assumptions concerning the ideality of the solution and experimental difficulties. The transference number is the net number of Faradays of current carried by a constituent ion (either the cation or the anion) upon the passage of one Faraday of charge through the cell *(120)*. The transport number refers to the charge flow associated with a single charged species, whereas the transference number is the resultant charge flow due to all species of an element. The transference and transport numbers are the same for a fully dissociated species at infinite salt dilution. For the case of a binary salt MX (with cation and anion of univalent charge) which dissolves in polymer forming species $M^+$, $X^-$, $[MX]^0$, $[M_2X]^+$ and $[MX_2]^-$, transport numbers exist for each species and the transference number refers the transport of one ion ($M^+$ or $X^-$) by all charged species. For the above example the transference and transport numbers are related as follows *(18)*.

$$T_{X^-} = t_{X^-} + 2t_{MX_2^-} - t_{M_2X^+} \quad (2.3)$$

$$T_{M^+} = t_{M^+} + 2t_{M_2X^-} - t_{MX_2^-} \quad (2.4)$$

$$T_{M^+} + T_{X^-} = 1 \quad (2.5)$$

In polymer electrolytes, determining individual transport numbers is difficult due to the presence of multiple species, and therefore transference numbers are predominantly measured. Recent results using electrophoretic NMR have obtained cation and anion transference numbers which sum to unity which establishes this method as viable for determining transference numbers in concentrated solutions *(120)*. Negative transference numbers have been reported by a number of groups and have been the subject of some discussion and disagreement *(68-70)*. A negative cationic transference number indicates that the dominant species carrying cations are anionic complexes *(120)*. Transference numbers have also been found to be a function of salt concentration which is attributed to a decrease in anion mobility with increasing salt concentration *(121)*. The ideal lithium transference number is unity, and transference numbers other than unity lead to salt concentration gradients within an operational battery *(69, 111)*. The importance of measuring transference numbers rather than only the ionic conductivity for optimizing electrolyte performance for batteries has been emphasized in recent literature *(122)*.

Diffusion coefficients describe the flow of matter in a concentration gradient. Diffusion coefficients are calculated from a number of techniques including pulse field gradient NMR and DC polarization experiments *(11, 107, 108, 114, 116, 123)*. Diffusion coefficients have been shown to a function of temperature and salt concentration *(107, 108, 124)*. It is generally found that in binary polymer electrolytes, the diffusion coefficient of the anion is larger than the diffusion coefficient of the cation, i.e. $D_- > D_+$ *(108, 124, 125)*. This

observation is consistent with the weak solvation of the anions by the polymer and the low value of the cation transference numbers. At low salt concentrations, the cation diffusion coefficient follows VTF-like behavior (described in the following section) *(107)*. However, at high salt concentration, the temperature dependence of the cation diffusion coefficient is not VTF-like, and this suggests that a different cation transport mechanism (other that VTF-like) is present at high salt concentrations *(108)*. Therefore this implies that in addition to the coupling of the ionic transport to polymer relaxation processes which is implied by VTF-like behavior, additional factors such as interionic interactions are involved in ionic transport.

2.5.2 Models of ionic transport

Empirical models: Ionic transport in polymer electrolytes has been described by a number of empirical and theoretical models. The temperature dependence of the ionic conductivity, often presented in an Arrhenius-type plot of log $\sigma(T)$ vs. $T^{-1}$, has been described by the empirical equations of Vogel-Tammann-Fulcher (VTF) and Williams-Landers-Ferry (WLF). Thorough treatments of these models applied to polymer electrolytes are presented elsewhere *(18, 112)*. Historically, the VTF equation was developed to describe the viscosity properties of supercooled liquids *(126-128)*. An equation which describes the ionic conductivity as a function of temperature can be derived from the VTF equation and expressed as *(18)*

$$\sigma(T) = \sigma_0 \exp[-B/R(T-T_0)] \qquad (2.6)$$

where $\sigma_0$ is a prexponential factor, B is a constant with dimensions of energy, and $T_0$ is the reference temperature. The equation can be expressed in different forms with some of the forms having a $T^{1/2}$ term in the prexponential factor. The reference temperature $T_0$ has been described as an 'equilibrium glass transition temperature', the temperature at which the free

volume disappears, and this quantity is related to the thermodynamic glass transition temperature $T_g$, the temperature at which endotherms are observed *(112)*. The two temperatures are related empirically by the equation $T_0 \approx T_g - 50$ K *(106)*. In an Arrhenius-type plot of log $\sigma(T)$ vs. $T^{-1}$, a bent line is characteristic of VTF behavior, and for many systems the temperature dependence of the ionic conductivity can be well described by the VTF equation *(2, 129)*. For some systems, the VTF equation does not adequately describe the temperature dependence of the ionic conductivity, and Arrhenius behavior is also observed as well as combinations of Arrhenius and VTF behavior *(112)*.

The Williams-Landel-Ferry (WLF) equation is based on empirical observations of polymer relaxation times and is found to apply to many disordered systems including glasses and pure polymers *(130)*. The equation expresses a characteristic property in terms of a shift factor that is the ratio of a property at temperature T to the property at a reference temperature $T_s$. The temperature dependence of the ionic conductivity can be written in the WLF form *(18)*

$$\log \frac{\sigma(T)}{\sigma(T_s)} = \frac{-C_1(T - T_s)}{(C_2 + T - T_s)} \qquad (2.7)$$

where $\sigma(T_s)$ is the ionic conductivity at temperature $T_s$ and $C_1$ and $C_2$ are constants that can be obtained experimentally. Empirically the constants $C_1$ and $C_2$ have been found to be 8.9 and 102 K respectively, independent of the measured property. The WLF form of the ionic conductivity is based on the empirical VTF equation, and eq. 2.6 and 2.7 can be shown to be equivalent expressions. Although $T_s$ is an arbitrary temperature, the value often taken to be 50 K above the equilibrium glass transition temperature, and the WLF form can be written using $T_g$ in place of $T_s$ *(18, 112)*.

The VTF and WLF equations are useful to describe the temperature dependence of a number of transport properties including conductivity, diffusivity and viscosity. Both equations are related to the properties of the polymer and are centered around reference temperatures that are related to the glass transition temperature $T_g$. The agreement of the experimental ionic conductivity to these empirical equations establishes that the relationship of the ionic conductivity to the temperature relative to the glass transition temperature. From this relationship, it follows that ionic transport is intimately coupled to the local relaxation processes of the polymer. The application of simple models to describe $\sigma(T)$ is limited by a number of factors including (a) the inhomogeneity of the ionically conducting phase (b) complications due to ion pairing, and (c) varying carrier number and many-particle effects. Transport of the ions is related to the motion of the polymer but is not governed exclusively by it, .i.e. VTF behavior for the ions does not directly follow from VTF behavior for the polymer *(112)*.

Theoretical models: The predominant theoretical models used to describe ionic transport in polymer electrolytes are the free volume model, the configurational entropy model and dynamic bond percolation model. The free-volume model is widely used to describe viscosity and diffusion in polymeric systems and has also been used to describe ionic motion in fused salts and fluids *(131)*. The availability of free volume is a function of the temperature above the equilibrium glass transition temperature $T_{\infty}$, and at the equilibrium glass transition temperature free volume vanishes. The dependence of temperature and molecular weight on free volume in PEO was investigated by positron lifetime experiments *(132)*. The basic assumption of the free volume model is that diffusion occurs as a result of the redistribution of free volume. Pockets of free volume are produced, and polymer segments, ionic species or solvated molecules can move into the local voids. Molecules are

considered to be confined within their cages unless a hole is created which is large enough for the molecule to diffuse into. This minimum size is defined as $V^*$, the critical free volume for transport. A number of expressions can be written which relate the ionic conductivity to the free volume. The ionic conductivity can be expressed as a function of free volume using a WLF shift factor *(18)*,

$$\ln\left[\frac{\sigma(T)}{\sigma(T_g)}\right] = -\left(\frac{V_i^*}{V_p^*}\right)\ln a_T, \qquad (2.8)$$

where $V_i^*$ and $V_p^*$ are the critical free volumes for ions and polymer segment motion respectively, and $a_T$ is the WLF shift factor. The ratio $V_i^*/V_p^*$ is found to be very close to unity which suggests that these values depend of the same process. The free volume model is conceptually the simplest way to understand transport behavior in polymer electrolytes *(112)*.

The configurational entropy model *(133, 134)* is similar to free volume models in that it only concerns properties of the polymer. In this model, the mass transport occurs by a cooperative rearrangement of the chain. The average probability of rearrangement is related to the minimum configurational entropy required for rearrangement. The configurational entropy model has been applied to polymer electrolytes *(129, 135)*, and the ionic conductivity can be expressed as

$$\sigma(T) = A\exp\left(\frac{-K_\sigma}{T - T_0}\right) \qquad (2.9)$$

where A is a preexponential factor, $K_\sigma = \Delta\mu S_c^* T_0/k_B$, $S_c^*$ is the minimum configurational entropy required for rearrangement, $\Delta\mu$ is the free energy barrier per mole which opposes the rearrangement, and $k_B$ is Boltzmann's constant. Transport properties described using the configurational entropy model are in agreement with VTF and WLF equations *(112)*.

The configurational entropy model has some advantages compared to the free volume model, but both models suffer from not taking into account microscopic mechanisms. A drawback of the free volume and configurational entropy models is that they are static pictures based on thermodynamic arguments, and therefore they do address dynamics or kinetic factors. The motions of the polymer are described by various relaxation processes with characteristic time scales or frequencies. The frequency dependent properties of polymer electrolytes have been studied by a variety of techniques including mechanical relaxation, dielectric relaxation and loss, ac conductivity, Brillouin scattering, NMR relaxation, and quasielastic neutron scattering *(8-10)*. Some major deficiencies common to these models is that they do not address interactions between the ions and do not predict the effect of variables such as ion size, ion paring, polarizability, solvation strength, ion concentration, polymer structure and chain length on the ionic conductivity *(18)*.

The most comprehensive model describing ionic transport in polymer electrolytes is the dynamic bond percolation (DBP) model, and a detailed description of this model is presented elsewhere *(5, 6, 112, 136)*. The DBP model has a number of advantages over free volume and configurational entropy models in that it considers frequency dependent properties and can account for interionic interactions *(106)*. The dynamic bond percolation model starts from the static percolation models which define a set of sites in which mobile species reside. The motion of the mobile species, or carriers, is described by the 'master equation',

$$\frac{dP_i(t)}{dt} = \sum_j (-W_{ij}P_i + W_{ji}P_j). \qquad (2.10)$$

where $P_i$ is the probability of finding an ion at site i. $W_{ij}$ is the probability per unit time that a carrier will jump from site j to site i, i.e. the hopping rate, and is defined as zero except between neighboring sites. The value $W_{ij}$ can take on two values

$$W_{ij} = \begin{Bmatrix} 0, probability = 1-f \\ w, probability = f \end{Bmatrix} \qquad (2.11)$$

where $w$ is the hopping rate between neighboring sites, $f$ denotes the fraction of bonds that are open or available, and $1-f$ is the fraction of bonds closed or unavailable. The DPB model has three characteristic parameters: $w$, $f$, and $\tau_{ren}$. These parameters determine the probability of particle hopping and can be related to the parameters present in the system such as ion size, free volume, temperature and pressure. The hopping rate $w$ is related to the time scale for changing the coordination shell, which involves breaking and reforming bonds, and has been related to the ion velocity divided by the lattice constant *(136)*. The parameter $f$ has been related to the availability of critical free volume *(136)*. The parameter $\tau_{ren}$ is a distribution of relaxation times that correspond to orientational and configurational changes of the polymer host, and hopping probabilities renew their values based on $\tau_{ren}$. The DBP model is successful in describing dynamical properties of polymer electrolytes and incorporating ionic interactions within ionic transport.

2.5.3 Microscopic descriptions

What is lacking in the theoretical models including DBP is that they do not provide a microscopic description of ionic transport. A number of microscopic descriptions of ionic conductivity have been proposed, but none has stood the test of time and experiment. The first of these descriptions was put forth by Armand, who suggested that alkali metal ions were the dominant charge carriers, and ionic conduction occurs mainly in the crystalline phase inside the PEO helices *(2)*.Subsequent experiments demonstrated that ionic transport

is not limited to cation motion along helical channels *(137)*. This finding suggested that ion transport may also occur between chains. A number of studies, namely vibrational spectroscopic studies *(109)*, transference number measurements *(68-70, 120)*, diffusion coefficients measurements *(108)*, and molecular dynamics simulations *(62-67)*, suggest that at moderate and high salt concentrations interionic interactions contribute in some manner to ionic transport. A number of groups have suggested that ionic transport may occur through correlated motions of cations and anions *(11, 138)*. The role of clusters or salt-rich regions in ionic transport has been considered *(108)*. The contribution of ion pairs in the ionic conductivity is the subject of some debate within the field. Uncharged ion pairs are considered to contribute to the diffusion coefficient but not contribute to the ionic conductivity. However, ion pairs may be involved in some correlated transport mechanism where the cation hops between ionic clusters *(11)*. It is clear that the microscopic mechanism of ionic transport in polymer electrolytes is quite complex.

## 2.6 Recent developments

A variety of new systems and approaches are being developed to improve the properties both the transport and mechanical properties of polymer electrolyte systems. Since for many systems the ionic conductivity has been shown to occur predominantly in the amorphous phase, research efforts have been focused on producing entirely amorphous polymer electrolytes *(37)*. A variety of new polymer architectures have been developed *(34, 139)*. Due to the strong correlation of segmental motion and ionic transport, efforts have been aimed at creating new polymer systems with lower glass transition temperatures *(35)*. Another strategy has been to investigate polymer systems in which ionic transport is decoupled from the polymer host dynamics *(140-142)*. Single ion conductors, which allow

only cationic migration, are being developed *(143-146)*. Polymer systems which incorporate anion binding sites within the polymer can decrease ion association and increase the cationic transference number *(147)*. Increased conductivities were obtained for stretched polymer electrolyte films which suggests that there may be enhanced ionic transport along certain orientations *(148, 149)*.

The area of composite polymer electrolytes has attracted considerable attention. New types of inorganic-organic polymer electrolyte systems are being investigated *(150-152)*. It has been determined that ceramic additives such as $SiO_2$, $Al_2O_3$, $TiO_2$ increase the ionic conductivity, increase the fraction of the amorphous phase, improve the mechanical properties, and improve the interfacial properties in a number of polymer electrolyte systems *(153-162)*. The addition of the inorganic particles also changes the lithium transference number *(159-161, 163)*. Understanding and improving the properties of polymer electrolytes continues to be of significant scientific interest.

# Chapter 3. Experimental Methods

## 3.1 Sample preparation

Chemicals: Poly(ethylene oxide), with $M_v=1\cdot10^5$ and $4\cdot10^6$ and abbreviated as PEO, was obtained from Aldrich and dried at 50 °C for 24 to 48 h prior to use. Ethylene glycol dimethyl ether (99.9%, monoglyme), di(ethylene glycol) dimethyl ether (99.5%, diglyme), tri(ethylene glycol) dimethyl ether (99%, triglyme), and tetra(ethylene glycol) dimethyl ether (99%, tetraglyme) were obtained from Aldrich and used as received. Lithium trifluoromethanesulfonate $LiCF_3SO_3$ (99.995%), also called lithium triflate and abbreviated here as LiTf, was obtained from Aldrich and heated under vacuum at 120°C for 48 h prior to use. Sodium trifluoromethanesulfonate $NaCF_3SO_3$ (97 %), also called sodium triflate and abbreviated here as NaTf, was obtained from Fluka and heated under vacuum at 120°C for 48 h prior to use. All reagents were stored and manipulated in a dry nitrogen glovebox (Vacuum Atmospheres Company, ≤ 1ppm $H_2O$).

Polymer-salt crystals: For preparation of the polymer-salt compounds, both solution and solid-state synthesis methods were used. The best results were obtained using PEO with $M_v=1\cdot10^5$ rather than with $M_v = 4\cdot10^6$ and mixing solid powders of the polymer and the salt. For the crystalline $P(EO)_3$:LiTf compound, stoichiometric amounts of the dry powders were thoroughly ground together in the glovebox with a mortar and pestle. The powders were transferred to an 8 mm glass ampoule that was sealed under vacuum. To promote intimate mixing of the reagents, the samples were heated at 100 °C for 12 to 24 hours. The samples were then heated to 170 °C for 4 hours and further annealed at 100 °C for 9 days. The annealed samples were transferred back to the glovebox. An identical procedure was used to prepare the crystalline P(EO):NaTf compound except for the heating temperatures. After

heating the glass ampoule containing the PEO and NaTf powders at 100 °C for 12-24 hours, the sample was heated to 275 °C for 5 hours and then annealed at 100 °C for 5 to 6 days.

Polymer-salt films: Polymer-salt films were prepared according to the standard solvent casting technique *(46)*. Stoichiometric amounts of the polymer and salt were measured and combined with acetonitrile to give solutions of ~2-10% weight (polymer + salt). The solutions were stirred for 24 h, and then films were cast onto either Teflon or glass slides. The cast films were left in the glovebox for 24 h to evaporate solvent and then heated at 50°C for 24 h under vacuum. Samples were also heated at 75°C or 100°C depending on the desired heat treatment. A heating temperature of 50°C was chosen for most samples to avoid heating the film above the melting point of PEO. The same sample preparation, heating temperature and time were used for the various specimens to enable direct comparison of the data.

Glyme-salt solutions. The salt was combined with the solvent in stoichiometric amounts to yield solutions of the desired ether oxygen to metal cation ratio (O:M). The solutions were stirred in the glovebox for at least 48 h prior to measurement.

Glyme-salt crystals: Glyme-salt crystals were prepared from concentrated glyme-salt solutions. The exact salt concentration used for each system was different. For the lithium systems, the concentrations of the solutions, described by the ether oxygen: sodium cation ratios, were 2.5:1, 3:1 and 4:1 for the monoglyme-LiTf, diglyme-LiTf and triglyme-NaTf respectively. For the sodium systems, the concentrations of the solutions, described by the ether oxygen: sodium cation ratios, were 5:1, 5:1, 6:1 and 5:1 for the monoglyme-NaTf, diglyme-NaTf, triglyme-NaTf and tetraglyme-NaTf solutions respectively. Salt concentrations were chosen to allow the maximum amount of salt to dissolve in the solvent. The solutions were stirred for at least ~48 h and left inside the glovebox at room

temperature. Some systems, namely diglyme-NaTf and triglyme-LiTf, were stored at both –20°C and 4°C to promote crystal growth. The other solutions were left at room temperature. In all systems, an intermediate gel-like phase appeared within a week to many months, which then became crystalline after a number of months. Single crystals specimens were isolated from the concentrated solution.

### 3.2 Raman spectroscopy

Raman spectra were recorded on an I.S.A. Jobin-Yvon T64000 in the triple subtractive mode with a 16 s acquisition time and 10-16 accumulations using both 180° and 90° scattering geometries. The 514 nm line of an Argon laser operating at 100-300 mW (measured at the laser head) was used for excitation. For the backscattering geometry, the laser was focused through an 80x microscope lens. Possible thermal heating of the samples from the focused Raman laser was examined by comparing spectra taken through the microscope to spectra taken in the 90° scattering geometry, and no differences between the spectra were observed. High temperatures measurements were obtained using an Omega CN9000A temperature controller and a Harrick temperature cell that was adapted for the Raman experimental configuration. Low temperature measurements were taken using a MMR Technologies K-20 Temperature Controller. Bands in the Raman spectra were curve-fit using a non-linear least-squares method with a commercial program, Grams 386 ® (Galactic Industries) using a straight base line and one Gaussian-Lorentzian product function for each band.

### 3.3 Infrared spectroscopy

Infrared spectra were recorded with a Bruker IFS66V FT-IR spectrometer in the region 400-4000 $cm^{-1}$ and at a resolution of 1.0 $cm^{-1}$. IR data of solid samples were obtained using both the KBr pellet and Nujol mull methods. Spectra of polymer films were taken as free standing films or using ZnSe windows in an evacuated sample chamber. IR spectra of liquid samples were obtained using ZnSe plates and a dry-air purge. The temperature was controlled (est. ±2 K) using an Omega CN9000A temperature controller and a Harrick temperature cell. Bands in the IR were curve-fit using a non-linear least-squares method with a commercial program, Grams 386 ® (Galactic Industries) using a straight base line and one Gaussian-Lorentzian product function for each band.

### 3.4 X-ray diffraction

X-ray powder patterns were recorded at ambient conditions from $5 \leq 2\theta \leq 70$ in $2\theta$ steps of 0.05° on a Rigaku D/4MAX automated diffractometer using Cu $K_\alpha$ radiation. For single crystal samples, x-ray diffraction patterns were collected at 173(2) K on a Siemans P4 diffractometer using Mo $K_\alpha$ radiation ($\lambda$=0.71873 Å). The data were corrected for Lorentz and polarization effects; an absorption correction was not applied since it was judged to be insignificant. The structure was solved by the direct method using the SHELXTL system, and refined by a full matrix least squares on $F^2$ using all reflections. Further details of the structural refinement methods used for each crystal structure are presented in the respective publications.

### 3.5 Differential scanning calorimetry

Differential scanning calorimetry (DSC) measurements were taken on a Mettler DSC 820 calorimeter at a rate of 10 °C/min under an 87 mL/min nitrogen purge. The samples were sealed in aluminum crucibles in the glovebox.

# Chapter 4. Glyme-salt systems

*Studies of glyme-salt systems are contained in papers I, IV, V and VI.*

## 4.1 Glymes as models

Systems of PEO with dissolved inorganic salts are of significant interest since PEO shows a particular propensity to solvate and transport ions. In addition to systems based on pure PEO, various polymer architectures containing ethylene oxide (EO) units continue to be investigated *(34, 35, 142, 164, 165)*. Compounds with the general formula $CH_3(OCH_2CH_2)_nOCH_3$ with n usually $\leq 6$, known as glymes (glyme=glycol dimethyl ether), are useful for modeling PEO and polymer systems with EO units. Glyme-salts systems are useful models for the amorphous phase of polymer electrolytes with the understanding that the mechanism of ionic transport is different in low molecular weight oligomers systems compared to high molecular weight PEO systems. This is because the oligomers can diffuse with the ions below the critical entanglement limit. Glymes are also used as solvents in liquid and gel electrolytes and as plasticizers in polymer electrolytes *(123, 166-171)*. The study of glyme-salt systems using glymes with different numbers of ethylene oxide units allows an investigation of how local structure changes with chain length. The relationship between chain length and local structure is an important issue in polymer electrolytes and applies to a number of different systems. For example a number of polymer architectures including copolymers and comb-branched polymers have $(EO)_n$ units with varying n *(34-37, 139, 142, 165, 172)*. Investigation of phosphazenes with ethylene oxide chains of different lengths shows that the number of ethylene oxide units in the chain affects the ionic conductivity *(172)* and local structure *(173)*.

Glymes have been used to model pure poly(ethylene oxide) *(84, 89, 91-93, 174-184)*. Ab initio and quantum chemical calculations of glyme-salt systems have yielded insights into binding energies, coordination geometries, conformational energy minima and energetic barriers for ionic transport *(179, 185-199)*. Vibrational spectroscopic studies of glyme-salt systems have provided insight into conformation changes of the PEO backbone induced by cation coordination *(94, 200, 201)*. Cation complexation induces changes the torsional angles of the bonds in the polymer backbone.

Molecular dynamics (MD) simulations of glymes are useful models of structure and dynamics of PEO *(202-207)*, and MD simulations of glyme-salt systems are particularly useful models of structure and dynamics in polymer electrolytes *(62-65, 67, 208-213)*. MD simulations have been useful to identify the presence of ionic clusters *(62-66)* and salt-rich domains *(67)*, and provided insight into the contribution of various ionic species to the ionic conductivity *(64)*. In addition, MD simulations have provided particular insight into cation complexation and chain conformation *(65, 212)*. MD simulations have been used to model diffusion *(208, 210, 211, 213)* and bond lifetimes *(213)* in polymer electrolytes.

To date, research in glyme-salt systems has focused mainly on gas and solution phases, and crystalline glyme-salt phases have not been widely studied. A few crystalline glyme-salt compounds have been previously reported including (monoglyme)$_2$:$LiBF_4$ *(214)*, tetraglyme:$(CdCl_2)_2$ *(215)*, and tetraglyme:$HgCl_2$ *(216)*. The investigation of crystalline phases has the advantage that x-ray diffraction methods can be used to determine structure in these systems. The comparison of spectra crystalline and solution phases allows the determination of structures present in solution.

**Table 4.1.** Crystalline phases in glyme-salt systems where C = crystalline phase identified and x-ray structure determined; C,C= two phases identified and determined; I = crystalline phase identified; and I,I=two phases identified.

| | $LiCF_3SO_3$ | $NaCF_3SO_3$ |
|---|---|---|
| $CH_3(OCH_2CH_2)_1OCH_3$ | C,C | C |
| $CH_3(OCH_2CH_2)_2OCH_3$ | C | C |
| $CH_3(OCH_2CH_2)_3OCH_3$ | C | I, I |
| $CH_3(OCH_2CH_2)_4OCH_3$ | I | C |

## 4.2 Glyme-salt crystalline phases

### 4.2.1 X-ray structures

A significant result of this investigation is the determination of glyme-salt crystalline phases and their corresponding x-ray structures. Table 4.1 shows crystalline phases which have been identified for systems with the general formula $CH_3(OCH_2CH_2)_nOCH_3$:MX, where n=1-4 and MX=$LiCF_3SO_3$ or $NaCF_3SO_3$. X-ray structures for tetraglyme:LiTf and triglyme:NaTf were not determined due to the difficulty of growing adequate single crystal specimens below room temperature (for triglyme:NaTf) or the long kinetics of crystallization (for tetraglyme:LiTf). For a number of systems, multiple crystalline phases were present in the temperature range studied. Multiple crystalline phases may exist for a single glyme:salt concentration, as is the case for monoglyme:$(LiTf)_2$, and for different glyme:salt concentrations (there is preliminary evidence for this in triglyme-LiTf.). The isolation of a number of crystalline phases for this series suggests that crystalline phases are a general behavior of these systems and therefore crystalline phases may also be present for systems of salts and glymes with $n \geq 5$.

**Table 4.2.** Glyme-salt crystalline phases whose structures were determined and their corresponding crystal systems and space groups.

| Compound | Crystal system | Space group | Paper |
|---|---|---|---|
| Monoglyme:$(LiTf)_2$ α | Triclinic | $P\bar{1}$ | V |
| Monoglyme:$(LiTf)_2$ β | Triclinic | $P\bar{1}$ | V |
| Monoglyme:NaTf | Monoclinic | $P2_1/c$ | VI |
| Diglyme:LiTf | Monoclinic | $P2_1/c$ | IV |
| Diglyme:NaTf | Orthorhombic | $P2_12_12_1$ | VI |
| Triglyme:$(LiTf)_2$ | Triclinic | $P\bar{1}$ | Ref 217 |
| Tetraglyme:NaTf | Monoclinic | $P2_1/c$ | VI |

X-ray diffraction methods yielded structures for a number of these crystalline phases. Crystal systems and space groups for structures that were determined are presented in Table 4.2. Thermal transition temperatures have also been measured and reported in the respective publications. Visual representations of monoglyme:LiTf α, diglyme:LiTf and triglyme:LiTf are presented in Figure 4.1. Visual representations of the monoglyme:NaTf , diglyme:NaTf and tetraglyme:NaTf are presented in Figure 4.2. Single crystal specimens were obtained for these systems, which presents the opportunity to study ionic conductivity and other properties along different crystal orientations.

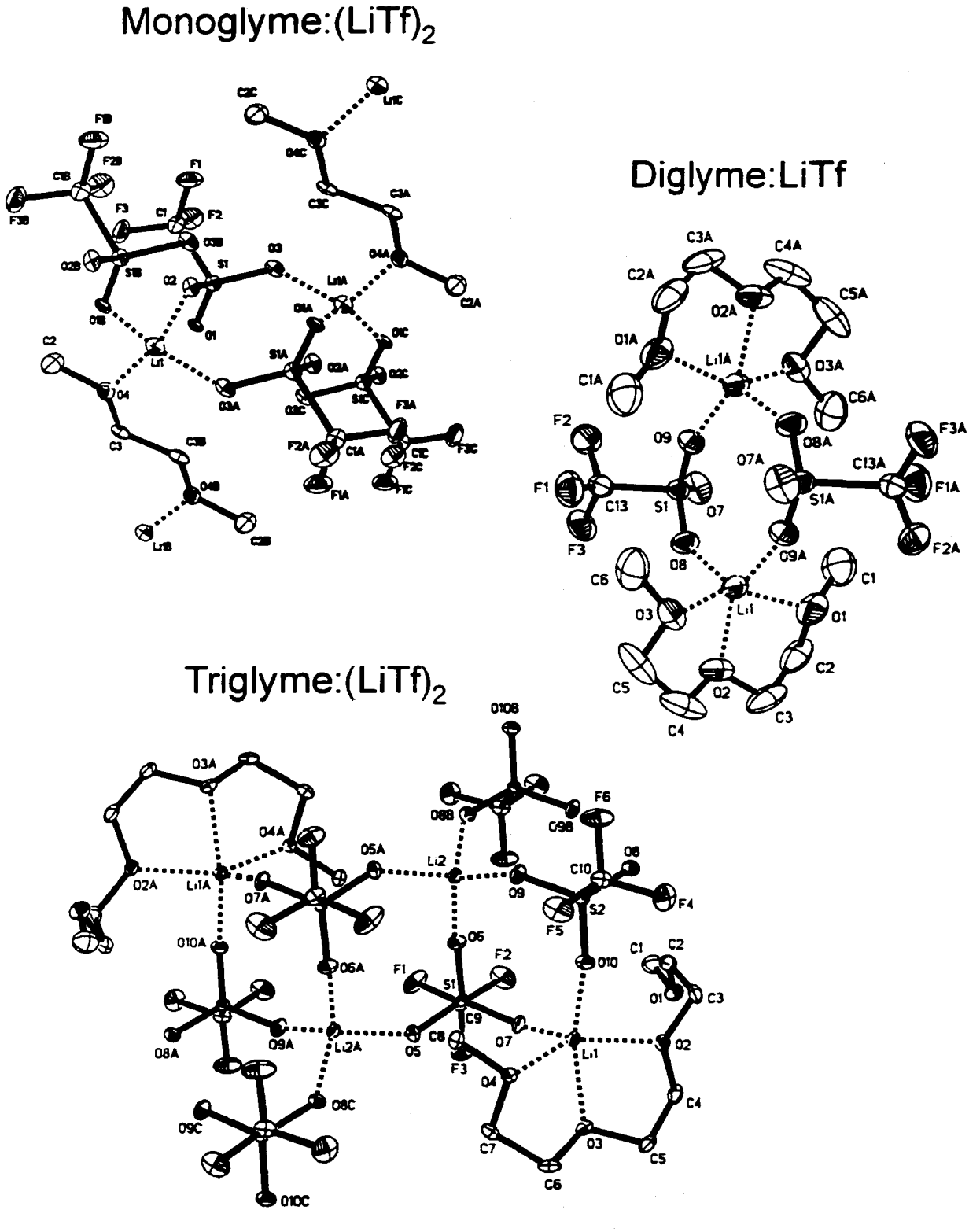


*Figure 4.1. Structures for crystalline phases of monoglyme:$(LiTf)_2$, diglyme:LiTf and triglyme:$(LiTf)_2$.*

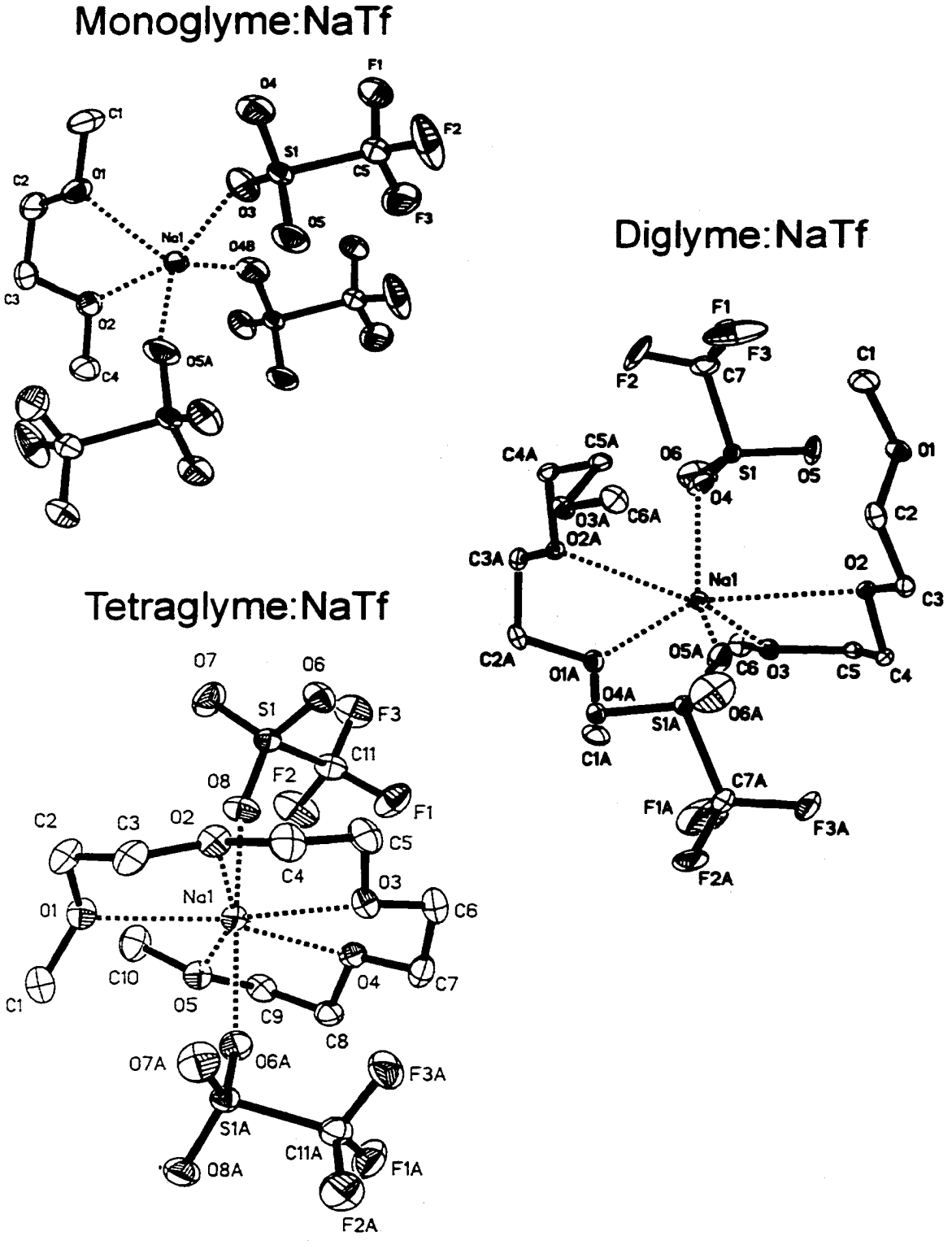


*Figure 4.2. Structures for crystalline phases of monoglyme:NaTf, diglyme:NaTf and tetraglyme:NaTf.*

4.2.2 Comparison of crystal structures

It is of interest to compare three aspects of local structure within the glyme-salt systems: cation coordination, anion coordination, and backbone conformation. The comparison of glyme-salt systems consisting of glymes with different numbers of ethylene oxide units and the same salt allows the effect of chain length on local structure to be investigated. A comparison of the cation environments, anion environments and conformation in the glyme-LiTf systems, $CH_3(OCH_2CH_2)_nOCH_3$:LiTf with n=1, 2 and 3, and $P(EO)_3$:LiTf is presented in Table 4.3. A comparison of the cation environments, anion environments and conformation in the glyme-NaTf systems, $CH_3(OCH_2CH_2)_nOCH_3$:NaTf with n=1, 2 and 4, and P(EO):NaTf is presented in Table 4.4. In all of the structures, the cation is coordinated by both ether oxygens and triflate oxygens, and the relative numbers of ether oxygens and triflate oxygens coordinated to the cation is different in each structure. The overall coordination number and the relative contribution of ether and triflate oxygens results from a number of factors, in particular conformational energies and crystal packing effects.

A number of trends are of interest in the glyme-salt and PEO-salt systems. For the lithium systems, the coordination of Li is four or five in all the structures. In these structures Li is coordinated to both ether and triflate oxygens, and the relative contribution of ether oxygens and triflate oxygens to the overall coordination number varies. The triflate anion is coordinated to either two or three cations in all the structures, which indicates similar anion environments. The conformation is described by the sequence of C-O-C-C, O-C-C-O and C-O-C-C torsional angles using the abbreviation t for a trans angle (180 ± 60°), g for a gauche angle (60 ± 60°), and $\bar{g}$ for a gauche minus angle (270 ± 60°). The torsional angle sequences in the glymes can be viewed as a series of triads, which each consist of three

**Table 4.3.** Comparison of cation environment, anion environment, and conformation for the crystalline phases monoglyme:$(LiTf)_2$ α, diglyme:LiTf, triglyme:$(LiTf)_2$ and $P(EO)_3$:LiTf. The parameters for $P(EO)_3$:LiTf were obtained from the reported crystal structure *(234)*.

| | *Cation environment* | | | *Anion environment* | *Conformation* |
|---|---|---|---|---|---|
| | Total $Li^+$ coordination | Ether oxygens | Triflate oxygens | No. of cations | Torsional sequence |
| Monoglyme:$(LiTf)_2$ | 4 | 1 | 3 | 3 | ttt |
| Diglyme:LiTf | 5 | 3 | 2 | 2 | tgtt$\bar{g}$t |
| Triglyme: $(LiTf)_2$ | 4<br>5 | 0<br>3 | 4<br>2 | 3 | tgtt$\bar{g}$t$\bar{g}$gt |
| $P(EO)_3$:LiTf | 5 | 3 | 2 | 2 | tgtt$\bar{g}$ttgt |

torsional angles. The conformations of the glyme-LiTf structures show similar torsional angle sequences of either tgt or t$\bar{g}$t with the exception of the monoglyme:$(LiTf)_2$ which shows a ttt conformation. The ttt conformer has a lower energy than the tgt conformer in the gas phase *(177, 185, 218)*, and the ttt conformation is stabilized in monoglyme:$(LiTf)_2$ by the lithium ions and their coordination to the triflate anions. It is particularly interesting that a similar local structure is observed in diglyme:LiTf, triglyme:LiTf and $P(EO)_3$:LiTf. In this local structure $Li^+$ is five-fold coordinated by three ether oxygens and two triflate oxygens from different triflate ions. The specific torsional angle sequence is tgtt$\bar{g}$t, and this conformation allows three ether oxygens to coordinate to $Li^+$. The presence of this torsional angle sequence in the three structures suggests that is structure is particularly stable in these systems.

As presented in Table 4.4, the coordination number of $Na^+$ in the structures is five, six or seven, and there is a significant variation in the relative contribution of the ether

**Table 4.4.** Comparison of cation environment, anion environment, and conformation for crystalline phases of monoglyme:NaTf, diglyme:NaTf, tetraglyme:NaTf and P(EO):NaTf. The parameters for P(EO):NaTf were obtained from the reported crystal structure *(229)*.

| | *Cation environment* | | | *Anion environment* | *Conformation* |
|---|---|---|---|---|---|
| | Total $Na^+$ coordination | Ether oxygens | Triflate oxygens | No. of cations | Torsional sequence |
| Monoglyme:NaTf | 5 | 2 | 3 | 3 | tgt |
| Diglyme:NaTf | 6 | 4 | 2 | 2 | tgttgt |
| Tetraglyme: NaTf | 7 | 5 | 2 | 2 | $tgtt\bar{g}ttgtt\bar{g}\bar{g}$ |
| P(EO):NaTf | 6 | 2 | 4 | 4 | $tggt\bar{g}\bar{g}$ |

oxygens and triflate oxygens. For diglyme:NaTf and tetraglyme:NaTf, the ether oxygens contribute more than the triflate oxygens to the overall coordination number. For monoglyme:NaTf and P(EO):NaTf, the triflate oxygens contribute more than the ether oxygens to the overall coordination number. Structural differences are related to the energy minima for these molecules packing within a crystalline phase. The terminal groups in the glymes, which are neglected in P(EO):NaTf, play a role in the observed structure. In addition, sodium can adopt a number of different coordination states. The triflate anion is coordinated to two, three or four sodium ions in the structures, which shows the different types of anion environments that can occur in these systems. Similar triad sequences of either tgt or $t\bar{g}t$ are observed in all the structures, however very different overall conformations are observed. Significant differences in the cation environment, anion environment and conformation are observed between the glyme-NaTf structures,

particularly between tetraglyme:NaTf, and P(EO):NaTf. A further discussion of the glyme-NaTf structures is presented in paper VI.

The comparison of crystalline glyme-salt structures to crystalline PEO-salt structures is useful to determine the effect of the terminal methoxy groups on the local structure. Crystalline phases have been determined for glyme-salt systems for glymes with $1 \leq n \leq 4$. The glyme-salt structures are different than the PEO-salt structures. Crystalline phases of PEO:salt systems have been made using PEO of molecular weights as low as $M_w = 1000$, and similar x-ray patterns and d-spacings were observed between the structures using PEO with $M_w = 1000$ and with $M_w = 100{,}000$ *(219)*. This suggests that the crystalline structure of high molecular weight PEO with salts can be obtained using PEO with molecular weights as low as $M_w = 1000$ (n~22). Therefore region of glymes with n=5 to n=22 with salts may exhibit different crystalline structures. At some critical chain length between n=5 and n=22, the structure of the crystalline glyme-salt phase (as determined by x-ray) will be isomorphous with the crystalline polymer-salt phase using PEO with $n \geq 22$. Below this critical chain length, the structures for crystalline glyme-salt phases will be different than the structure of the crystalline polymer-salt compound obtained with PEO ($n \geq 22$).

Spectroscopic studies of the glyme-salt structures are useful to further spectra-structure correlations in these systems, particularly the anion and glyme modes. The monoglyme$(LiTf)_2$ $\alpha$ structure demonstrates the existence of a $[Li_3Tf]^{2+}$ species and its corresponding frequency (presented in paper V). The spectral comparison of the $\nu_s(SO_3)$ and $\delta_s(CF_3)$ modes in the glyme-NaTf crystals shows that the frequencies of these modes are highly sensitive to the local potential environment of the triflate anion (presented in paper VI).

## 4.3 Glyme-salt solutions

It is of interest to examine glyme-salt solutions since their structure is not a result of crystal packing effects and therefore may be a good structural model of the amorphous phase of polymer electrolytes. Since the crystal structures of a number of different glyme-salt systems was determined as presented above, it if of interest to compare the local structure in the crystal to the local structure in solution. Vibrational spectroscopy is ideal for the experimental comparison of the crystalline and solution phases since the vibrational modes are sensitive to local structure. To present representative behaviors, two glyme-salt systems are presented: monoglyme-LiTf and diglyme-LiTf. Other systems including diglyme-NaTf (paper I), tetraglyme-LiTf *(65)*, and tetraglyme-NaTf *(220)* have also been investigated.

### 4.3.1 Monoglyme-LiTf

The spectra of crystalline monoglyme:$(LiTf)_2$ β is compared to spectra of monoglyme-LiTf solutions in Figure 4.3. The 800-1000 $cm^{-1}$ region contains modes that are composed of $CH_2$ twisting, $CH_2$ wagging and C-O stretching motions, and these modes have been shown to be sensitive to conformation and coordination to cations *(79, 92, 94, 176, 183, 184, 200)*. The intensity of the 864 $cm^{-1}$ band in the monoglyme-LiTf solution increases with increasing salt concentration and has been assigned to a monoglyme molecule in a tgt conformation interacting with $Li^+$ *(221)*. The frequency of this mode is also affected by coordination of $Li^+$ by one or more triflate anions *(221)*. In contrast, the 920 and 933 $cm^{-1}$ bands in crystalline monoglyme:$(LiTf)_2$ result from monoglyme in a ttt conformation. This spectral comparison shows that the conformation of monoglyme interacting with $Li^+$ in solution is very different than in the crystalline phase. The comparison of the triflate modes in the two phases also shows differences. The $\delta_s(CF_3)$ mode of the triflate anion is sensitive

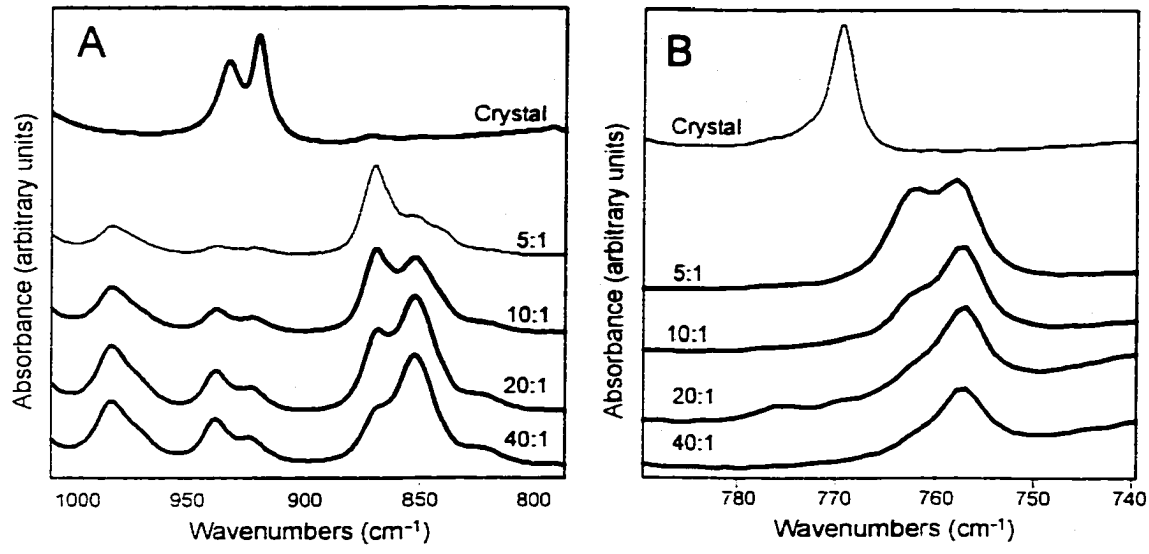


*Figure 4.3. Infrared spectra in the 800-1000 $cm^{-1}$ region (A) and 740-780 $cm^{-1}$ region (B) of crystalline monoglyme:$(LiTf)_2$ and solutions of monoglyme-LiTf with concentrations described by the ether oxygen to metal cation ratio (O:M).*

to the local potential energy environment, and in particular to the number of cations which are coordinated to the triflate anion *(60, 61)*. Spectra of the solutions in the $\delta_s(CF_3)$ region show bands which can be resolved by curve-fitting to bands at 753, 758, 762 and 766 $cm^{-1}$, which correspond to "free" triflate species, contact ion pairs, $[Li_2Tf]^+$ aggregates and $[Li_3Tf]^{2+}$ aggregates. These assignments are based on studies of triflate with different cations in numerous solvent systems *(61, 77, 78, 222)*. The predominant triflate anion species in solution is the contact ion pair species, and the 766 $cm^{-1}$ band has a very minor intensity. The spectra of the crystalline monoglyme:$(LiTf)_2$ has a single band at 769 $cm^{-1}$ which corresponds a triflate anion that is coordinated to three lithium ions. The spectral comparison of the $\delta_s(CF_3)$ mode in the crystal and in solution shows that the predominant triflate anion environment is very different in solution than in the crystalline phase.

4.3.2 Diglyme-LiTf

Raman spectra of crystalline diglyme:LiTf, diglyme-LiTf solutions and pure diglyme are presented in Figure 4.4. The mode at 871 $cm^{-1}$ observed in the spectra of crystalline diglyme:LiTf is assigned to $CH_2$ twisting/$CH_2$ wagging motions of a diglyme molecule in a tgtt$\bar{g}$t conformation which is coordinated to lithium. The 871 $cm^{-1}$ band is also observed in the 10:1 solution of diglyme-LiTf which indicates that the conformation of diglyme interacting with lithium, tgtt$\bar{g}$t, is also observed in solution. The $\delta_s(CF_3)$ region of crystalline diglyme:LiTf and a 10:1 diglyme-LiTf solution is also presented in Figure 4.4. Crystalline diglyme:LiTf (structure shown in Figure 4.1) shows a single band at 762 $cm^{-1}$ in the $\delta_s(CF_3)$ region that is due to a triflate anion coordinated to two lithium ions. In contrast, the spectrum of the 10:1 diglyme-LiTf solution shows the presence of different triflate anion species. Bands in $\delta_s(CF_3)$ region can be curve-fit using bands at 752 $cm^{-1}$, 757 $cm^{-1}$ and 762 $cm^{-1}$ which correspond to "free" triflate anions, contact ion pairs and $[Li_2Tf]^+$ aggregate species, respectively. The predominant triflate anion species in solution is the contact ion pair. In the diglyme-LiTf system, the structure present in the crystalline phase is also present in solution, and in addition other structures as well. The existence of the dimer structure in solution is not surprising since this structure may be a particularly stable geometry. The monoglyme-LiTf and diglyme-LiTf data demonstrate that the local structure in solution can be similar to the local structure present in the crystal, or it can be quite different.

Based on the spectral comparison, proposed local structures for "free" ions, contact ion pair species and aggregate species which occur in solution are presented in Figure 4.5. The aggregate species exists in within a dimer which has analogous structure to that of the dimer in crystalline diglyme:LiTf. A dynamic equilibrium exists between these species in solution, and the relative amounts of these species depend on salt concentration as reported

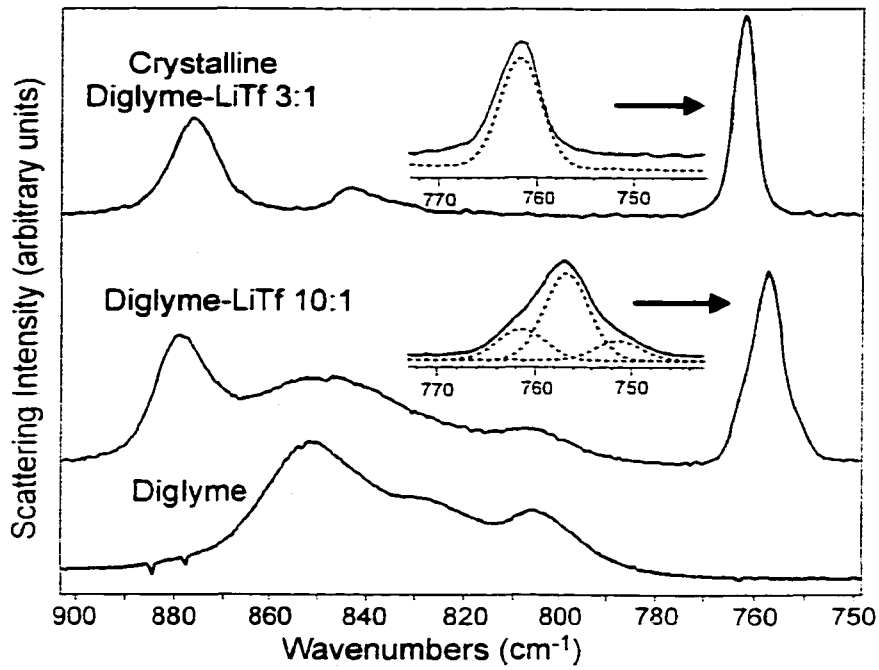


*Figure 4.4. Raman spectra in the 750-900 $cm^{-1}$ region of crystalline diglyme:LiTf, a 10:1 solution of diglyme-LiTf and pure diglyme.*

previously *(223)*. These structures represent possible coordination environments of $Li^+$ and triflate and correspond with the spectral data. In the proposed "free" ion structure, $Li^+$ is six-coordinate and is coordinated by ether oxygens from two diglyme molecules. The tgtt$\bar{g}$t diglyme conformation interacting with $Li^+$ was determined to be a local energy minima structure from ab initio studies *(186)*. In the contact ion pair species, $Li^+$ is four-coordinate consisting of three ether oxygens from a diglyme in a tgtt$\bar{g}$t conformation and a single oxygen from a triflate anion. In the dimer structure, lithium is five-coordinate consisting of three ether oxygens and two triflate oxygens from different triflate anions. These $Li^+$ coordination numbers are consistent with those of similar ether systems *(81)*. Cation

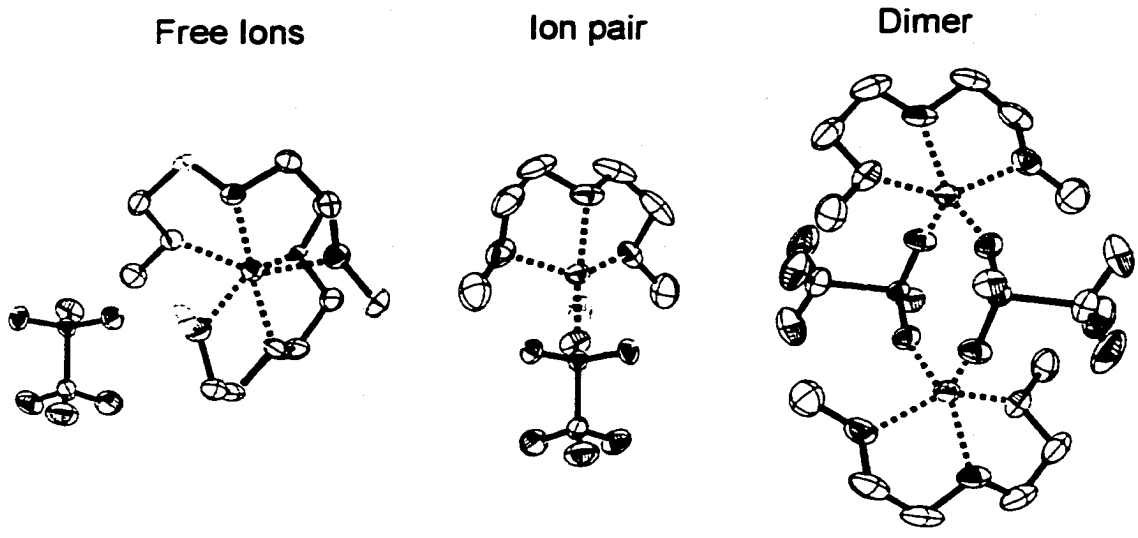


*Figure 4.5. Proposed local structure in diglyme-LiTf solution consisting of a contact ion pair and a single diglyme molecule in a tgt-t$\bar{g}$t conformation.*

environments, anion environments and conformations present in glyme-salt solutions and crystalline phases suggest stable local structures which may also be present in PEO-salt systems. The application of these structures to high molecular weight PEO-salt systems is presented in section 5.2 and has been presented in the literature (paper VI).

# Chapter 5. Polymer-salt systems

*Studies of polymer-salt systems are contained in papers I, II, III and IV.*

## 5. 1 Crystalline phases in polymer-salt systems

The study of crystalline phases, both PEO and PEO:salt compounds, provides substantial insight into the microscopic structure of polymer electrolytes. Pure PEO is a semicrystalline polymer having two known crystalline forms, a helix with seven monomeric units turn two times per fiber period shown in Figure 5.1 *(83, 224)*, and a second crystalline structure, a planar zigzag, that has been identified upon stretching *(225)*. Vibrational spectroscopic studies of pure PEO establish modes and frequencies for the crystalline phase and provide a basis for understanding the structure of the amorphous phase *(83-87, 89-91, 93, 224-226)*.

The study of crystalline polymer-salt compounds is motivated by a number of factors. In a number of PEO-salt systems where crystalline and amorphous phases coexist, the ionic conductivity occurs primarily in the amorphous phase *(3, 4)*. Recently, Bruce and coworkers reported a crystalline phases which has a higher ionic conductivity than the corresponding amorphous phase *(7)*. The specific reason for the higher ionic conductivity of the crystalline phase has not been precisely determined but underscores the importance of examining crystalline polymer-salt phases. Motivation for studying crystalline polymer-salt compounds also lies in their ability to provide insight into local structure in polymer electrolytes. The structures of the crystalline polymer-salt phases have been used to infer structures present in the amorphous phases of polymer electrolytes *(227-229)*. A vibrational spectroscopic study of crystalline $P(EO)_3$:$LiCF_3SO_3$ above its melting point suggested that the structure of the amorphous phase is similar structure to structure of the crystalline phase

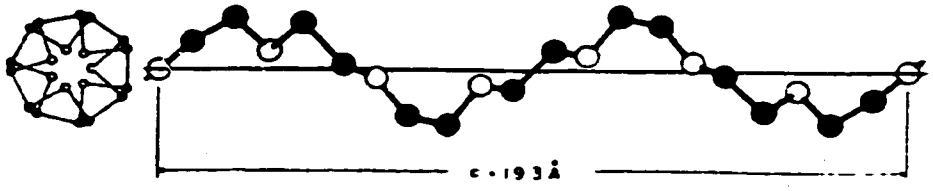


*Figure 5.1. Structure of crystalline poly(ethylene oxide) (83).*

*(230)*. The comparison of crystalline phases to amorphous phases provides insight into the structure of the amorphous phase *(231)*.

Crystalline polymer-salt complexes have been useful to examine local structure in polymer electrolytes *(227)*. Using x-ray and neutron diffraction techniques, structures for a number of polymer-salt complexes have been solved including $P(EO)_3$:NaI *(232)*. $P(EO)_3$:NaSCN *(233)*. $P(EO)_3:LiCF_3SO_3$ *(234)*. $P(EO)_3:LiN(SO_2CF_3)_2$ *(235)*, $PEO:NaCF_3SO_3$ *(236)*, $P(EO)_6:LiAsF_6$ *(237)*, $P(EO)_6:LiPF_6$ *(7)*, and $P(EO)_6:LiSbF_6$ *(7)*. The x-ray structures of $P(EO)_3:LiCF_3SO_3$ and $P(EO):NaCF_3SO_3$ are presented in Figure 5.2. Crystalline polymer-salt complexes have revealed coordination geometries, polymer conformations and interactions of the ions with the polymer. In a number of crystalline polymer-salt compounds, PEO is in a helical conformation within the crystal, and the cation is located within the helix. However within a number of structures, the geometry of the PEO is a zigzag, rather than a helix. The cation may be coordinated by the polymer and the anion, or entirely by the polymer. The interaction of the anion with the polymer can be characterized by weak van der Waals interactions. Polymer-salt complexes also provide insight into the nature of ionic crosslinking. The predominant ionic crosslinks within these structures are *intra-chain* crosslinks with the cation and anion interactions within a single chain, as seen in the structure of $P(EO)_3:LiCF_3SO_3$ in Figure 5.2. A notable exception is the crystalline

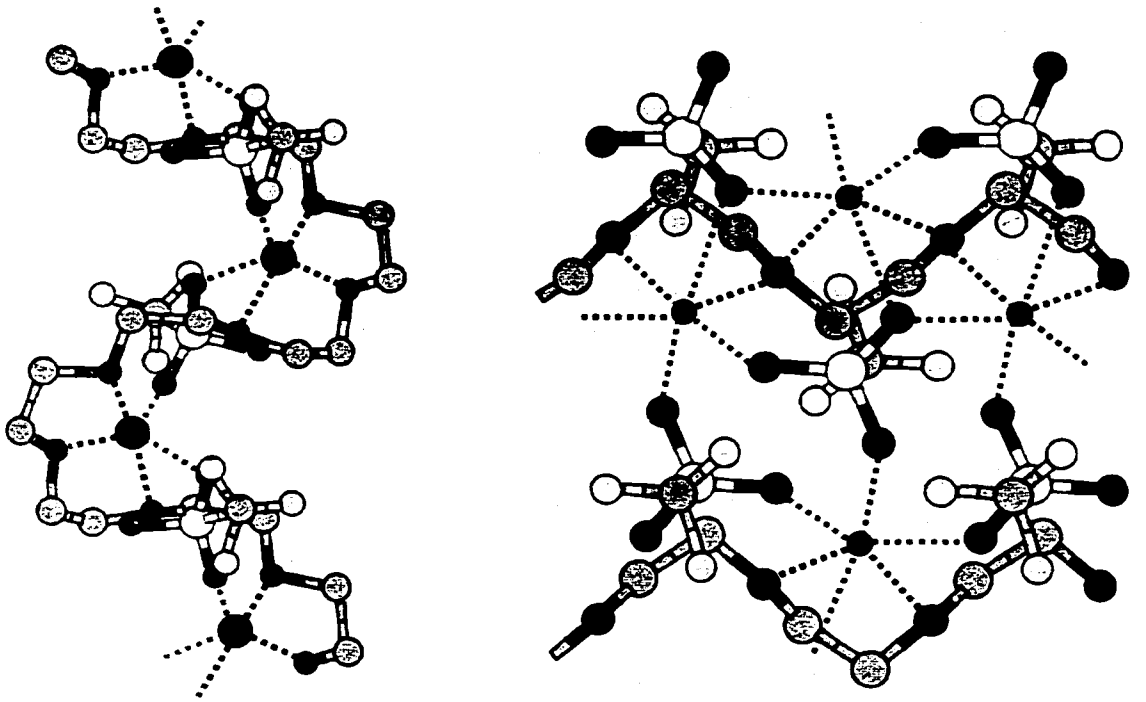

*Figure 5.2. X-ray structures of P(EO)$_3$:LiCF$_3$SO$_3$, left. (234) and P(EO):NaCF$_3$SO$_3$, right (236). The hydrogen atoms are not shown.*

P(EO):NaCF$_3$SO$_3$ compound, where anions are coordinated to cations from different chains, resulting in anion-assisted *inter-chain* crosslinking as presented in Figure 5.2.

## 5.2 Symmetry-based vibrational analysis

A thorough vibrational analysis of polymer-salt crystals has not been previously reported. The vibrational modes in a crystal are a function of the unit cell and the symmetries thereof. The full factor group, which neglects specific bonding interactions, describes the vibrational modes within the unit cell of a crystal and predicts more modes than observed in PEO-salt crystalline compounds *(238)*. The factor group correlation field method, which includes specific bonding interactions of distinct polyatomic species such as

the triflate anion, provides a description of correlated molecular vibrations in terms of the irreducible representations of the factor group *(239)*. Other symmetry-based analyses are also possible, and in particular a helical group analysis provides useful insight into the nature of these modes in polymer-salt compounds *(240)*.

The factor group correlation field method has been used to analyze the triflate anion, $CF_3SO_3^-$ or Tf, bands in $P(EO)_3$:LiTf and P(EO):NaTf (paper II) and the hexafluoroarsentae anion, $AsF_6^-$, bands in $P(EO)_6$:$LiAsF_6$ (paper III). The analysis of the triflate bands in $P(EO)_3$:LiTf and P(EO):NaTf is presented here, and the analysis of the $AsF_6^-$ bands in $P(EO)_6$:$LiAsF_6$ is presented in the respective publication. For this analysis all atoms in the unit cell other than the atoms of the triflate anions are neglected. The isolated triflate anion is taken as having $C_{3v}$ symmetry (staggered configuration). For an isolated triflate anion with $C_{3v}$ point group symmetry, the anion gives 3N-6=18 fundamental vibrational modes which belong to the irreducible representations,

$$\Gamma\ (CF_3SO_3^-) = 5A_1 + A_2 + 6E. \qquad (5.1)$$

The frequencies and symmetries of these modes in triflate anions and triflate anions coordinated to cations in a variety of solvents have been previously analyzed by experimental and computational methods *(61, 222, 241-243)*. A number of modes have been used to examine the association of triflate with cations, particularly the symmetric $SO_3$ stretching mode $\nu_s(SO_3)$ of $A_1$ symmetry, the symmetric $CF_3$ deformation mode $\delta_s(CF_3)$ of $A_1$ symmetry, and the antisymmetric $SO_3$ stretching mode $\nu_{as}(SO_3)$ of E symmetry. Thus the analysis is focused on modes of $A_1$ and E symmetry.

**Table 5.1.** Factor group correlation of intramolecular triflate vibrations in a $C_{2h}^5$ crystal

| Mode | Point Group ($C_{3v}$) | Site Group ($C_1$) | Factor Group ($C_{2h}^5$) |
|---|---|---|---|
| $\nu_s(SO_3)$, $\delta_s(CF_3)$, $\delta_s(SO_3)$ | $A_1$ | A | $A_g$ |
| | | | $B_g$ |
| $\delta_{as}(CF_3)$, $\delta_{as}(SO_3)$ | E | | $A_u$ |
| | | | $B_u$ |

Within a crystal the vibrations of the triflate anions are not isolated from each other but are correlated through intermolecular forces. The unit cells of both P(EO)$_3$:LiTf and P(EO):NaTf belong to the $C_{2h}^5$ space group and contain four triflate anions per unit cell. The factor group method provides a description of the correlated molecular vibrations as they transform according to the irreducible representations of the factor group. The center of mass of the triflate anion occupies a specific Wyckoff site of $C_1$ symmetry, and the site group is a subgroup of the unit cell space group $C_{2h}^5$. The general procedure presented elsewhere [Fateley, 1972 #16] correlates the irreducible representations of the point group to those of the site group which are in turn correlated to the factor group. A visual representation of the factor group correlation applied to $A_1$ and E modes in a $C_{2h}^5$ crystal is presented in Table 5.1. The result of the analysis is that four isolated Tf anion modes of $A_1$ symmetry give four factor group modes whose symmetries are described in Eq. 5.2. Similarly, the correlation of four isolated triflate E modes results in eight factor group modes whose symmetries are described in Eq. 5.3,

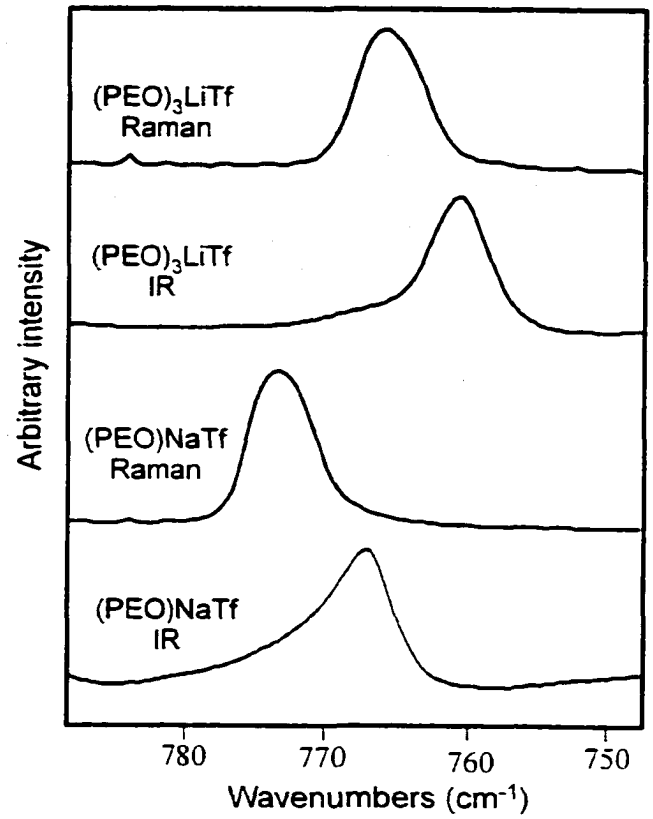


*Figure 5.3. Raman and IR spectra in the $\delta_s(CF_3)$ region of $P(EO)_3$:LiTf and P(EO):NaTf.*

$$\Gamma(A_1) = A_g + B_g + A_u + B_u \quad (5.2)$$

$$\Gamma(E) = 2A_g + 2B_g + 2A_u + 2B_u \quad (5.3)$$

Under the symmetry of the $C_{2h}^5$ space group, the $A_g$ and $B_g$ modes are Raman active and the $A_u$ and $B_u$ modes are IR active. Of course the frequencies and intensities of the bands cannot be predicted by symmetry methods. This analysis applies to both the crystalline $P(EO)_3$:LiTf and P(EO):NaTf compounds.

The symmetry-based vibrational analysis is useful to explain the multiple bands present in the vibrational spectra. Raman and infrared spectra in the $\delta_s(CF_3)$ region of P(EO)$_3$:LiTf and P(EO):NaTf are presented in Figure 5.3. The symmetry analysis predicts two Raman active and two IR active modes. The experimental spectra show a single band in both the Raman and IR spectra which may be composed of two bands which are close in frequency. In each compound, the frequencies of the predominant $\delta_s(CF_3)$ Raman and IR bands are noncoincident and exhibit a ~5 $cm^{-1}$ difference. The frequency difference indicates a modest amount of dynamical coupling between the vibrational modes in the crystal which results from the highly ordered structure in the crystalline material. A similar frequency difference is not observed in crystalline diglyme:LiTf where the triflate anion is in a similar local environment but exists in the unit cell within an isolated dimeric structure. In both P(EO)$_3$:LiTf and P(EO):NaTf, the triflate anions exist within a linear chain, rather than an isolated dimer. This suggests that the coupling of these modes is dependent on the relative orientation of the anions within the unit cell.

## 5.3 Structure in the amorphous phase

Since the ionic conductivity occurs primarily in the amorphous phase for a number of polymer-salt systems, determining the structure of the amorphous phase has been of primary importance. The structure of the amorphous phase has not been well characterized due in part to its heterogeneity. Vibrational spectroscopy has been particularly useful to identify the presence and relative concentrations of different ionic species *(60, 61, 244)* and changes in the polymer conformation due to cation complexation *(52, 79, 94, 96, 129, 200, 245)*. NMR studies have identified different relaxation times corresponding to nuclei in the crystalline and amorphous phase *(3, 4)* and have determined that the addition of salt

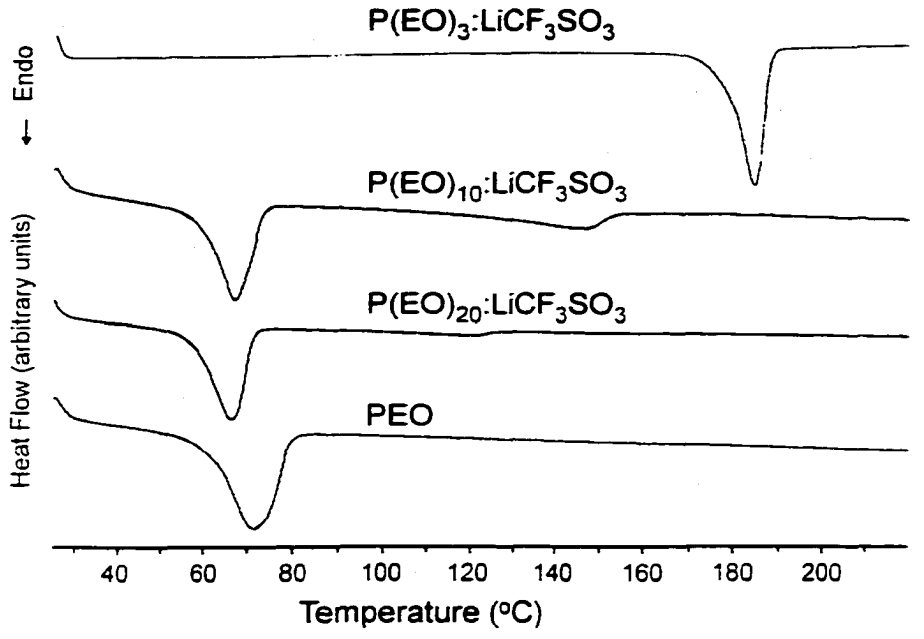


*Figure 5.4. Differential scanning thermograms of PEO, $P(EO)_{20}$:LiTf, $P(EO)_{10}$:LiTf and $P(EO)_3$:LiTf in the range 25°C to 220°C.*

increases the segmental relaxation time *(56, 80, 97, 98, 246, 247)*. The $^{13}C$ chemical shift in the amorphous phase of PEO-LiTf was similar to the $^{13}C$ chemical shift in the crystalline $P(EO)_3$:LiTf which indicates that the local structure in the amorphous phase is similar to the local structure in the crystalline phase *(59)*. DSC measurements have shown that increase in the glass transition temperature with the addition of salt *(16, 53.)* Previous results have suggested that the structure of the amorphous phase is similar to the structure of the crystalline polymer-salt phase *(59, 230, 231)*. Therefore, a direct comparison of the structures of the amorphous and crystalline polymer-salt phases is of interest.

DSC, x-ray diffraction and vibrational spectroscopy were used to examine the amorphous and crystalline phases of PEO-LiTf. At room temperature, films of PEO-LiTf consist of multiple phases, and the relative amounts of these phases depends on

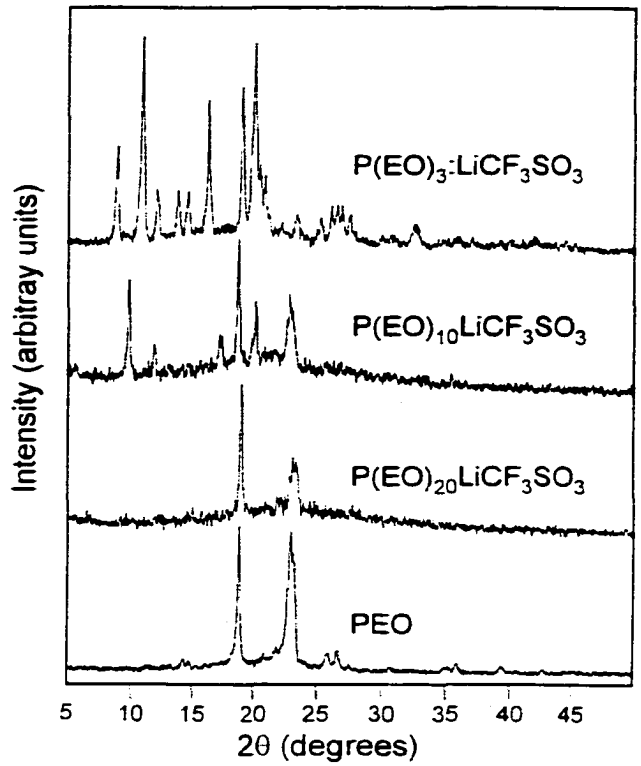


*Figure 5.5. Powder x-ray diffraction patterns of PEO, $P(EO)_{20}$:LiTf, $P(EO)_{10}$:LiTf and $P(EO)_3$:LiTf*

temperature, salt concentration, the molecular weight of the polymer *(43)*, thermal history *(44)*, time *(45)*, and preparation method *(46)*. Films for DSC, x-ray and Raman measurements were prepared in an identical manner in order to facilitate a direct comparison of the results. Data for films with 10:1 and 20:1 concentrations were compared with data for both crystalline PEO and $P(EO)_3$:LiTf. DSC data is presented in Figure 5.4. The 10:1 and 20:1 films exhibit very small endotherms which indicate the presence of small domains of $P(EO)_3$:LiTf, in agreement with the published phase diagram.

X-ray data of the 10:1 and 20:1 films, presented in Figure 5.5, show the presence of crystalline PEO domains, which is consistent with the DSC data. However, the data shows

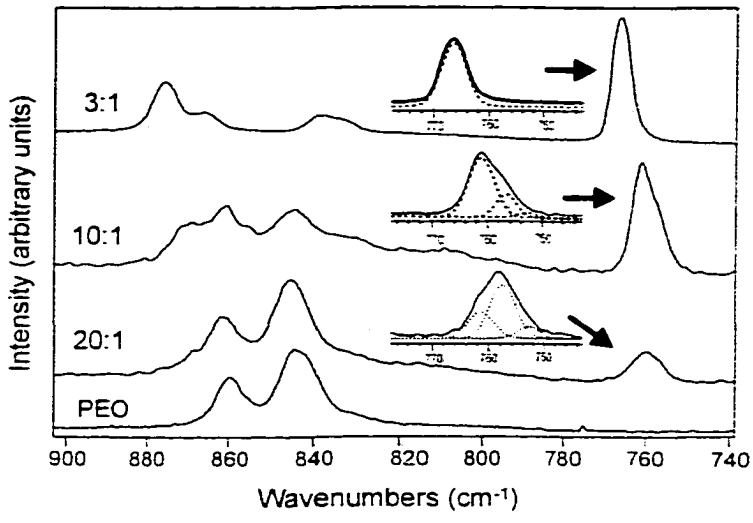


*Figure 5.6. Raman spectra in the 740-900 $cm^{-1}$ region of PEO, $P(EO)_{20}$:LiTf, $P(EO)_{10}$:LiTf and $P(EO)_3$:LiTf.*

that the 20:1 film contains domains of $P(EO)_3$:LiTf whose sizes are sufficiently small so that distinct peaks are not observed by x-ray diffraction. In addition, the 10:1 sample show different 2θ values than present in $P(EO)_3$:LiTf, which indicates a structure with a different ordering than that present in $P(EO)_3$:LiTf. A number of the diffraction peaks have similar values to those of $P(EO)_3$:LiTf, so this suggests some similar ordering is present.

Vibrational spectra are presented in Figure 5.6. The analysis of the $\delta_s(CF_3)$ region shows the existence of "free" ions, ion pairs and aggregate species with frequencies of 752 $cm^{-1}$, 757 $cm^{-1}$ and 762 $cm^{-1}$ respectively. Of particular interest is the frequency of the aggregate species in the PEO-LiTf films, 762 $cm^{-1}$, which is different than the frequency of the aggregate species in the crystalline $P(EO)_3$:LiTf compound, 767 $cm^{-1}$. The frequency difference suggests that the triflate anion in the PEO-LiTf films exists within a local structure which is less ordered than the local structure of the triflate anion in the crystalline

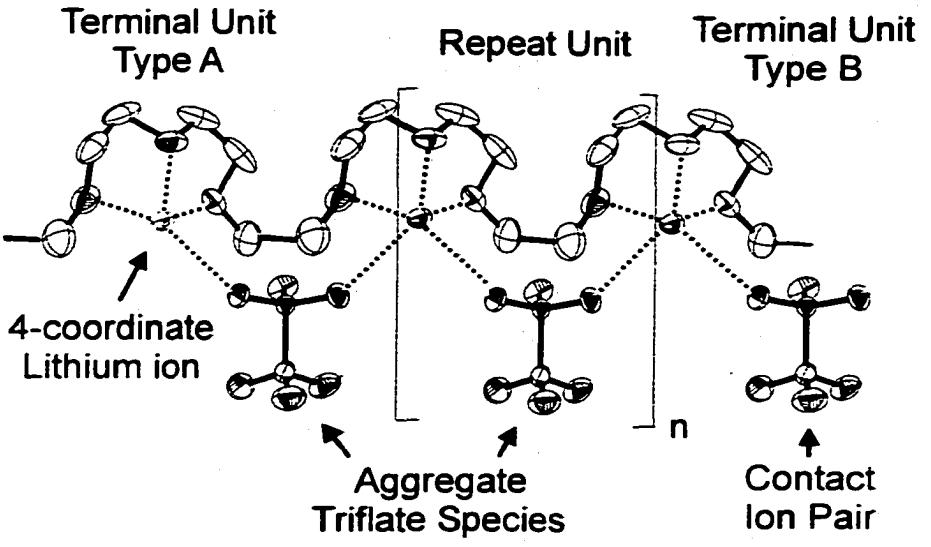


*Figure 5.7. Proposed local structure in PEO-LiTf systems.*

$P(EO)_3$:LiTf. The PEO modes in the 800-900 $cm^{-1}$ region contain mixtures of $CH_2$ rocking, $CH_2$ twisting and CO stretching motions *(86, 87, 92)*. The frequencies of these modes are highly sensitive to both the conformation and the interaction of the ether oxygens with the $Li^+$ cation *(92, 94, 200, 221)*. The analysis of the 800-1000 $cm^{-1}$ region shows that in the PEO-LiTf films, the region of the polymer which interact with $Li^+$ have a similar, but not identical, local structure to that present in $P(EO)_3$:LiTf.

Based on the combination of the DSC, x-ray and vibrational spectroscopic data, local structures which exist in PEO-LiTf systems are proposed, and a pictorial representation is presented in Figure 5.7. The proposed local structure contains local structures which are similar to the local structure present in the crystalline $P(EO)_3$:LiTf compound, namely five coordinate Li ions, tgttg´t torsional angle sequences and aggregate triflate species. The proposed local structure also contains terminal units of two different types. The terminal unit consisting of a 4-coordinate $Li^+$ (Type A) is suggested by the vibrational study of the

diglyme-LiTf system (presented in 4.3). For PEO-salt systems, experimental evidence for the presence of salt-rich regions and local structures thereof has not been previously reported. The presence of local salt-rich regions with terminal units is consistent with molecular dynamics simulations which identified the presence of ionic clusters and salt-rich domains *(62-66)*. The existence of microdomains within the amorphous phase of polymer electrolytes was observed in poly(propylene oxide)-sodium salt electrolytes where two glass transition temperatures were observed corresponding salt-rich and salt-poor microdomains within the "amorphous" phase *(248)*.

### 5.4 Implications for ionic transport

The mechanism of ionic transport in polymer electrolytes is complex and remains not well understood. Determining the relationship of local structure to ionic transport is crucial to improving the transport properties of polymer electrolytes. An understanding of local structure, specifically cation-polymer and cation-anion interactions is needed. The relationship between ionic transport and local polymer relaxation processes has been established *(5, 82, 112)*. The role of ion-ion interactions in ionic transport in polymer electrolytes has not been well described. The importance of cation-anion interactions is apparent from transference number measurements *(120)*, diffusion coefficients *(107, 125)*, and the failure of the Nernst-Einstein relationship to describe the experimental ionic conductivity *(108-110, 114)*. It is recognized that in these systems, both cations and anions are mobile and the ionic mobility of the anion is generally greater than the cation *(108, 110, 125)*. For the application of polymer-salt systems as electrolytes in rechargeable batteries, transport of the cation is needed. Mobility of the anion leads to concentration gradients in the operational cell, i.e. cell polarization *(101)*. A number of results suggest that ionic

transport of the cation is affected by the anion. Transport of the cation may occur via transport of cation-anion aggregate species as suggested by the negative cation transference numbers observed in some systems *(68-70)*. Ionic transport may also occur via hopping between ionic clusters and/or correlated motions of cations and anions *(11, 108, 138)*. The ionic transport mechanism may also vary from system to system, especially in regards to the role of the anion. It is possible that ionic transport of the cation may be higher in systems where the anion is entirely mobile or semi-mobile. Monte Carlo simulations of polyelectrolytes demonstrated that increased local anion motion increases the cation conductivity *(146)*.

The proposed local structure presented above suggests particular environments for cations and anions in the amorphous phas in which the contribution to the ionic conductivity is significantly enhanced. In particular, the terminal units of the local complex contain lithium ions in potential energy environments which are less deep than the than five-fold coordinated lithium in crystalline domains of $P(EO)_3$:$LiCF_3SO_3$. In addition, the potential energy environment of the lithium ions is dynamically disordered through polymer segmental motion. Therefore it is proposed that lithium ions in part of a terminal unit of a localized complex or an isolated $[Li_2CF_3SO_3]^+$ contribute to the ionic conductivity in the amorphous phase. It is also possible that contact ion pair species contribute to the ionic conductivity. Clearly, an isolated contact ion species is neutral and as such does not directly contribute to the ionic conductivity. However, a contact ion pair species may contribute to the ionic conductivity through a dissociative process that is part of the dynamical nature of the equilibrium between the various ionic species.

# Chapter 6. Concluding Remarks

An understanding of local structure and its relationship to ionic transport is needed to improve the properties of polymer electrolytes. For this investigation, some of the major results are the following:

(a) Discovery of a series of glyme-salt crystalline phases and elucidation of their structures which allows the determination of the effect of chain length on local structure,

(b) Spectroscopic comparison of glyme-salt crystalline and solution phases showing that in solution both similar and different local structures are observed,

(c) Application of factor group correlation method to the vibrational analysis of polymer-salt crystals,

(d) Demonstration of anion mode coupling in crystalline phases of polymer electrolytes,

(e) Proposed local structures in the amorphous phase of PEO-LiTf and the contribution of such structures to the ionic conductivity.

The glyme-salt systems further our understanding of coordination environments in PEO-salt systems. The current study suggests a number of new directions for future research efforts. Since the formation of crystalline phases seems a general property of the system, a similar chain length study with a different, less coordinating anions would reveal different cation coordination environments. Determining the critical chain length where glyme-salt crystal structures are isomorphous with PEO-salt crystals is of interest, as well as investigating the regime below the critical chain length. The study of the glyme-salt systems

can provide insight into the optimal number of EO units for coordination. It should also be possible to determine the number of EO units for optimal transport. The optimal number of EO units may depend on the anion and the polymer system. This information could be applied to a number of copolymer and comb-branch polymer systems.

The microscopic mechanism of ionic transport in polymer electrolytes is still not well understood, and the relationship between ionic transport and local structure has not been well established. In particular, an understanding of the role of the anion in the transport of the cation is needed. If the cation is transported via anionic clusters or some correlated cation-anion mechanism, it should be possible to design new systems which optimize the ionic transport of the cation. Such systems may be a matrix which includes anions with appropriate intermolecular spacings and mobilities.

## References


1. D. E. Fenton, J. M. Parker, P. V. Wright, *Polymer* **14**, 589 (1973).
2. M. B. Armand, J. M. Chabagno, M. J. Duclot, in *Fast Ion Transport in Solids*. P. Vashista, J. M. Mundy, G. K. Shenoy, Eds. (Elsevier, Amsterdam, 1979) pp. 131-136.
3. C. Berthier, W. Gorecki, M. Minier, *Solid State Ionics* **11**, 91 (1983).
4. M. Minier, C. Berthier, W. Gorecki, *J. Physique* **45**, 739 (1984).
5. M. A. Ratner, A. Nitzan, *Faraday Discuss. Chem. Soc.* **88**, 19 (1989).
6. A. Nitzan, M. A. Ratner, *J. Phys. Chem.* **98**, 1765 (1994).
7. Z. Gadjourova, D. M. Marero, K. H. Andersen, Y. G. Andreev, P. G. Bruce, *Chem. Mater.* **13**, 1282 (2001).
8. J. R. MacCallum, C. A. Vincent, Eds., *Polymer Electrolyte Reviews* (Elsevier Applied Science, New York, 1987) vol. 1.
9. J. R. MacCallum, C. A. Vincent, Eds., *Polymer Electrolyte Reviews* (Elsevier Applied Science, New York, 1989) vol. 2.
10. F. M. Gray, *Solid Polymer Electrolytes: Fundamentals and Technological Applications* (VCH Publishers, Inc., New York, 1991).
11. P. G. Bruce, C. A. Vincent, *J. Chem. Soc. Faraday Trans.* **89**, 3187 (1993).
12. P. G. Bruce, Ed., *Solid State Electrochemistry* (University Press, Cambridge, 1995).
13. D. Baril, C. Minchot, M. Armand, *Solid State Ionics* **94**, 35 (1997).
14. W. H. Meyer, *Adv. Mater.* **10**, 439 (1998).
15. F. B. Dias, L. Plomb, J. B. J. Veldhuis, *J. Power Sources* **88**, 169 (2000).
16. J. R. Stevens, S. Schantz, *Polym. Commun.* **29**, 330 (1988).
17. G. G. Cameron, M. D. Ingram, in *Polymer Electrolyte Reviews*. J. R. MacCallum, C. A. Vincent, Eds. (Elsevier Applied Science, New York, 1989) vol. 2, chap. 5.
18. P. G. Bruce, F. M. Gray, in *Solid State Electrochemistry*. P. G. Bruce, Ed. (Cambridge University Press, Cambridge, 1995) pp. 119-162.
19. K. M. Abraham, *Solid State Ionics* **7**, 199 (1982).
20. J. Y. Cherng, M. Z. A. Munshi, B. B. Owens, W. H. Smyrl, *Solid State Ionics* **28-30**, 857 (1988).
21. M. Z. A. Munshi, A. Gilmour, W. H. Smyrl, B. B. Owens, *J. Electrochem. Soc.* **136**, 1847 (1989).
22. M. Z. A. Munshi, W. H. Smyrl, *Solid State Ionics* **45**, 183 (1991).
23. M. Z. A. Munshi, W. H. Smyrl, C. Schmidtke, *Chem. Mater.* **2**, 530 (1990).
24. M. M. Doeff, M. Y. Peng, Y. Ma, L. C. De Jonghe, *J. Electrochem. Soc.* **141**, L145 (1994).
25. M. M. Doeff, et al., *Electrochimica Acta* **40**, 2205 (1995).
26. M. Morita, N. Yoshimoto, S. Yakushiji, M. Ishikawa, *Electrochem. Solid State Lett.* **4**, A177 (2001).
27. J. R. Owen, in *Electrochemical Science and Technology of Polymers*. R. G. Linford, Ed. (Elsevier Applied Science, New York, 1987) vol. 1, chap. 3.
28. P. V. Wright, in *Polymer Electrolyte Reviews*. J. R. MacCallum, C. A. Vincent, Eds. (Elsevier Apllied Science, New York, 1989), vol. 2, chap. 3..
29. V. Gutmann, *Coordination Chemistry in Nonaqueous Solvents* (Springer-Verlag, Vienna, 1968).
30. H. Honda, K. Ono, K. Murakami, *Macromolecules* **23**, 515 (1990).

31. R. G. Pearson, *J. Am. Chem. Soc.* **85**, 3533 (1963).
32. P. G. Bruce, F. Krok, C. A. Vincent, *Solid State Ionics* **27**, 81 (1988).
33. J. M. G. Cowie, S. H. Cree, in *Annu. Rev. Phys. Chem.*, H. L. Strass, G. T. Babcock, C. B. Moore, Eds. (Annual Reviews Inc., Palo Alto, 1989) vol. 40, pp. 85-113.
34. A. Nishimoto, M. Watanabe, Y. Ikeda, S. Kohjiya, *Electrochim. Acta* **43**, 1177 (1998).
35. J. Qiao, Y. Chen, G. L. Baker, *Chem. Mater.* **11**, 2542 (1999).
36. M. Kono, E. Hayashi, M. Wantanabe, *J. Electrochem. Soc.* **145**, 1521 (1998).
37. H. R. Allcock, et al., *Electrochim. Acta* **43**, 1145 (1998).
38. M. Stainer, L. C. Hardy, D. H. Whitmore, D. F. Shriver, *J. Electrochem. Soc.* **131**, 784 (1984).
39. C. D. Robitaille, D. Fauteux, *J. Electrochem. Soc.* **133**, 315 (1986).
40. A. Vallée, S. Besner, J. Prud'homme, *Electrochim. Acta* **37**, 1579 (1992).
41. S. Besner, A. Vallée, G. Bouchard, J. Prud'homme, *Macromolecules* **25**, 6480 (1992).
42. S. Lascaud, M. Perrier, A. Vallée, S. Besner, J. Prud'homme, *Macromolecules* **27**, 7469 (1994).
43. A. Brodin, B. Mattsson, K. Nilsson, L. M. Torell, J. Hamara, *Solid State Ionics* **85**, 111 (1996).
44. L. Yang, A. Zhang, B. Qiu, J. Yin, Q. Liu, *Solid State Ionics* **28-30**, 1029 (1988).
45. S. Chintapalli, R. Frech, *Electrochimica Acta* **43**, 1395 (1998).
46. J. E. Weston, B. C. H. Steele, *Solid State Ionics* **7**, 81 (1982).
47. W. J. Barnes, F. P. Price, *Polymer* **5**, 283 (1964).
48. K. Song, S. Krimm, *Macromolecules* **23**, 1946 (1990).
49. Y. K. Godovsky, G. L. Slonimsky, N. M. Garbar, *J. Polymer Sci. C* **38**, 1 (1972).
50. J. Q. G. Maclaine, C. Booth, *Polymer* **16**, 680 (1975).
51. M. Armand, M. Gauthier, in *High Conductivity Solid Ionic Conductors*, T. Takahashi, Ed. (World Scientific Press, New Jersey, 1989) pp. 114-145.
52. B. L. Papke, M. A. Ratner, D. F. Shriver, *J. Phys. Chem. Solids* **42**, 493 (1981).
53. D. Martin-Vosshage, B. V. R. Chowdari, *J. Electrochem. Soc.* **140**, 3531 (1993).
54. H. M. N. Bandara, W. S. Schlindwein, R. J. Latham, R. G. Linford, *J. Chem. Soc. Faraday Trans.* **90**, 3549 (1994).
55. R. G. Linford, *Chem. Soc. Rev.* **24**, 267 (1995).
56. M. E. Ries, M. G. Brereton, J. M. Cruickshank, P. G. Klein, I. W. Ward, *Macromolecules* **28**, 3282 (1995).
57. J. McBreen, *Electrochem. Soc. Proc.* **96**, 162 (1996).
58. S. Wong, D. B. Zax, *Electrochim. Acta* **42**, 3513 (1997).
59. J. Spevacek, J. Dybal, *Macromol. Rapid Commun.* **20**, 435 (1999).
60. S. Schantz, J. Sandahl, L. Borjesson, L. M. Torell, J. R. Stevens, *Solid State Ionics* **28-30**, 1047 (1988).
61. W. Huang, R. Frech, R. A. Wheeler, *J. Phys. Chem.* **98**, 100 (1994).
62. L. Xie, G. C. Farrington, *Solid State Ionics* **53-56**, 1054 (1992).
63. V. A. Payne, et al., *Electrochim. Acta* **40**, 2087 (1995).
64. J. A. Payne, et al., *J. Chem. Phys.* **103**, 8746 (1995).
65. J. Hyun, H. Dong, C. P. Rhodes, R. Frech, R. A. Wheeler, *J. Phys. Chem. B* **105**, 3329 (2001).
66. M. Forsyth, V. A. Payne, M. A. Ratner, S. W. de Leeuw, D. F. Shriver, *Solid State Ionics* **53-56**, 1011 (1992).
67. O. Borodin, G. D. Smith, *Macromolecules* **31**, 8396 (1998).
68. Y. Ma, et al., *J. Electrochem. Soc.* **142**, 1859 (1995).

69. M. M. Doeff, P. Georen, J. Qiao, J. Kerr, L. C. De Jonghe, *J. Electrochem. Soc.* **146**, 2024 (1999).
70. A. Ferry, M. M. Doeff, L. C. DeJonghe, *Electrochim. Acta* **43**, 1387 (1998).
71. M. Kakihana, S. Shantz, L. M. Torell, *J. Chem. Phys.* **94**, 6271 (1990).
72. B. L. Papke, M. A. Ratner, D. F. Shriver, *J. Electrochem. Soc.* **129**, 1434 (1982).
73. M. Kakihana, S. Schantz, L. M. Torell, *Solid State Ionics* **40/41**, 641 (1990).
74. D. Battisti, G. A. Nazri, B. Klassen, R. Aroca, *J. Phys. Chem.* **97**, 5826 (1993).
75. B. Klassen, R. Aroca, M. Nazri, G. A. Nazri, *J. Phys. Chem. B* **102**, 4795 (1998).
76. B. Klassen, R. Aroca, G. A. Nazri, *J, Phys. Chem.* **100**, 9334 (1996).
77. R. Frech, W. Huang, M. A. K. L. Dissanayake, *Mat. Res. Soc. Symp. Proc.* **369**, 523 (1995).
78. R. Frech, W. Huang, *J. Solution Chem.* **23**, 469 (1994).
79. A. Bernson, J. Lindgen, W. Huang, R. Frech, *Polymer* **36**, 4471 (1995).
80. A. Lauenstein, J. Tegenfeldt, *J. Phys. Chem.* **101**, 3311 (1997).
81. U. Olsher, R. M. Izatt, J. S. Bradshaw, N. K. Dalley, *Chem. Rev.* **91**, 137 (1991).
82. M. A. Ratner, D. F. Shriver, *Chem. Rev.* **88**, 109 (1988).
83. T. Yoshihara, H. Tadokoro, S. Murahashi, *J. Chem. Phys.* **41**, 2902 (1964).
84. K. Machida, T. Miyazawa, *Spectrochim. Acta* **20**, 1865 (1964).
85. H. Matsuura, T. Miyazawa, *Spectrochim. Acta* **23A**, 2433 (1967).
86. H. Matsuura, T. Miyazawa, *Bull. Chem. Soc. Japan* **41**, 1798 (1968).
87. H. Matsuura, T. Miyazawa, *J. Polym. Sci., Pt. A-2* **7**, 1735 (1969).
88. K. Liu, J. L. Parsons, *Macromolecules* **2**, 529 (1969).
89. H. Matsuura, T. Miyazawa, K. Machida, *Spectrochim. Acta* **29A**, 771 (1973).
90. J. Maxfield, I. W. Shepherd, *Polymer* **16**, 505 (1975).
91. H. Matsuura, K. Fukuhara, H. Tamaoki, *J. Sci. Hiroshima Univ., Ser. A* **49**, 89 (1985).
92. H. Matsuura, K. Fukuhara, *J. Polym. Sci. B* **24**, 1383 (1986).
93. X. Yang, Z. Su, D. Wu, S. Hsu, H. Stidham, *Macromolecules* **30**, 3796 (1997).
94. R. Frech, W. Huang, *Macromolecules* **28**, 1246 (1995).
95. S. Yoon, K. Ichikawa, W. J. MacKnight, S. L. Hsu, *Macromolecules* **28**, 4278 (1995).
96. M. A. K. L. Dissanayake, R. Frech, *Macromolecules* **28**, 5312 (1995).
97. A. Johansson, A. Wendsjo, J. Tegenfeldt, *Electrochim. Acta* **37**, 1487 (1992).
98. I. M. Ward, N. Boden, J. Cruickshank, S. A. Leng, *Electrochim. Acta* **40**, 2071 (1995).
99. M. M. Doeff, L. Edman, S. E. Sloop, J. Kerr, L. C. De Jonghe, *J. Power Sources* **89**, 227 (2000).
100. P. G. Bruce, in *Polymer Electrolyte Reviews*, J. R. MacCallum, C. A. Vincent, Eds. (Elsevier Applied Science, New York, 1987) vol. 1, chap. 8.
101. D. W. Dees, et al., *J. Power Sources* **89**, 249 (2000).
102. M. Z. A. Munshi, B. B. Owens, *Polymer J.* **20**, 577 (1988).
103. P. E. Rouse, *J. Chem. Phys.* **21**, 1272 (1953).
104. B. H. Zimm, *J. Chem. Phys.* **24**, 269 (1956).
105. P. G. De Gennes, *Scaling Concepts in Polymer Physics* (Cornell Univ. Press, Ithaca, 1979).
106. M. A. Ratner, P. Johansson, D. F. Shriver, *MRS Bulletin* **25**, 31 (2000).
107. S. E. Lindsey, D. H. Whitmore, W. P. Halperin, *Polym. Prepr. (Am. Chem. Soc., Div. Polym. Chem.)* **30**, 442 (1989).
108. S. Arumugam, J. Shi, D. P. Tunstall, C. A. Vincent, *J. Phys.: Condens. Matter* **5**, 153 (1993).
109. A. Ferry, G. Orädd, P. Jacobson, *J. Chem. Phys.* **108**, 7426 (1998).
110. M. G. McLin, C. A. Angell, *J. Phys. Chem. B* **100**, 1181 (1996).

111. M. Doyle, J. Newman, *J. Electrochem. Soc.* **142** (1995).
112. M. A. Ratner, in *Polymer Electrolyte Reviews,* J. R. MacCallum, C. A. Vincent, Eds. (Elsevier Applied Science, New York, 1987), vol. 1, chap. 7.
113. N. Balabai, D. H. Waldeck, *J. Phys. Chem. B* **101**, 2339 (1997).
114. P. G. Bruce, *Faraday Discuss. Chem. Soc.* **88**, 43 (1989).
115. P. G. Bruce, C. A. Vincent, *Solid State Ionics* **40-41**, 607 (1990).
116. P. G. Bruce, M. T. Hardgrave, C. A. Vincent, *Electrochim. Acta* **37**, 1517 (1992).
117. A. Bouridah, F. Dalard, D. Deroo, M. B. Armand, *J. Applied Electrochem.* **17**, 625 (1987).
118. M. Z. A. Munshi, B. B. Owens, S. Nguyen, *Polymer J.* **20**, 597 (1988).
119. H. P. Fritz, A. Kuhn, *J. Power Sources* **41**, 253 (1993).
120. H. J. Walls, T. A. J. Zawodzinski, *Electrochem. Solid-State Lett.* **3**, 321 (2000).
121. L. Edman, M. M. Doeff, A. Ferry, J. Kerr, L. C. D. Jonghe, *J. Phys. Chem. B* **104**, 3476 (2000).
122. K. E. Thomas, S. E. Sloop, J. B. Kerr, J. Newman, *J. Power Sources* **89**, 132 (2000).
123. M. J. Williamson, J. P. Southall, H. V. S. A. Hubbard, G. R. Davies, I. M. Ward, *Polymer* **40**, 3945 (1999).
124. W. Gorecki, M. Jeannin, E. Belorizky, C. Roux, M. Armand, *J. Phys.: Condens. Matter* **7**, 6823 (1995).
125. S. Bhattacharja, S. W. Smoot, D. H. Whitmore, *Solid State Ionics* **18&19**, 306 (1986).
126. H. Vogel, *Phys. Z.* **22**, 645 (1921).
127. G. Tammann, W. Hesse, *Z. Anorg. Allg. Chem.* **156**, 245 (1926).
128. G. S. Fulcher, *J. Am. Chem. Soc.* **8**, 339 (1925).
129. B. L. Papke, M. A. Ratner, D. F. Shriver, *J. Electrochem. Soc.* **129**, 1694 (1982).
130. M. L. Williams, R. F. Landel, J. D. Ferry, *J. Am. Chem. Soc.* **77**, 3701 (1955).
131. M. H. Cohen, D. Turnball, *J. Chem. Phys.* **31**, 1164 (1959).
132. A. O. Porto, G. G. Silva, W. F. Magalhaes, *J. Poly. Sci. B* **37**, 219 (1999).
133. E. A. DiMarzio, J. H. Gibbs, *J. Chem. Phys.* **28**, 807 (1958).
134. G. Adams, J. H. Gibbs, *J. Chem. Phys.* **43**, 139 (1965).
135. D. F. Shriver, R. Dupon, M. Stainer, *J. Power Sources* **9**, 383 (1983).
136. S. D. Druger, M. A. Ratner, A. Nitzan, *Solid State Ionics* **9 & 10**, 1115 (1983).
137. R. Dupon, B. L. Papke, M. A. Ratner, D. H. Whitmore, D. F. Shriver, *J. Am. Chem. Soc.* **104**, 6247 (1982).
138. N. Boden, S. A. Leng, I. M. Ward, *Solid State Ionics* **45**, 261 (1991).
139. K. Y. Cho, K. Lee, J. Park, *Polymer J.* **32**, 537 (2000).
140. X. Wei, D. F. Shriver, *Chem. Mater.* **10**, 2307 (1998).
141. D. R. MacFarlane, J. Huang, M. Forsyth, *Nature* **402**, 792 (1999).
142. C. T. Imrie, M. D. Ingram, G. S. McHattie, *Adv. Mater.* **11**, 832 (1999).
143. J. M. G. Cowie, G. H. Spence, *Solid State Ionics* **123**, 233 (1999).
144. K. Onishi, M. Matsumoto, K. Shigehara, *J. Power Sources* **92**, 120 (2001).
145. L. C. Reibel, B. Azimipour, N. Parizel, *Polymeric Materials: Science and Engineering* **84**, 1043 (2001).
146. J. F. Snyder, M. A. Ratner, D. F. Shiver, *J. Electrochem. Soc.* **148**, A858 (2001).
147. J. McBreen, H. S. Lee, X. Q. Yang, X. Sun, *J. Power Sources* **89**, 163 (2000).
148. S. H. Chung, Y. Wang, S. G. Greenbaum, D. Golodnitsky, E. Peled, *Electrochem. Solid State Lett.* **2**, 553 (1999).
149. D. Golodnitsky, et al., *J. Electroanal. Chem.* **491**, 203 (2000).
150. O. Dag, A. Verma, G. A. Ozin, C. T. Kresge, *J. Mater. Chem.* **9**, 1475 (1999).

151. V. D. Noto, D. Barreca, C. Furlan, L. Armelao, *Polym. Adv. Technol.* **11**, 108 (2000).
152. G. J. d. A. A. Soler-Illia, C. Sanchez, *New J. Chem.* **24**, 493 (2000).
153. F. Capuano, F. Croce, B. Scrosati, *J. Electrochem. Soc.* **138**, 1918 (1991).
154. F. Croce, B. Scrosati, G. Mariotto, *Chem. Mater.* **4**, 1134 (1992).
155. F. Croce, G. B. Appetecchi, L. Persi, B. Scrosati, *Nature* **394**, 456 (1998).
156. E. Morales, J. L. Acosta, *Solid State Ionics* **111**, 109 (1998).
157. W. Wieczorek, A. Zalewska, D. Raducha, Z. Florjanczyk, J. R. Stephens, *J. Phys. Chem. B* **102**, 352 (1998).
158. W. Wieczorek, P. Lipka, G. Zukowska, H. Wycislik, *J. Phys. Chem. B* **102**, 6968 (1998).
159. B. Kumar, L. G. Scanlon, *Solid State Ionics* **124**, 239 (1999).
160. C. Capiglia, P. Mustarelli, E. Quartarone, C. Tomasi, A. Magistris, *Solid State Ionics* **118**, 73 (1999).
161. H. Y. Sun, H.-J. Sohn, O. Yamamoto, Y. Takeda, N. Imanishi, *J. Electrochem. Soc.* **146**, 1672 (1999).
162. B. Kumar, L. G. Scanlon, R. J. Spry, *J. Power Sources* **96**, 337 (2001).
163. F. Croce, et al., *Electrochim. Acta* **46**, 2457 (2001).
164. K. Nagaoka, H. Naruse, I. Shinohara, *J. Polym. Sci., Polym. Lett.* **22**, 659 (1984).
165. H. R. Allcock, M. E. Napierala, D. L. Olmeijer, S. A. Best, K. M. Merz, Jr., *Macromolecules* **32**, 732 (1999).
166. S. Chintapalli, R. Frech, *Macromolecules* **29**, 3499 (1996).
167. A. G. Bishop, D. R. MacFarlane, D. McNaughton, M. Forsyth, *J. Phys. Chem.* **100**, 2237 (1996).
168. D. Golodnitsky, G. Ardel, E. Peled, *Solid State Ionics* **85**, 231 (1996).
169. S. F. Johnston, I. M. Ward, J. Cruickshank, G. R. Davies, *Solid State Ionics* **90**, 39 (1996).
170. Y. Saito, H. Yamamoto, H. Kageyama, O. Nakamura, *J. Mater. Sci.* **35**, 809 (2000).
171. I. Geoffroy, P. Willmann, K. Mesfar, B. Carré, D. Lemordant, *Electrochim. Acta* **45**, 2019 (2000).
172. H. R. Allcock, S. J. M. O'Connor, D. L. Olmeijer, M. E. Napierala, C. G. Cameron, *Macromolecules* **29**, 7544 (1996).
173. S. York, E. C. Kellam, H. R. Allcock, R. Frech, *Electrochim. Acta* **46**, 1553 (2001).
174. Y. Ogawa, et al., *Bull. Chem. Soc. Japan* **50**, 650 (1977).
175. E. E. Astrup, *Acta. Chem. Scand. , Ser. A* **33**, 655 (1979).
176. M. A. Murcko, R. A. DiPaola, *J. Am. Chem. Soc.* **114**, 10010 (1992).
177. R. L. Jaffe, G. D. Smith, D. Y. Yoon, *J. Phys. Chem.* **97**, 12745 (1993).
178. F. Muller-Plathe, W. v. Gunsteren, *Macromolecules* **27**, 6040 (1994).
179. S. P. Gejji, J. Tegenfeldt, J. Lindgren, *Chem. Phys. Lett.* **226**, 427 (1994).
180. Y. Yokoyama, H. Uekusa, Y. Ohashi, *Chem. Lett.* **6**, 443 (1996).
181. H. Yoshida, T. Tanaka, H. Matsuura, *Chem. Lett.* , 637 (1996).
182. A. Sutjianto, L. A. Curtis, *Chem. Phys. Lett.* **264**, 127 (1997).
183. H. Yoshida, H. Matsuura, *J. Phys. Chem. A* **102**, 2691 (1998).
184. N. Goutev, K. Ohno, H. Matsuura, *J. Phys. Chem. A* **104**, 9226 (2000).
185. G. D. Smith, R. L. Jaffe, D. Y. Yoon, *J. Phys. Chem.* **97**, 12752 (1993).
186. S. P. Gejji, P. Johansson, J. Tegenfeldt, J. Lindgren, *Comput. Polym. Sci.* **5**, 99 (1995).
187. P. Johansson, S. P. Gejji, J. Tegenfeldt, J. Lindgren, *Solid State Ionics* **86-88**, 297 (1996).
188. D. J. Williams, K. B. Hall, *J. Phys. Chem.* **100**, 8224 (1996).

189. D. Ray, D. Feller, M. B. More, E. D. Glendening, P. B. Armentrout, *J. Phys. Chem.* **100**, 16116 (1996).
190. P. T. Boinske, L. Curtiss, J. W. Halley, B. Lin, A. Sutjianto, *J. Comput.-Aided Mater. Des.* **3**, 385 (1996).
191. T.-S. Yeh, T.-M. Su, *J. Phys. Chem. A* **101**, 1672 (1997).
192. G. D. Smith, R. L. Jaffe, H. Partridge, *J. Phys. Chem. A* **101**, 1705 (1997).
193. S. E. Hill, D. Feller, E. D. Glendening, *J. Phys. Chem. A* **102**, 3813 (1998).
194. P. Johansson, J. Tegenfedlt, J. Lindgren, *J. Phys. Chem. A* **102**, 4660 (1998).
195. A. Sutjianto, L. A. Curtiss, *J. Phys. Chem. A* **102**, 968 (1998).
196. V. Mujica, M. Malaver, F. Ruette, *J. Phys. Chem. A* **103**, 89 (1999).
197. A. G. Baboul, P. C. Redfern, A. Sutjianto, L. A. Curtiss, *J. Am. Chem. Soc.* **121**, 7220 (1999).
198. P. Johansson, J. Tegenfeldt, J. Lindgren, *Polymer* **40**, 4399 (1999).
199. P. Johansson, *Polymer* **42**, 4367 (2001).
200. R. Frech, W. Huang, *Solid State Ionics* **72**, 103 (1994).
201. W. Huang, R. Frech, P. Johansson, J. Lindgren, *Electrochim. Acta* **40**, 2147 (1995).
202. S. Neyertz, D. Brown, J. O. Thomas, *J. Chem. Phys.* **101**, 10064 (1994).
203. H. Liu, F. Muller-Plathe, W. F. van Gunsteren, *J. Chem. Phys.* **102**, 1722 (1995).
204. G. D. Smith, et al., *J. Chem. Phys.* **106**, 3798 (1997).
205. M. M. Fuson, K. H. Hanser, M. D. Ediger, *Macromolecules* **30**, 5714 (1997).
206. M. M. Fuson, M. D. Ediger, *Macromolecules* **30**, 5704 (1997).
207. D. Bedrov, G. D. Smith, *J. Chem. Phys.* **109**, 8118 (1998).
208. C. R. A. Catlow, G. E. Mills, *Electrochim. Acta* **40**, 2057 (1995).
209. S. Neyertz, D. Brown, J. O. Thomas, *Electrochim. Acta* **40**, 2063 (1995).
210. K. Laasonen, M. L. Klein, *J. Chem. Soc., Faraday Trans.* **91**, 2633 (1995).
211. S. Neyertz, D. Brown, *J. Chem. Phys.* **104**, 3797 (1996).
212. B. K. Annis, M. Kim, G. D. Wignall, O. Borodin, G. D. Smith, *Macromolecules* **33**, 7544 (2000).
213. O. Borodin, G. D. Smith, *J. Phys. Chem. B* **104**, 8017 (2000).
214. V. N. Plakhotnik, Y. V. Kovtun, V. B. Tul'chinskii, *Vopr. Khim. Khim. Tekhnol.* **81**, 29 (1986).
215. R. Iwamoto, H. Wakano, *J. Am. Chem. Soc.* **98**, 3764 (1976).
216. R. Iwamoto, *Bull. Chem. Soc. Japan* **46**, 1114 (1973).
217. R. Frech, C. P. Rhodes, *Polymer Preprints* (submitted).
218. H. Yoshida, I. Kaneko, H. Matsuura, Y. Ogawa, M. Tasumi, *Chem. Phys. Lett.* **196**, 601 (1992).
219. Z. Gadjourova, Y. G. Andreev, D. P. Tunstall, P. G. Bruce, *Nature* **412**, 520 (2001).
220. H. Dong, J. Hyun, C. P. Rhodes, R. Frech, R. A. Wheeler, submitted to *J. Phys. Chem.*
221. S. E. Boesch, C. P. Rhodes, R. Frech, R. A. Wheeler, (in progress).
222. D. H. Johnston, D. F. Shriver, *Inorg. Chem.* **32**, 1045 (1993).
223. M. Petrowsky, C. P. Rhodes, R. Frech, *J. Soln. Chem.* **30**, 171 (2001).
224. Y. Takahashi, H. Tadokoro, *Macromolecules* **6**, 672 (1973).
225. Y. Takahashi, I. Sumita, H. Tadokoro, *J. Polym. Sci.* **11** (1973).
226. H. Tadokoro, Y. Chatani, T. Yoshihara, S. Tahara, S. Murahashi, *Makromol. Chem.* **73**, 109 (1964).
227. P. G. Bruce, *Electrochim. Acta* **40**, 2077 (1995).
228. R. J. Latham, R. G. Linford, *Solid State Ionics* **85**, 193 (1996).
229. Y. G. Andreev, P. G. Bruce, *Electrochim. Acta* **45**, 1417 (2000).

230. R. Frech, S. Chintapalli, P. G. Bruce, C. A. Vincent, *Chem. Commun.* 157 (1997).
231. R. Frech, S. Chintapalli, P. G. Bruce, C. A. Vincent, *Macromolecules* **32**, 808 (1999).
232. Y. Chatani, S. Okamura, *Polymer* **28**, 1815 (1987).
233. Y. Chatani, Y. Fujii, T. Takayanagi, A. Honma, *Polymer* **31**, 2238 (1990).
234. P. Lightfoot, M. A. Mehta, P. G. Bruce, *Science* **262**, 883 (1993).
235. Y. G. Andreev, P. Lightfoot, P. G. Bruce, *Chem. Comm.* , 2169 (1996).
236. Y. G. Andreev, G. S. MacGlashan, P. G. Bruce, *Phys. Rev. B* **55**, 12011 (1997).
237. G. S. MacGlashan, Y. G. Andreev, P. G. Bruce, *Nature* **398**, 792 (1999).
238. R. Frech, C. P. Rhodes, S. S. York, *Mat. Res. Soc. Symp. Proc.* **548**, 335 (1999).
239. W. G. Fateley, F. R. Dollish, N. T. McDevitt, F. F. Bentley, *Infrared and Raman Selection Rules for Molecular and Lattice Vibrations: The Correlation Method* (John Wiley & Sons, Inc., New York, 1972).
240. R. Frech, *Macromolecules* **33**, 9432 (2000).
241. S. P. Gejji, K. Hermansson, J. Lindgren, *J. Phys. Chem.* **97**, 3712 (1993).
242. S. P. Gejji, K. Hermansson, J. Tegenfeldt, J. Lindgren, *J. Phys. Chem.* **97**, 11402 (1993).
243. W. Huang, R. A. Wheeler, R. Frech, *Spectrochimica Acta* **50A**, 985 (1994).
244. S. Schantz, L. M. Torell, J. R. Stevens, *J. Chem. Phys.* **94**, 6862 (1991).
245. S. Chintapalli, C. Quinton, R. Frech, C. A. Vincent, *Macromolecules* **30**, 7472 (1997).
246. H. Menge, T. Steurich, *Electrochim. Acta* **39**, 1971 (1994).
247. M. Mortimer, E. A. Moore, M. A. K. Williams, *J. Chem. Soc. Faraday Trans.* **91**, 2871 (1995).
248. M. Bégin, C. Vachon, C. Labrèche, B. Goulet, J. Prud'homme, *Macromolecules* **31**, 96 (1998).

# I

ELSEVIER

Reproduced with permission from *Solid State Ionics* 121, 91-99 (1999)

SOLID STATE IONICS

# Cation–anion and cation–polymer interactions in $(PEO)_nNaCF_3SO_3$ ($n = 1$–$80$)

Christopher P. Rhodes, Roger Frech*

*Department of Chemistry and Biochemistry, University of Oklahoma, Norman, OK 73019-0370, USA*

Received 18 November 1997; accepted 4 December 1998

**Abstract**

Cation–anion interactions and cation–polymer interactions in the system $(PEO)_nNaCF_3SO_3$ ($1 \leq n \leq 80$) have been studied using Raman and FTIR spectroscopy. In the dilute salt region ($80 \geq n \geq 50$) there are predominately 'free' ions and ion pairs present. However at increasing salt concentration, two aggregate species are observed. The symmetric $SO_3$ stretching mode of one of the aggregate species appears at a frequency which is lower than that of the 'free' triflate anion ($CF_3SO_3^-$), in contrast to behavior seen in the PEO–lithium triflate system. The cation–polymer interactions in high molecular weight PEO–sodium triflate do not appear to involve a local distortion of the –O–C–C–O– torsional angle, consistent with the crystal structure reported for the compound $(PEO)NaCF_3SO_3$. However such a distortion does appear to be present in the diglyme–sodium triflate system at salt concentrations $n \leq 20$. 

*Keywords:* Polymer electrolyte; Poly(ethylene oxide); Sodium triflate; Ionic association; Raman spectroscopy

## 1. Introduction

Although most of the interest in polymer electrolytes has focused on lithium ion-conducting systems, their sodium ion-conducting analogs have also been the subject of much attention. Polyethers containing dissolved sodium trifluoromethanesulfonate (triflate), $NaCF_3SO_3$, or sodium perchlorate, $NaClO_4$, have proven to be particularly fruitful systems for vibrational spectroscopic studies of ionic association, since the frequencies of several intramolecular modes of these anions are sensitive to cation–anion interactions. A recent study of the polyethylene oxide–sodium triflate system suggests that aggregate species may be involved in charge transfer [1]. Therefore the nature and concentration of the various ionic species is important to understand the overall mechanism of conductivity. The recent elucidation of the crystal structure of a polyethylene oxide–sodium triflate compound with a 1:1 stoichiometry [2], here abbreviated as (PEO)NaTf, provides useful guidance in examining ionic association in the $(PEO)_nNaTf$ system. One of the earliest studies of cation–anion interactions in a polyether containing dissolved sodium triflate was a study of sodium triflate in 4000 molecular weight poly(propylene glycol) reported by Schantz et al. [3]. The authors interpreted the three spectral features seen in the $SO_3$ symmetric stretching region as due to dissociated or 'free' ions, ion pairing, and multiple

*Corresponding author.

0167-2738/99/$ – see front matter 
PII: S0167-2738(98)00534-7

ion aggregates. They further noted a shift to a more highly associated ionic species with increasing salt concentration. In a later work, Schantz et al. studied the temperature dependence of ionic association in the same system [4]. Two previous vibrational studies of the $PEO_nNaTf$ system using low molecular weight PEO were conducted. Concentration-dependent and temperature-dependent Raman spectra were reported by Kakihana et al. using PEO of molecular weight 400 [5], and Brodin et al. using PEO of molecular weight 400 and 1000 [6].

A number of other techniques have been used to characterize the $(PEO)_nNaTf$ system. Vosshage et al. reported work using X-ray photoelectron spectroscopy, differential scanning calorimetry (DSC), thermogravimetric analysis, and X-ray diffraction [7]. Conductivity studies are reported by three groups [1,8–10]. $^{23}Na$ NMR measurements have also been conducted [10]. The goal of this paper is to examine the cation–anion interactions and cation–polymer interactions using vibrational spectroscopy in $(PEO)_nNaTf$ and $(diglyme)_nNaTf$ over a wide range of PEO/oligomer–salt concentrations, described in this paper by the ether oxygen:metal cation ratio O:M.

## 2. Experimental

### 2.1. Sample preparation

Poly(ethylene oxide) (PEO) with an average molecular weight of $4 \times 10^6$ was obtained from Aldrich and was dried in a vacuum oven at ~50°C for 24 h. Sodium trifluoromethane sulfonate (NaTf) was obtained from two sources, Aldrich and Fluka, and was dried under vacuum at ~100°C for 24 h. 2-Methoxyethyl ether (diglyme) was obtained from Aldrich and was used without further purification. Acetonitrile (<0.3% $H_2O$) from EM Science was kept dry with molecular sieves. All reagents were stored in an argon glovebox.

Stoichiometric amounts of PEO and NaTf were dissolved in acetonitrile and stirred overnight, then cast onto Teflon sheets and left standing at least 8 h to evaporate the solvent. Films were then placed in a vacuum oven and heated at ~50°C for ~12 h. Diglyme complexes were prepared by dissolving appropriate amounts of NaTf directly in diglyme and stirred overnight. All preparation, casting and evaporation of $(PEO)_nNaTf$ films and preparation of diglyme solutions were performed in an argon glovebox.

Raman spectra were recorded on an I.S.A. Jobin-Yvon T64000 spectrometer in the triple subtractive mode with a scan time of 16 s and 10 accumulations. Data were recorded using a backscattering geometry with the laser focused through the 80× objective lens of an Olympus microscope. The 514.5 nm line of an argon ion laser operating at 300 mW power was used for excitation. Due to the possibility of thermal excitation of the sample from the Raman laser focused through the microscope, no direct comparison of Raman and IR band intensities was attempted.

Infrared spectra were recorded with a Bruker IFS66V FT-IR spectrometer over a range of 4000 $cm^{-1}$ to 400 $cm^{-1}$ at a resolution of 1 $cm^{-1}$. For the PEO–NaTf complexes, IR spectra of the free-standing films were taken in an evacuated sample chamber. IR spectra of diglyme–NaTf complexes were recorded using NaCl windows and a dry air-purged sample chamber. All Raman and IR spectra were recorded at ambient room temperature.

In comparing spectra of PEO–NaTf films taken of different samples at the same nominal concentration, some differences in relative intensities of triflate bands were observed for the 50:1 to 20:1 concentration range. This may be due to slow crystallization kinetics present in this concentration range.

All spectra were taken of thin films or liquid complexes except for the 1:1 PEO–NaTf Raman spectrum presented in Fig. 1. This compound was a solid that precipitated out of solution before casting and was subsequently filtered and heated under vacuum. DSC data of this compound was collected with a Mettler DSC 820 calorimeter over a range of −100°C to 350°C. Analysis revealed the presence of an endotherm at ~320°C which was attributed to the presence of crystalline (PEO)NaTf which has a reported melting point of 330°C [2].

Curve fitting analysis was accomplished using a commercial program (Grams 386, Galactic Indus-

tries). Spectra were curve-fit to a straight base line and one Gaussian–Lorentzian product function for each band using a non-linear least squares method.

## 3. Results and discussion

### 3.1. Raman and IR spectra of the $\nu_s(SO_3)$ region of PEO–$NaCF_3SO_3$

The concentration-dependent Raman spectra in the $\nu_s(SO_3)$ region are presented in Fig. 1. The Raman spectrum of pure PEO exhibits bands at 1073 $cm^{-1}$ and 1062 $cm^{-1}$ and very weak features near 1040 $cm^{-1}$ which are subsequently observed as weak shoulders on the triflate bands. The feature at 1060 $cm^{-1}$ at the 40:1 composition is attributed to the combination of the PEO band and a band from a triflate aggregate species whose band intensity increases with increasing salt concentration. The broad band centered at 1034 $cm^{-1}$ is shown by curve fitting (Fig. 3) to consist of two component bands, one at ~1032 $cm^{-1}$ which is assigned to 'free' triflate ions and the other at ~1037 $cm^{-1}$ to contact ion pairs. These data and corresponding assignments are in agreement with observations by Kakihana et al. in a study of poly(propylene oxide)–NaTf [11] and in studies of low $M_w$ PEO–NaTf by Kakihana et al. and Brodin et al. [5,6]. In the concentration range from pure PEO to 50:1, the presence of mostly 'free' ions and ion-pairs is observed. At the 40:1 composition there is a very weak band at 1050 $cm^{-1}$ and a band centered at 1058 $cm^{-1}$ which are attributed to ionic species designated as aggregate I and aggregate II, respectively. The 1058 $cm^{-1}$ band is also reported by Kakihana et al. and Brodin et al. [5,6]. From the 20:1 system to the 1:1 system, the relative intensity of aggregate II increases strongly, the intensity of aggregate I increases slightly, and the intensities of 'free' ions and ion pairs decrease. Aggregate II is clearly the dominant species at high salt concentration.

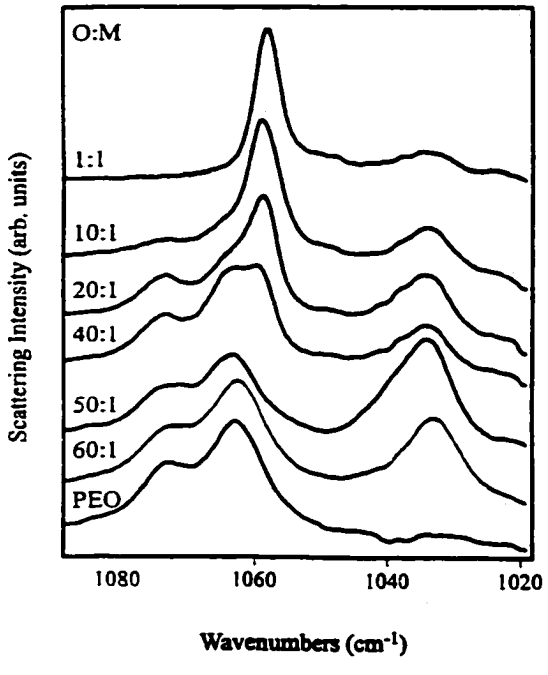


Fig. 1. Raman spectra of $(PEO)_xNaCF_3SO_3$ in the $\nu_s(SO_3)$ spectral region.

Fig. 2 presents the infrared spectra of $PEO_xNaTf$ in the $\nu_s(SO_3)$ region. The 1061 $cm^{-1}$ PEO band decreases in relative intensity with increasing salt concentration. The $\nu_s(SO_3)$ mode is strongly Raman active and only weakly IR active as expected, since this is a symmetric stretching mode. In the 80:1 system, 'free' ions at ~1032 $cm^{-1}$ and ion pairs at ~1037 $cm^{-1}$ are observed. At 40:1, a broad feature centered at 1052 $cm^{-1}$ and an additional weak feature at ~1025 $cm^{-1}$ occur. The curve-fitted spectrum (shown in Fig. 4) shows the broad band centered at 1052 $cm^{-1}$ to be composed of bands at ~1050 $cm^{-1}$ and ~1056 $cm^{-1}$. The intensities of the 1025 $cm^{-1}$, 1050 $cm^{-1}$, and 1056 $cm^{-1}$ bands increase with increasing salt concentration.

The lower frequency band occurring at ~1025 $cm^{-1}$ in the IR spectrum is not observed with any appreciable intensity in the Raman spectrum. The phenomenon of a $\nu_s(SO_3)$ frequency lower than the 'free' ion frequency has also been reported in polyethers containing dissolved triflate salts of lead [12,13], tin [12], dysprosium, europium, lanthanum, ytterbium [14], and neodymium [14,15]. Although the increase of the 1024 $cm^{-1}$ band intensity appears to be coincident with the increase of the 1050 $cm^{-1}$

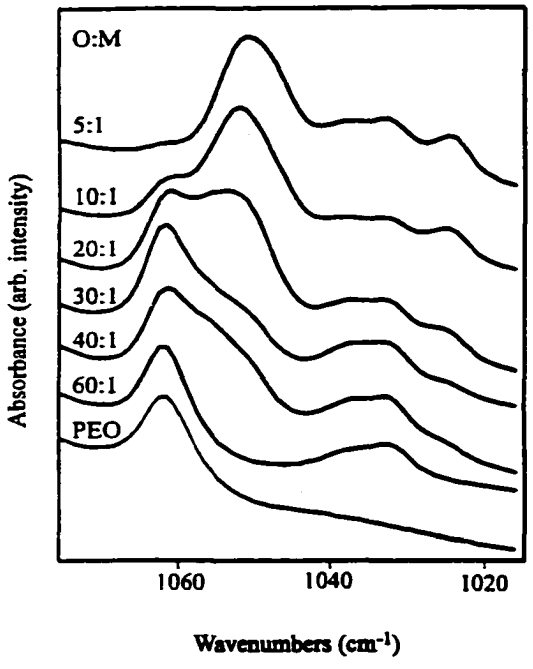


Fig. 2. IR spectra of $(PEO)_nNaCF_3SO_3$ in the $\nu_s(SO_3)$ spectral region.

and 1056 $cm^{-1}$ band intensities, the data in this study do not allow a firm conclusion that the aggregate band(s) and the low frequency band originate in the same species. The existence of two $\nu_s(SO_3)$ bands originating in the same triflate species is expected if the species is comprised of at least two triflate ions. For example, coordination of two oxygen atoms, one each from two triflate anions, through a common sodium cation can easily result in the dynamical coupling necessary to produce two $\nu_s(SO_3)$ modes at different frequencies.

The Raman and IR spectra of the PEO–NaTf system in the $\nu_s(SO_3)$ region at high salt concentrations show a very strong band at a frequency indicating a highly associated species. However, there are also much weaker bands at triflate ion frequencies attributed to 'free' ions, ion pairs, and aggregate I. It is likely that the 1:1 system in this study consists primarily of the crystalline 1:1 compound, along with some amorphous PEO containing dissolved NaTf. At lower salt concentration where the aggregate II band is also seen, it is not possible to spectroscopically distinguish between the 1:1 compound and a region in the polymer where a number of sodium ions interact with several triflate anions in addition to the ether oxygens of several adjacent PEO molecules to produce a local structure which mimics the structure of the compound.

Insight into the nature of the aggregate II species is facilitated by examination of the reported crystal structure for crystalline (PEO)NaTf compound [2]. Each $SO_3$ end of the triflate is coordinated to four sodium ions. Two oxygens, O(1) and O(2), coordinate a single sodium ion, and the third oxygen, O(3) coordinates two sodium ions. The O(1) oxygen coordinates a sodium that is linked to a separate chain, resulting in extensive anion crosslinking of the chains. Thus, the triflate species in the crystalline compound is very highly associated, leading to an unusually high Raman frequency of 1058 $cm^{-1}$. Highly associated species are also observed in diglyme complexes with sodium triflate (shown later in Fig. 5) and sodium triflate dissolved in 2-MTHF (data not shown), where there is an intense band at 1056 $cm^{-1}$ in both systems.

The relative intensity of the high frequency aggregate II species appears to depend on the PEO chain length. In the low $M_w$ PEO complexes reported by Kakihana et al. and Brodin et al., the band due to aggregate II is lower in relative intensity than the bands of 'free' ions and ion pairs over the reported concentration range [5,6]. In high $M_w$ PEO, the intensity of the aggregate II band is much greater than the intensities of 'free' ion and ion pair bands at high salt concentration.

### 3.2. Comparison of Raman and IR spectra of 20:1 PEO–NaTf in the $\nu_s(SO_3)$ region

Raman and IR spectra of the same 20:1 PEO–NaTf film were recorded. The 20:1 composition is presented as a representative sample, as similar ionic association effects are observed throughout the concentration range. Fig. 3 presents the curve-fitted Raman spectrum. The two high frequency bands at 1073 $cm^{-1}$ and 1061 $cm^{-1}$ are PEO bands which are clearly visible in the Raman spectrum of pure PEO (Fig. 1). The curve-fitted spectrum identifies four triflate bands due to the triflate anion whose fre-

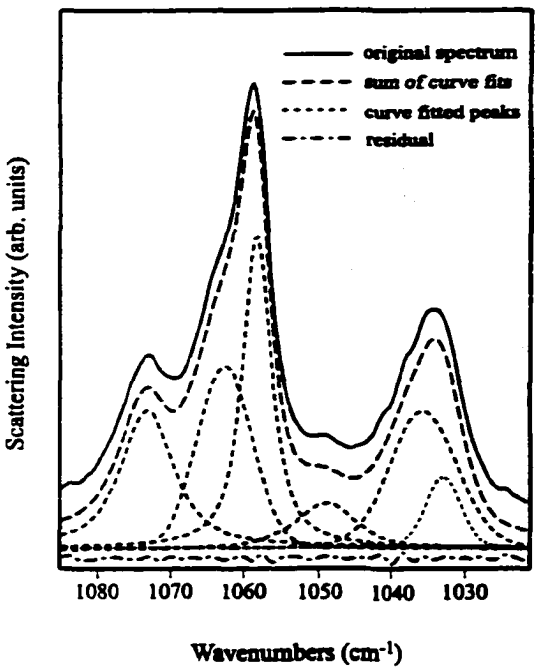


Fig. 3. Curve-fitted Raman spectra of $(PEO)_{20}NaCF_3SO_3$ in the $\nu_s(SO_3)$ spectral region.

quencies and assignments are presented in Table 1. The curve-fitted infrared spectrum of the same $(PEO)_{20}NaTf$ system is presented in Fig. 4. The 1061 $cm^{-1}$ band is present in pure PEO at the same frequency. The remaining five bands in the curve-fit spectrum are triflate anion species whose band frequencies and assignments are summarized in Table 1.

In the IR spectrum of the 20:1 complex, both the 'free' ion band and ion-pair band occur at or about the same frequencies as in the Raman spectrum. The aggregate I species is observed at the same frequency in both the Raman and IR spectrum, however the intensities relative to other species are very different. In the Raman spectrum, aggregate I appears as a relatively weak band, however in the IR spectrum the aggregate I species is observed with a greater band intensity than any other species. The frequency difference of the aggregate II species between the Raman and IR spectrum lies within the outer limits of experimental error and may not be significant.

Table 1
Band frequencies and assignments of $(PEO)_{20}NaCF_3SO_3$ obtained from spectral curve fitting (a) and band frequencies and assignments of $(diglyme)_2NaCF_3SO_3$ in the $\nu_s(SO_3)$ region (b)

(a)

| $\nu_s(SO_3)$ region Raman freq. ($cm^{-1}$) | IR freq. ($cm^{-1}$) | Assignment |
|---|---|---|
| – | 1025 | (Aggregate) |
| 1032 | 1032 | Free anions |
| 1037 | 1037 | Ion pairs |
| 1050 | 1050 | Aggregate I |
| 1058 | ~1056 | Aggregate II |

| $\delta_s(CF_3)$ region Raman freq. ($cm^{-1}$) | Assignment |
|---|---|
| 753 | Free anions |
| 756 | Ion pairs |
| 761 | Aggregate I |
| 769 | Aggregate II |

(b)

| Raman freq. ($cm^{-1}$) | Assignment |
|---|---|
| 1032 | Free anions |
| 1037 | Ion pairs |
| 1044 | Aggregate I |
| 1056 | Aggregate II |

### *3.3. Raman spectra of $\delta_s(CF_3)$ region of PEO–NaTf*

The $\delta_s(CF_3)$ region is also sensitive to ionic association primarily through redistribution of electron density in the triflate anion when a cation interacts with the $SO_3$ end [16]. Fig. 5 presents the Raman spectra of the PEO–NaTf system in this region. The absence of polymer bands in this region compared with the $\nu_s(SO_3)$ region allows an unambiguous assignment of bands due solely to the triflate anion. Curve fitting establishes the frequencies of the ionic species as follows: 'free' ions ~753 $cm^{-1}$, ion-pairs ~756 $cm^{-1}$, aggregate I ~761 $cm^{-1}$, and aggregate II ~769 $cm^{-1}$. These data are summarized in Table 1. Similar frequencies are also observed in the same region of diglyme–NaTf complexes (not shown). In the composition range from pure PEO to the 50:1 system, 'free' ions, ion-pairs, and the aggregate I species are present, although the latter is present as a weak band in the curve-fit spectrum. At the 40:1 concentration, aggregate II appears as a strong band and aggregate I

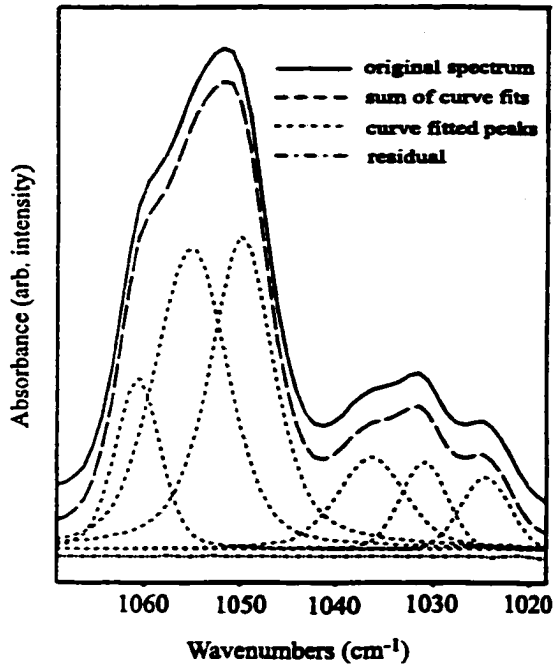


Fig. 4. Curve-fitted IR spectra of $(PEO)_{20}NaCF_3SO_3$ in the $\nu_s(SO_3)$ spectral region.

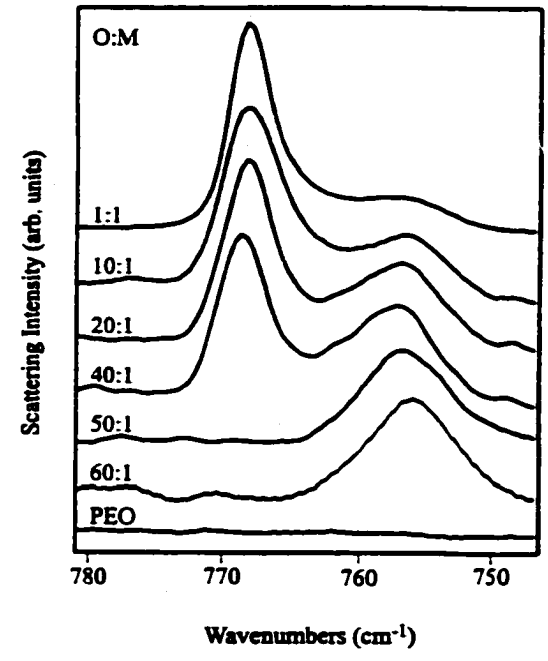


Fig. 5. Raman spectra of $(PEO)_nNaCF_3SO_3$ in the $\delta_s(CF_3)$ spectral region.

increases in relative intensity, clearly visible as a shoulder on the broad feature centered at 757 $cm^{-1}$. From 20:1 to 1:1, the aggregate II species increases in relative intensity, with 'free' ions and ion-pairs decreasing in intensity.

### *3.4. Infrared spectra of $CH_2$ rocking region of $PEO–NaCF_3SO_3$*

The bands occurring in the region of 825 $cm^{-1}$ to 870 $cm^{-1}$ of pure PEO have been assigned to modes consisting of $CH_2$ rocking motions mixed with some CO stretching motion in which the –O–C–C–O– torsional angles of two adjacent monomeric units are in gauche configurations [17]. This assignment is in agreement with the observation of an 844 $cm^{-1}$ IR-active $CH_2$ rocking mode in crystalline PEO which has all –O–C–C–O– torsional angles in gauche conformations [18]. Comparative spectroscopic studies of glymes, $CH_3(OCH_2CH_2)OCH_3$ with $n = 1$ to 4, conducted in our laboratory suggest that the $CH_2$ rocking vibrations of one $OCH_2CH_2$ unit are significantly decoupled from the $CH_2$ rocking vibrations of adjacent monomeric units [19]. Studies of the PEO–LiTf system show that the new bands appearing in this region upon the addition of the salt originate in the $CH_2$ rocking vibrations of a chain conformation in which the –O–C–C–O– torsional angle is decreased relative to its value in PEO [20]. This local structural modification of the backbone is caused by the cations interacting with the oxygen atoms as the lithium ions are coordinated by the polymer. The infrared spectra of PEO–NaTf in the $CH_2$ rocking region are presented in Fig. 6. There is a slight shift in band frequency and band broadening which occurs at high salt concentration, but no additional bands appear up to a concentration of 5:1. A comparison with the lithium system argues that in high molecular weight PEO, there is no significant local distortion of the PEO backbone resulting from the coordination of the sodium ion by

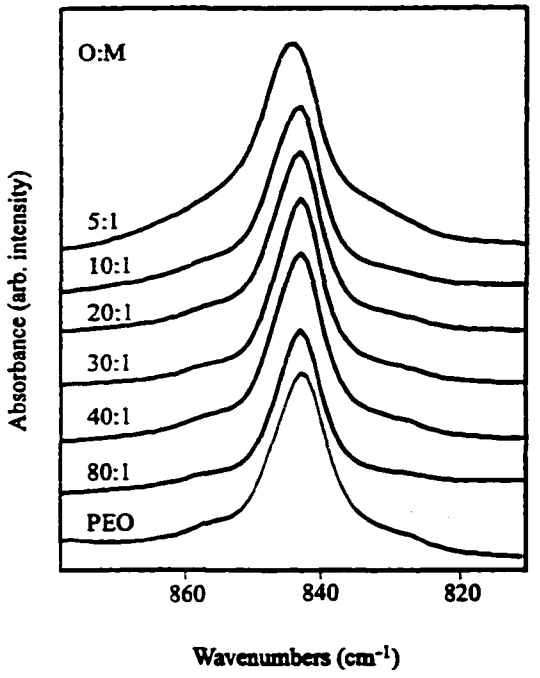


Fig. 6. IR spectra of $(PEO)_nNaCF_3SO_3$ in the $CH_2$ rocking region.

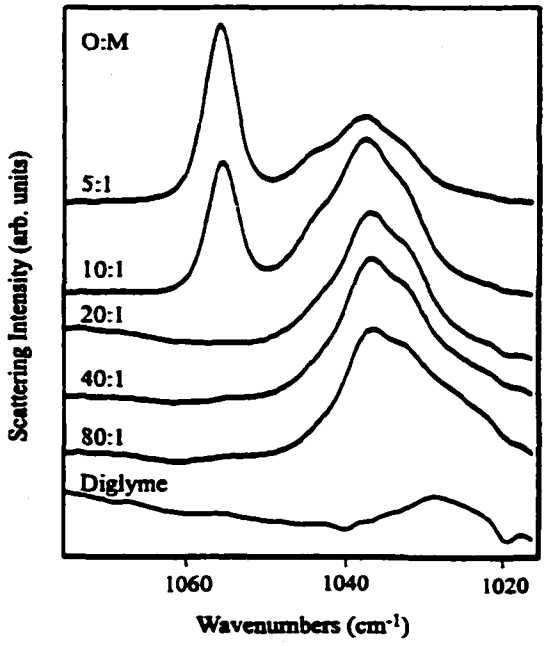


Fig. 7. Raman spectra of $(diglyme)_nNaCF_3SO_3$ in the $\nu_s(SO_3)$ spectral region.

the polyether oxygen atoms. This is consistent with the crystal structure of (PEO)NaTf, which has a similar O–C–C–O torsional angle (66°) to crystalline PEO (68.4° average) [2,18]. The spectra in this region further show that there is no local distortion of the polymer backbone by the sodium ion by the polyether backbone at any concentration of NaTf.

### *3.5. Raman spectra of $\nu_s(SO_3)$ region of diglyme–$NaCF_3SO_3$*

Diglyme is a low molecular weight oligomer of PEO. In the comparison of high molecular weight PEO and diglyme, end effects and chain length effects might be expected to lead to differences in ionic association and cation–ether oxygen interactions. The Raman spectra of diglyme–NaTf complexes are presented in Fig. 7. The presence of four triflate species present are easily discernible over the concentration range. As presented in Table 1, the 'free' ion frequency occurs at ~1032 $cm^{-1}$, the ion pair occurs at ~1037 $cm^{-1}$, aggregate I at ~1044 $cm^{-1}$, and aggregate II at ~1056 $cm^{-1}$. 'Free' ions and ion pairs occur at the same frequency as in high molecular weight PEO, whereas the bands of aggregate I and aggregate II occur at lower frequencies than their counterparts in high $M_w$ PEO. This carries the implication that the aggregate I and aggregate II species in diglyme may be structurally different than their counterparts in high $M_w$ PEO. Fig. 7 shows 'free' ions, ion-pairs and relatively small amounts of aggregate I species present at very dilute salt concentrations up to the 20:1 system. At 10:1 the intensity of the band due to aggregate I species increases and there is a new band corresponding to aggregate II which is present in relatively high intensity. The appearance of aggregate II with increasing concentration is rather abrupt compared to the relatively smaller concentration dependence of the band intensities from the other species. The aggregate II species increases in relative intensity at

a higher salt concentration of 5:1. Similar trends in aggregate speciation with increasing salt concentration are also observed in sodium triflate complexes with high $M_w$ PEO (Fig. 1).

### 3.6. IR spectra of $CH_2$ rocking region of diglyme–$CF_3SO_3$

Short chain length analogs of PEO, namely $CH_3(OCH_2CH_2)_nOCH_3$ with $n = 2$, 3 and 6, have been found to be good models of PEO in analyzing the normal vibrations of the polymer. Matsuura et al. have conducted detailed normal coordinate analysis on conformers of these model molecules and determined that the terminal-group vibrations do not complicate the vibrations of the monomeric units [17]. The result of this analysis is a well-defined correlation between conformation and vibrational spectra of the extended poly(ethylene oxide) chain. Vibrational spectroscopy can be used to compare local structure of ethylene oxide units between diglyme–NaTf complexes and the local structure of the ethylene oxide units in high $M_w$ PEO–NaTf complexes. Fig. 8 shows the growth of a higher frequency band at 864 $cm^{-1}$ and a lower frequency band at 840 $cm^{-1}$ which are clearly visible in the 10:1 and 20:1 systems. As stated previously, the growth of high and low frequency bands observed in PEO–LiTf systems have been attributed to a change of the –O–C–C–O– torsional angle [20]. By analogy to the lithium system, the presence of these additional bands suggests that the coordination of the sodium ion by the PEO chain involves a change in the –O–C–C–O– torsional angle. As presented in Section 3.4, high $M_w$ PEO–NaTf complexes do not appear to involve a significant change in the –O–C–C–O– torsional angle. The PEO–sodium triflate system is therefore different than the PEO–lithium triflate system where the conformation of the diglyme–LiTf complex is similar to the local conformation of the PEO–LiTf complex [20].

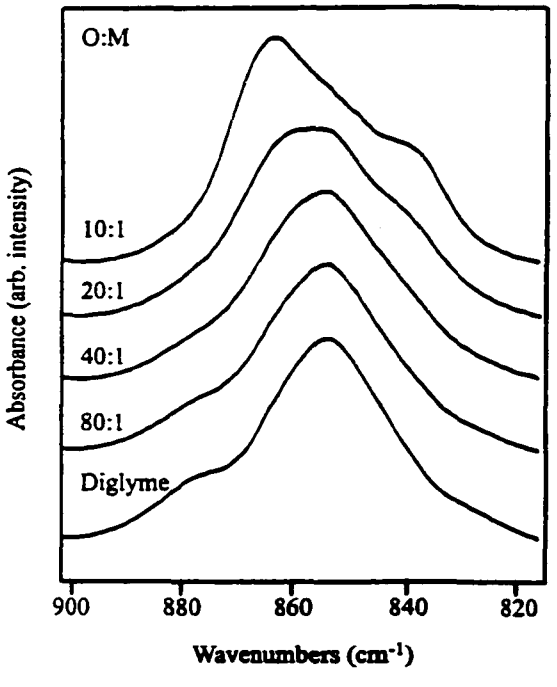


Fig. 8. IR spectra of (diglyme)$_n$NaCF$_3$SO$_3$ in the $CH_2$ rocking region.

## 4. Conclusions

The published phase diagram describes two crystalline phases, PEO and the (PEO)NaTf compound, in the concentration range (PEO)$_n$NaTf ($n = 1$–60) at room temperature [21]. This study shows that over this range there is also an amorphous PEO phase containing dissolved NaTf. This observation has consequences for battery applications, since conductivity has been found to occur mostly in the amorphous regions of these polymer–salt systems. In the PEO–NaTf system there are at least four triflate species present: 'free' ions, ion-pairs, aggregate I, aggregate II, and (possibly) the species responsible for the band at 1024 $cm^{-1}$. Aggregate II is attributed to the (PEO)NaTf compound, although at intermediate concentrations where aggregate II first appears, this species may be a localized structure which is similar to the extended PEO–sodium ion–triflate ion structure of the compound. Since the (PEO)NaTf compound is highly anion crosslinked [2], the presence of aggregate II suggests extensive intermolecular crosslinking at intermediate and high salt concentrations.

The relative intensity of the aggregate II species is significantly larger in high molecular weight PEO–

NaTf systems than in low molecular weight PEO–NaTf systems at similar O:M ratios. This suggests that in the high $M_w$ PEO system formation of the (PEO)NaTf compound (or local structures similar to the (PEO)NaTf compound) is energetically favored and probably involves a chain length effect. In addition, the coordination of the sodium ion by high $M_w$ PEO does not appear to involve a significant change in the –O–C–C–O– torsional angle whereas coordination of the sodium ion by diglyme does appear to shift the torsional angle.

## Acknowledgements

This work was partially supported by funds from the National Science Foundation EPSCoR Advanced Development Program (Grant No. EHR-9108771).

## References

[1] Y. Ma, M. Doyle, T.F. Fuller, M.M. Doeff, L.C. De Jonghe, J. Newman, J. Electrochem. Soc. 142 (1995) 1859.
[2] Y.G. Andreev, G.S. MacGlashan, P.G. Bruce, Phys. Rev. B 55 (1997) 12011.
[3] S. Schantz, J. Sandahl, L. Börjesson, L.M. Torell, Solid State Ionics 28–30 (1988) 1047.
[4] S. Schantz, L.M. Torell, J.R. Stevens, J. Phys. Chem. 94 (1991) 6862.
[5] M. Kakihana, S. Schantz, L.M. Torell, Solid State Ionics 40–41 (1990) 641.
[6] A. Brodin, B. Mattsson, K. Nilsson, L.M. Torell, J. Hamara, Solid State Ionics 85 (1996) 111.
[7] D. Martin-Vosshage, B.V.R. Chowdari, J. Electrochem. Soc. 140 (1993) 3531.
[8] E.A. Reitman, M.L. Kaplan, R.J. Cava, Solid State Ionics 25 (1987) 41.
[9] Y. Ma, M.M. Doeff, S.J. Visco, L.C. De Jonghe, J. Electrochem. Soc. 140 (1993) 2726.
[10] M.C. Wintersgill, J.J. Fontanella, Y.S. Pak, S.G. Greenbaum, A. Al-Mudaris, A.V. Chadwick, Polymer 30 (1989) 1123.
[11] M. Kakihana, S. Schantz, L.M. Torell, J. Chem. Phys. 92 (1990) 6271.
[12] P. Bergstrom, R. Frech, J. Phys. Chem. 99 (1995) 12603.
[13] Å. Wendsjö, J.O. Thomas, J. Lindgren, Polymer 34 (1993) 2243.
[14] A. Bernson, J. Lindgren, Solid State Ionics 60 (1993) 31.
[15] G. Peterson, L.M. Torell, S. Panero, B. Scrosati, C.J. da Silva, M. Smith, Solid State Ionics 60 (1993) 55.
[16] W. Huang, R. Frech, R.A. Wheeler, J. Phys. Chem. 98 (1994) 100.
[17] H. Matsuura, K. Fukuhara, J. Poly. Sci. B 24 (1986) 1383.
[18] Y. Takahashi, H. Tadokoro, Macromolecules 6 (1973) 672.
[19] R. Frech, W. Huang, Solid State Ionics 72 (1994) 103.
[20] R. Frech, W. Huang, Macromolecules 28 (1995) 1246.
[21] S. Besser, A. Vallée, G. Bouchard, J. Prud'homme, Macromolecules 25 (1992) 6480.

# II

ELSEVIER

Reproduced with permission from *Solid State Ionics* 136-137, 1131-1137 (2000)

SOLID STATE IONICS

www.elsevier.com/locate/ssi

# A symmetry-based analysis of Raman and infrared spectra of the compounds (poly(ethylene oxide))$_3$LiCF$_3$SO$_3$ and (poly(ethylene oxide))NaCF$_3$SO$_3$

Christopher P. Rhodes, Roger Frech*

*Department of Chemistry and Biochemistry, University of Oklahoma, Norman, OK 73071, USA*

**Abstract**

A symmetry-based factor group analysis is applied to the crystalline compounds (PEO)$_3$LiCF$_3$SO$_3$ and (PEO)NaCF$_3$SO$_3$, focusing on the vibrational modes originating in the intramolecular motion of the triflate anion. The dynamic coupling of the triflate anions in the unit cell yields a vibrational multiplet whose components exhibit different spectral activities. Experimentally, the Raman and IR spectra of the two compounds display multiple bands in the $\nu_s(SO_3)$ and $\delta_s(CF_3)$ spectral regions. In the $\delta_s(CF_3)$ spectral region of each compound, the frequencies of the Raman and IR bands are non-coincident and differ by $\sim 5\ cm^{-1}$. The frequency difference indicates a modest amount of dynamical coupling between the triflate anions in the crystal. The spectroscopic analysis of other modes such as $\delta_{as}(CF_3)$, $\delta_s(SO_3)$, and $\delta_{as}(SO_3)$ provides useful information about ionic interactions in the crystalline compounds. © 2000 Elsevier Science B.V. All rights reserved.

*Keywords:* Polymer electrolyte; Poly(ethylene) oxide; Lithium trifluoromethanesulfonate; Sodium trifluoromethanesulfonate; Raman spectroscopy; Infrared spectroscopy

## 1. Introduction

Polymer electrolytes have been the focus of intense research efforts due to their potential applications in rechargeable batteries and electrochemical sensors. Systems of poly(ethylene oxide) (PEO) with dissolved lithium trifluoromethanesulfonate ($LiCF_3SO_3$; LiTf) and PEO with dissolved sodium trifluoromethanesulfonate ($NaCF_3SO_3$; NaTf) have received considerable attention. At room temperature, these systems have been shown to be multiphase systems consisting of crystalline PEO, a crystalline polymer–salt complex, and an amorphous phase [1–5]. In this study we present a symmetry-based vibrational analysis of the crystalline 3:1 PEO–LiTf compound, abbreviated as (PEO)$_3$LiTf, and the crystalline 1:1 PEO–NaTf compound, abbreviated as (PEO)NaTf.

Vibrational analysis has been a powerful tool to determine the structure of polymer electrolytes. The intramolecular modes of the trifluoromethanesulfonate ($CF_3SO_3^-$) or triflate ($Tf^-$) anion, in particular the $SO_3$ symmetric stretch $\nu_s(SO_3)$ [6] and the $CF_3$ symmetric deformation $\delta_s(CF_3)$ [7,8], have been used to examine ionic association in polymer electrolytes containing this anion.

*Corresponding author. Fax: +1-405-325-6111.
*E-mail address:* rfrech@ou.edu (R. Frech).

0167-2738/00/$ – see front matter 
PII: S0167-2738(00)00608-1

There are a number of motivations for this study. Firstly, vibrational spectra show the bands of all the phases present. Earlier studies demonstrated that at moderate salt concentrations the $\nu_s(SO_3)$ and the $\delta_s(CF_3)$ modes have multiple bands in both the PEO–LiTf [9] and the PEO–NaTf systems [10], although only one band in each of these spectral regions would be predicted for the isolated triflate anion. It was unclear if the multiple bands originated in the crystalline compound or were due to the presence of an amorphous phase containing dissolved salt. Secondly, many of the previous studies have used exclusively either Raman or infrared spectroscopy. Studies using both techniques are needed for a full vibrational analysis. Given the space group and unit cell occupancies from the X-ray crystal structures of both crystalline $(PEO)_3LiTf$ [11] and crystalline (PEO)NaTf [12], factor group correlation methods can be applied to the systems and the results compared to observed spectra. This study will focus on the triflate anion modes of the compounds with the polymer modes to be presented in a further publication.

## 2. Experimental

Poly(ethylene oxide) with viscosity average molecular weight $M_v$ ca. $1 \times 10^5$ was obtained from Aldrich and dried under vacuum at 50°C for 48 h. Lithium trifluoromethanesulfonate (98%) was obtained from Aldrich and dried under vacuum at 100°C for 48 h. Sodium trifluoromethanesulfonate was obtained from Aldrich (98%) and Fluka (97%) and dried under vacuum at 100°C for 48 h. All reagents were stored and manipulated in a dry nitrogen glovebox (Vacuum Atmospheres) with $\leq 1$ ppm moisture.

For preparation of the crystalline $(PEO)_3LiTf$ compound, stoichiometric amounts of the dry powders were thoroughly ground together in the glovebox with a mortar and pestle. The powders were transferred to an 8-mm glass ampoule that was sealed under vacuum. To promote intimate mixing of the reagents, the samples were heated at 100°C for 12–24 h. The samples were then heated to 170°C for 4 h and further annealed at 100°C for 9 days. The annealed samples were transferred back to the glovebox. An identical procedure was used to prepare the crystalline (PEO)NaTf compound except for the heating temperatures. After heating the glass ampoule containing the PEO and NaTf powders at 100°C for 12–24 h, the sample was heated to 275°C for 5 h and then annealed at 100°C for 5–6 days.

Differential scanning calorimetry (DSC) measurements were taken on a Mettler DSC 820 calorimeter from 25 to 250°C for $(PEO)_3LiTf$ or 25–350°C for (PEO)NaTf at a rate of 10°C/min under a 87 ml/min nitrogen purge. The samples were sealed in aluminum crucibles in the glovebox. X-ray diffractograms were recorded at ambient conditions from $5 \leq 2\theta \leq 70$ in $2\theta$ steps of 0.05° on a Rigaku D/4MAX automated diffractometer using Cu Kα radiation.

Raman spectra were recorded on an I.S.A. Jobin-Yvon T64000 in the triple subtractive mode with a 16-s acquisition time and 10–16 accumulations using a backscattering geometry. The 514-nm line of an argon laser focused through an $\times 80$ microscope lens was used for excitation. Possible thermal heating of the samples from the focused Raman laser has been a concern. Due to fluorescence, the samples were bleached at 100 mW for at least 15 min prior to measurement. Longer bleaching times and a higher laser power (200 mW) resulted in better signal to noise ratios. Comparison of initial spectra to spectra taken with longer bleaching times and the higher laser power showed no observable differences. In addition, 90° Raman scattering of (PEO)NaTf in a sealed capillary tube was collected without sampling through the microscope and showed the same band frequencies and intensities as spectra taken in the backscattering geometry through the microscope.

Infrared spectra were recorded with a Bruker IFS66V FT-IR spectrometer in an evacuated sample chamber in the region 4000–200 $cm^{-1}$ and at a resolution of 1.0 $cm^{-1}$. Samples were prepared both as KBr pellets and as Nujol mulls. Both methods yielded essentially identical results. Bands in the IR and Raman spectra were curve-fit using a non-linear least-squares method with a commercial program, Grams 386® (Galactic Industries) using a straight base line and one Gaussian–Lorentzian product function for each band.

## 3. Results and discussion

### 3.1. Symmetry-based vibrational analysis

Recent vibrational studies of polymers with dissolved triflate salts have considered the environments of the triflate anions to be perturbations of the isolated triflate anion. Mode assignments for the observed bands of the isolated triflate anion and the triflate associated with lithium ion(s) have been made from ab initio calculations and isotopic substitution [7,13–15]. In the crystalline $(PEO)_3LiTf$ and (PEO)NaTf compounds, each triflate anion occupies symmetrically equivalent positions in the crystal lattice, therefore the potential energy environment of each triflate anion is necessarily the same. From our observation of multiple bands in the $\nu_s(SO_3)$ and $\delta_s(CF_3)$ modes in the PEO–NaTf system, we considered that coupling between multiple triflate anions may occur in the highly ordered crystalline complex.

The unit cells of both $(PEO)_3LiTf$ and (PEO)NaTf belong to the $C_{2h}^5$ space group and contain four triflate anions per unit cell [11,12]. The full factor group describes the vibrational modes within the unit cell of a crystal. In a previous publication we have shown that the full factor group analysis, which neglects specific bonding interactions, predicts more modes than observed [16]. The vibrational modes of the triflate anions are not independent from each other but rather are correlated through intermolecular forces. The factor group correlation field method provides a description of these correlated molecular vibrations in terms of the irreducible representations of the factor group [17]. In this case the isolated triflate anion is taken as having $C_{3v}$ symmetry (staggered configuration), i.e. its vibrations can be classified under the $C_{3v}$ point group, and all atoms in the unit cell other than the atoms of the triflate anions are neglected. The center of mass of the triflate anion occupies a specific Wyckoff site of $C_1$ symmetry. The site group is a subgroup of the unit cell space group $C_{2h}^5$. The general procedure presented elsewhere [17] correlates the irreducible representations of the point group to those of the site group. These irreducible representations in turn are correlated to the factor group. A visual representation is presented in Table 1. The result of the analysis is that a mode of $A_1$ symmetry in the isolated $Tf^-$ anion results in four factor group modes whose symmetry species are described by Eq. (1),

$$\Gamma(A_1) = A_g + B_g + A_u + B_u. \quad (1)$$

Similarly, the correlation of an isolated triflate $E$ mode to the factor group modes is described by Eq. (2),

$$\Gamma(E) = 2A_g + 2B_g + 2A_u + 2B_u. \quad (2)$$

The $A_g$ and $B_g$ modes are Raman active and the $A_u$ and $B_u$ modes are IR active. Of course the frequencies and intensities of the bands cannot be predicted by symmetry methods. This analysis applies to both the crystalline $(PEO)_3LiTf$ and (PEO)NaTf compounds.

### 3.2. Vibrational spectra of the triflate bands

The high degree of crystallinity of the materials was confirmed by XRD and DSC measurements. For

Table 1
Factor group correlation of intramolecular triflate vibrations in a $C_{2h}^5$ crystal

| Mode | Point group ($C_{3v}$) | Site group ($C_1$) | Factor group ($C_{2h}^5$) |
|---|---|---|---|
| $\nu_s(SO_3)$, $\delta_s(CF_3)$, $\delta_s(SO_3)$ | $A_1$ | A | $A_g$, $B_g$, $A_u$, $B_u$ |
| $\delta_{as}(CF_3)$, $\delta_{as}(SO_3)$ | E | | |

$(PEO)_3LiTf$, the DSC thermogram displays a single endotherm with an onset temperature of 172°C and a peak at 185°C corresponding to the melting of the crystalline compound [18]. X-ray diffraction patterns of the $(PEO)_3LiTf$ samples matched the published powder pattern [11]. For (PEO)NaTf, DSC measurements identified a single melting endotherm with an onset temperature of 310°C and a peak at 331°C which matched the reported melting temperature [12]. The measured X-ray diffraction peaks (PEO)NaTf were indexed to the published powder pattern [12].

The $CF_3$ symmetric deformation $\delta_s(CF_3)$ has been well established to reflect the ionic association of the triflate anion at the $SO_3$ end through electronic redistribution [7,8]. The irreducible representation of $\delta_s(CF_3)$ mode in the isolated anion is of $A_1$ symmetry so the vibrational multiplet structure in the crystal is described by Eq. (1). Fig. 1 displays the Raman and IR spectra of the crystalline $(PEO)_3LiTf$ and (PEO)NaTf compounds in the $\delta_s(CF_3)$ region. For the Raman spectrum, the symmetry analysis predicts two modes, one of $A_g$ and one of $B_g$ symmetry. The Raman spectrum of $(PEO)_3LiTf$ identifies a band centered at 766 $cm^{-1}$, which is either two coincident bands, or two bands that are very close in frequency. The IR spectrum of $(PEO)_3LiTf$ displays a slightly asymmetrical band centered at 761 $cm^{-1}$. Curve-fitting of the IR spectrum yields a minor band at 766 $cm^{-1}$ and a major band at 761 $cm^{-1}$. These modes are of $A_u$ and $B_u$ symmetry, however without polarized spectra of oriented single crystals, the symmetry labels of the bands cannot be unambiguously assigned.

For (PEO)NaTf, the symmetry analysis predicts as above that the Raman spectrum should contain an $A_g$ and a $B_g$ mode, and the IR spectrum should contain an $A_u$ and a $B_u$ mode. The Raman spectrum of (PEO)NaTf displays a feature centered at 773 $cm^{-1}$. It is possible that this band is a single band, but again the band may be the $A_g$ and $B_g$ modes that are either coincident or separated by a very small frequency difference. The IR spectrum of the $\delta_s(CF_3)$ mode of (PEO)NaTf is clearly asymmetrical. Curve-fitting of the IR spectrum of (PEO)NaTf identifies a band at 771 $cm^{-1}$ and a band at 767 $cm^{-1}$, one being the $A_u$ mode and the other the $B_u$ mode. Table 2 summarizes the Raman and IR

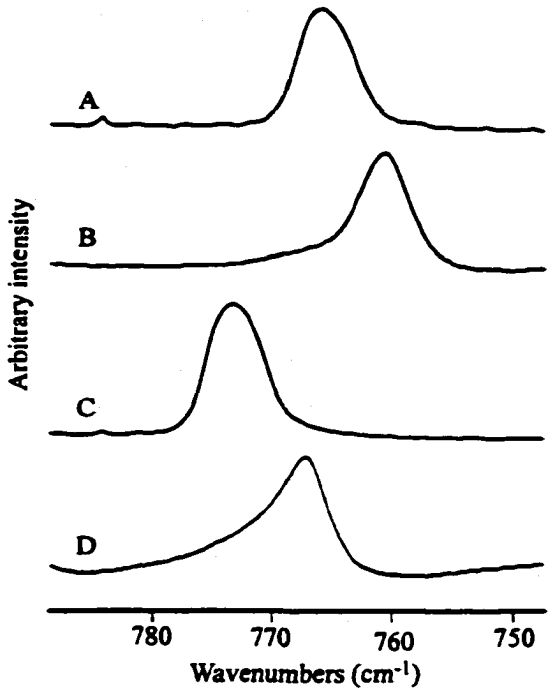


Fig. 1. Raman and IR spectra of the crystalline $(PEO)_3LiTf$ and (PEO)NaTf compounds in the $\delta_s(CF_3)$ region. (A) Raman spectrum of $(PEO)_3LiTf$; (B) IR spectrum of $(PEO)_3LiTf$; (C) Raman spectrum of (PEO)NaTf; (D) IR spectrum of (PEO)NaTf.

frequencies of the $\delta_s(CF_3)$ modes in the two compounds.

The $SO_3$ symmetric stretch $\nu_s(SO_3)$ is particularly sensitive to ionic association since the oxygens of the triflate interact directly with the cations of the salt [7]. Since the mode is also of $A_1$ symmetry, the $\nu_s(SO_3)$ modes in the crystal are also given by Eq. (1) with the same spectral activities. Fig. 2 displays the Raman and IR spectra of the crystalline $(PEO)_3LiTf$ and (PEO)NaTf compounds in the $\nu_s(SO_3)$ region. For $(PEO)_3LiTf$, curve-fitting of the Raman spectrum identifies bands at 1061 and 1051 $cm^{-1}$. Crystalline PEO has a Raman active band at about 1063 $cm^{-1}$ [10,19]. It is probable that the 1061 $cm^{-1}$ band in the Raman spectrum of $(PEO)_3LiTf$ is a PEO band. From this assumption, the 1050 $cm^{-1}$ band contains one or both of the $A_g$ and $B_g$ modes. The IR spectrum of $(PEO)_3LiTf$ in the $\nu_s(SO_3)$

Table 2
Raman and infrared frequencies of the triflate ion modes in $(PEO)_3LiTf$ and (PEO)NaTf

| Mode | Raman ($cm^{-1}$) | IR ($cm^{-1}$) |
|---|---|---|
| $(PEO)_3LiTf$ | | |
| $\nu_s(SO_3)$ | 1051 | |
| | | 1044 (broad) |
| $\delta_s(CF_3)$ | 766 | 766 |
| | | 761 |
| $\delta_s(SO_3)$ | 645 | |
| | | 641 (broad) |
| $\delta_{as}(CF_3)$ | | 588 |
| | 583 | 582 |
| | | 576 |
| $\delta_{as}(SO_3)$ | | 521 |
| (PEO)NaTf | | |
| $\nu_s(SO_3)$ | 1064 (?) | |
| | 1056 (?) | |
| | | 1049 (broad) |
| | 1030 (?) | |
| $\delta_s(CF_3)$ | 773 | 771 |
| | | 767 |
| $\delta_s(SO_3)$ | 655 | |
| | | 641 (broad) |
| $\delta_{as}(CF_3)$ | 588 | 584 |
| | | 577 |
| | | 526 (?) |
| $\delta_{as}(SO_3)$ | | 518 (?) |

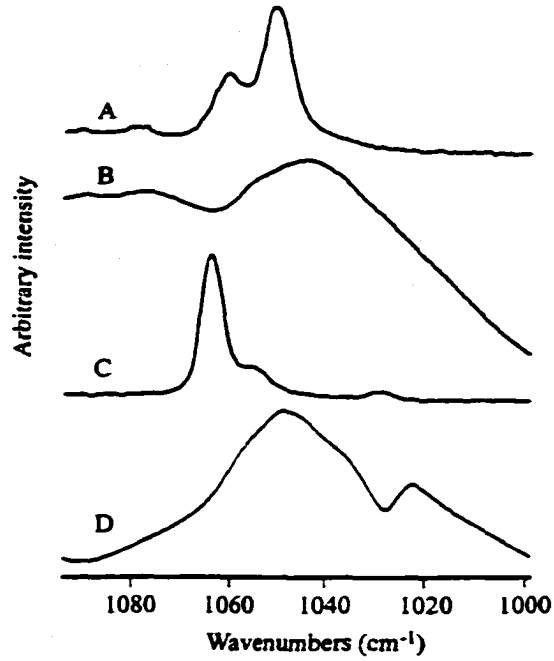


Fig. 2. Raman and IR spectra of the crystalline $(PEO)_3LiTf$ and (PEO)NaTf compounds in the $\nu_s(SO_3)$ region. (A) Raman spectrum of $(PEO)_3LiTf$; (B) IR spectrum of $(PEO)_3LiTf$; (C) Raman spectrum of (PEO)NaTf; (D) IR spectrum of (PEO)NaTf.

region is sufficiently broadened as to prevent useful spectral deconvolution. The high frequency shoulder at ~1054 $cm^{-1}$ shifts in the deuterated sample $(PEO\text{-}d_4)_3LiTf$ (unpublished data), and is therefore due to a polymer mode. Given that the broad feature centered at 1044 $cm^{-1}$ remains in the deuterated sample, the $A_u$ and $B_u$ modes must be contained within this broad feature.

For the $\nu_s(SO_3)$ region of (PEO)NaTf, curve-fitting of the Raman spectrum identifies bands at 1064, 1056 and a minor band at 1030 $cm^{-1}$. As mentioned above, crystalline PEO has a Raman-active band at 1063 $cm^{-1}$. The concentration-dependent spectra of $(PEO)_xNaTf$ with $x=1$–80 show the gradual disappearance of the 1063 $cm^{-1}$ crystalline PEO band with increasing salt concentration [10]. The intensity of the band at 1064 $cm^{-1}$ in (PEO)NaTf argues that this feature is due to a triflate anion $\nu_s(SO_3)$ mode of the compound. However without further data, the possibility of a polymer band in this region still exits. Therefore, one or both of the 1064- and 1056-$cm^{-1}$ bands are due to the $A_g$ and $B_g$ modes. The weak 1030 $cm^{-1}$ band is an interesting feature that deserves further analysis. Previously we have suggested that triflate anion coupling may be responsible for this band. The mode may also originate from vibrations of the PEO chain in the compound.

As in the case for $(PEO)_3LiTf$, the IR spectrum of (PEO)NaTf in the $\nu_s(SO_3)$ region is rather complicated with multiple bands clearly observed. From our symmetry analysis, we expect to see the triflate anion $A_u$ and $B_u$ modes somewhere within the broad feature centered at 1049 $cm^{-1}$. Despite the lack of resolution, the frequency difference of the $\nu_s(SO_3)$ modes in the Raman spectrum and the IR spectrum can be observed in Fig. 2. It is probable that polymer modes contribute to the complex band structure in this region. Further analysis with isotopic substitution will assist in band assignments. Table 2 summa-

rizes the Raman and IR frequencies of the $\nu_s(SO_3)$ modes in the two compounds.

In spectroscopic studies of triflate-containing polymer electrolytes, attention has been focused almost exclusively on the $\delta_s(CF_3)$ and $\nu_s(SO_3)$ modes. However, other triflate modes should show effects of both ionic association and coupling between the triflate anions in the crystalline compounds. Fig. 3 displays the Raman and infrared spectra for $(PEO)_3LiTf$ and (PEO)NaTf in the 700–500-$cm^{-1}$ region. Three triflate bands are identified in this region: the $SO_3$ symmetric deformation $\delta_s(SO_3)$, the $CF_3$ antisymmetric deformation $\delta_{as}(CF_3)$ and the $SO_3$ antisymmetric deformation $\delta_{as}(SO_3)$.

The bands around the 640 $cm^{-1}$ region have been assigned to predominately $\delta_s(SO_3)$ with a contribution of $\delta_s(CF_3)$ motion, from here on abbreviated as $\delta_s(SO_3)$ [13,14]. Since the $\delta_s(SO_3)$ mode is of $A_1$ symmetry, its vibrations in the crystal are given by

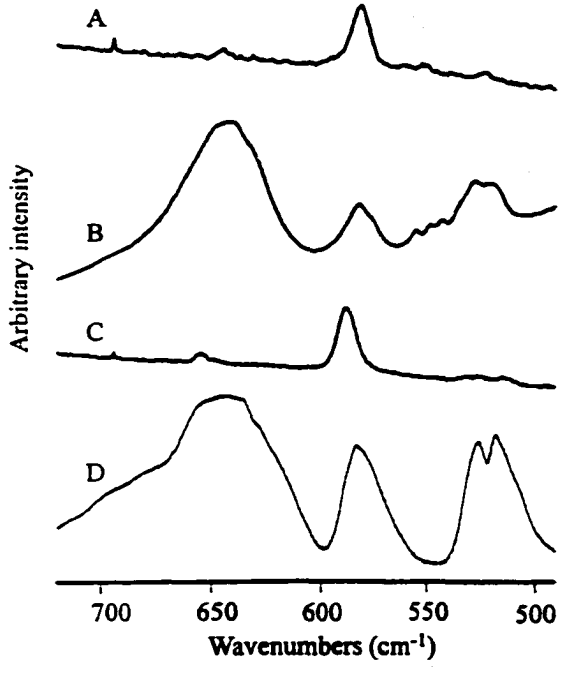


Fig. 3. Raman and IR spectra for $(PEO)_3LiTf$ and (PEO)NaTf in the 700–500-$cm^{-1}$ region. (A) Raman spectrum of $(PEO)_3LiTf$; (B) IR spectrum of $(PEO)_3LiTf$; (C) Raman spectrum of (PEO)NaTf; (D) IR spectrum of (PEO)NaTf.

Eq. (1). The Raman spectra of $(PEO)_3LiTf$ and (PEO)NaTf display very weak components at 645 and 655 $cm^{-1}$, respectively. The symmetry properties of these modes may be either $A_g$ or $B_g$. The IR spectrum of $(PEO)_3LiTf$ displays a very broad band centered at 641 $cm^{-1}$, and the IR spectrum of (PEO)NaTf also has a very broad band centered at a similar frequency. Although the presence of a polymer band may contribute to the broad feature, only two triflate anion bands are expected in this region.

The modes occurring around the 570 $cm^{-1}$ region have been assigned to $\delta_{as}(CF_3)$ with a contribution from $\delta_{as}(SO_3)$ motion, from here on abbreviated as $\delta_{as}(CF_3)$ [13,14]. This mode is of $E$ symmetry so the band structure is given by Eq. (2). The Raman spectrum of $(PEO)_3LiTf$ displays a single band at 583 $cm^{-1}$ which is either $A_g$ or $B_g$. The IR spectrum of $(PEO)_3LiTf$ spectrum is much better curve-fit with three bands than two, with frequencies of 588, 582 and 576 $cm^{-1}$. Multiple bands are expected since the symmetry analysis predicts four IR-active bands, $2A_u$ and $2B_u$. The Raman spectrum of (PEO)NaTf displays a single band of $A_g$ or $B_g$ symmetry at 588 $cm^{-1}$. Curve-fitting of the IR spectrum has band components of $A_u$ or $B_u$ symmetry at 584 and 577 $cm^{-1}$.

The region around 520 $cm^{-1}$ contains the modes assigned to $\delta_{as}(SO_3)$ with a significant contribution of $\delta_{as}(CF_3)$, from here on abbreviated as $\delta_{as}(SO_3)$ [13,14]. The mode is of $E$ symmetry so the bands are described by Eq. (2). This region is complicated by pure PEO bands in the Raman spectrum at 534 $cm^{-1}$ and in the IR spectrum at 529 and 509 $cm^{-1}$ [19]. No appreciable Raman activity of the $\delta_{as}(SO_3)$ modes is observed in $(PEO)_3LiTf$. While there appears to be at least two bands present in the IR spectrum of $(PEO)_3LiTf$, the component at 528 $cm^{-1}$ shifts in the deuterated $(PEO\text{-}d_4)_3LiTf$ and therefore results from a polymer mode. There may be one or two modes of either $A_u$ or $B_u$ symmetry contained within the 521 $cm^{-1}$ feature in the IR of $(PEO)_3LiTf$. The (PEO)NaTf compound shows similar patterns. No appreciable Raman activity for the $\delta_{as}(SO_3)$ mode is observed. Data for $(PEO\text{-}d_4)$NaTf is not presently available, but it is expected that the band at 526 $cm^{-1}$ is probably a polymer band. Therefore the 518 $cm^{-1}$ band in the IR spectrum of (PEO)NaTf may contain either or both of the $A_u$ and

$B_u$ modes. Triflate anion band frequencies and spectral activities for $(PEO)_3LiTf$ and (PEO)NaTf in the 700–500-$cm^{-1}$ region are summarized in Table 2.

## 4. Conclusions

A symmetry-based vibrational analysis using the factor group correlation method has been used to describe the vibrational multiplet structure observed in the crystalline compounds $(PEO)_3LiTf$ and (PEO)NaTf. The triflate intramolecular modes of interest here are either of $A_1$ or $E$ symmetry in the isolated anion. The multiple occupancy of the unit cell by four triflate anions in each compound requires that each isolated anion mode of $A_1$ ($E$) symmetry results in four (eight) independent modes in the crystal. The presence of an inversion center in the space group operations of both compounds divides the predicted vibrational multiplet of each spectral region equally into Raman active, infrared inactive modes and infrared active, Raman inactive modes. The effects of this are manifested in the general non-coincidence of band frequencies in the Raman and infrared spectra observed in each spectral region discussed in this paper. This non-coincidence is especially dramatic in the $\delta_s(CF_3)$ region as shown in Fig. 1, where there is a ~5-$cm^{-1}$ difference between the infrared-active and Raman-active modes. This frequency difference indicates a modest amount of dynamical coupling between the triflate anions in the crystal.

This work also emphasizes the importance of vibrational modes other than $\nu_s(SO_3)$ and $\delta_s(CF_3)$ in spectroscopic studies of triflate-containing polymer electrolytes. The observation of factor group multiplet structure in the $\delta_{as}(CF_3)$ spectral region of the two crystalline compounds suggests that this mode can provide useful insight into local structure and ionic interactions in these and related systems. In addition, multiple bands observed in the infrared spectra of the $\delta_s(SO_3)$ and $\delta_{as}(SO_3)$ regions may also yield useful information, although these regions are complicated by the presence of PEO bands. It is interesting to note that the Raman spectra in these two regions are almost featureless, possibly due to very weak polarizability derivatives associated with the $\delta_s(SO_3)$ and $\delta_{as}(SO_3)$ modes.

## Acknowledgements

This work has been partially supported by the Oklahoma Center for the Advancement of Science and Technology, Project No. AR982-013, and Eagle-Picher Technologies, LLC. We appreciate the assistance of Ronald Conlon and the use of the X-ray facilities in the Department of Geology and Geophysics.

## References

[1] C.D. Robitaille, D. Fauteux, J. Electrochem. Soc. 133 (1986) 315.
[2] S. Besner, A. Vallée, G. Bouchard, J. Prud'homme, Macromolecules 25 (1992) 6480.
[3] C. Berthier, W. Gorecki, M. Minier, Solid State Ionics 11 (1983) 91.
[4] M. Minier, C. Berthier, W. Gorecki, J. Phys. 45 (1984) 739.
[5] M.C. Wintersgill, J.J. Fontanella, Y.S. Pak, S.G. Greenbaum, A. Al-Mudaris, A.V. Chadwick, Polymer 30 (1989) 1123.
[6] G. Peterson, P. Jacobsson, L.M. Torell, Electrochim. Acta 37 (1992) 1495.
[7] W. Huang, R. Frech, R.A. Wheeler, J. Phys. Chem. 98 (1994) 100.
[8] R. Frech, W. Huang, M.A.K.L. Dissanayake, Mater. Res. Soc. Symp. Proc. 369 (1995) 523.
[9] R. Frech, S. Chintapalli, P.G. Bruce, C.A. Vincent, Macromolecules 32 (1999) 808.
[10] C.P. Rhodes, R. Frech, Solid State Ionics 121 (1999) 91.
[11] P. Lightfoot, M.A. Mehta, P.G. Bruce, Science 262 (1993) 883.
[12] Y.G. Andreev, G.S. MacGlashan, P.G. Bruce, Phys. Rev. B 55 (1997) 12011.
[13] W. Huang, R.A. Wheeler, R. Frech, Spectrochim. Acta 50A (1994) 985.
[14] E.L. Varetti, E.L. Fernández, A.B. Altabef, Spectrochim. Acta 47A (1991) 1767.
[15] D.H. Johnston, D.F. Shriver, Inorg. Chem. 32 (1993) 1045.
[16] R. Frech, C.P. Rhodes, S.S. York, Mater. Res. Soc. Symp. Proc. 548 (1999) 335.
[17] W.G. Fateley, F.R. Dollish, N.T. McDevitt, F.F. Bentley, in: Infrared and Raman Selection Rules for Molecular and Lattice Vibrations: The Correlation Method, Wiley, New York, 1972.
[18] R. Frech, S. Chintapalli, P.G. Bruce, C.A. Vincent, Chem. Commun. (1997) 157.
[19] T. Yoshihara, H. Tadokoro, S. Murahashi, J. Chem. Phys. 41 (1964) 2902.

# III

# Vibrational Study of the Polymer Electrolyte Poly(ethylene oxide)$_6$:LiAsF$_6$

**Christopher P. Rhodes and Roger Frech***

*Department of Chemistry and Biochemistry, University of Oklahoma, Norman, Oklahoma 73019*

*Received May 16, 2000; Revised Manuscript Received November 21, 2000*

ABSTRACT: A vibrational study of the polymer electrolyte compound poly(ethylene oxide)$_6$:LiAsF$_6$ is reported. A symmetry-based factor group correlation method is applied to interpret the observed bands. The Raman and infrared spectra of the compound are consistent with the reported crystal structure. The $\nu_1$ mode, which appears at 685 cm$^{-1}$, identifies the anions as being "spectroscopically free". Multiple bands in the $\nu_3$ spectral region are interpreted as resulting from the dynamical coupling of the four AsF$_6^-$ anions in the unit cell. The $\rho(CH_2)$ region shows multiple bands that arise from the complex conformations of the polymer backbone.

## 1. Introduction

Polymer electrolytes are of considerable interest due to their potential applications in rechargeable batteries and other electrochemical devices.[1-3] Investigation of cation−polymer and cation−anion interactions is essential to understanding the microscopic mechanism of ionic transport in polymer electrolytes. The study of crystalline phases in certain poly(ethylene oxide)−alkali metal salt systems yields the structures and bonding geometries in these systems[4,5] and provides insight into the local structure of the amorphous phase,[6,7] which is primarily where ionic conductivity occurs.[8,9]

Ionic transport in poly(ethylene oxide)−salt systems is coupled to the segmental motion of the polymer host.[10,11] Although the specific nature of the segmental motion is not known, it is generally considered that segmental motion involves changes in the conformation of the polymer backbone. Analysis of crystalline polymer−salt structures[4,5] and vibrational spectroscopic studies of polymer−salt systems[12-15] show that the conformation of the poly(ethylene oxide), PEO, backbone is altered upon complexation to cations. Ab initio calculations have been used to determine the relative energies of various conformational sequences and model the energetic barriers for the migration of a lithium ion.[16-20] Molecular dynamics simulations have been used to examine the relative populations of various conformational sequences.[21,22]

The extent and nature of ionic association is also a critical factor in the ionic conductivity and transport properties of the electroyte.[23] Vibrational spectroscopy has proven to be a powerful tool to examine the ionic association of the salt anion.[12,24-26] In particular, we consider the determining the vibrational signatures of the crystalline polymer−salt compounds to be crucial to investigating the local structure in amorphous and multiple-phase polymer electrolytes. We have recently studied the crystalline compounds P(EO):NaCF$_3$SO$_3$ and P(EO)$_3$:LiCF$_3$SO$_3$ and have interpreted multiple CF$_3$SO$_3^-$ anion bands as resulting from coupling of the vibrational modes in the crystal.[27]

The structure of the crystalline compound poly(ethylene oxide)$_6$:LiAsF$_6$ (abbreviated P(EO)$_6$:LiAsF$_6$), which was elucidated from X-ray diffraction patterns, has been recently reported.[28] This structure is strikingly different from those of other polymer−salt compounds in that there is no coordination of the lithium ions by the anions. Therefore, it is of interest to examine the local environment of the hexafluoroarsenate anions by vibrational spectroscopy, with the expectation that the AsF$_6^-$ mode frequencies would correspond to those of a "spectroscopically free" anion. A study of the polymer modes in P(EO)$_6$:LiAsF$_6$ furthers our knowledge of the relationship between vibrational frequencies and specific conformational sequences. Mid-infrared and Raman spectra of the P(EO)$_6$:LiAsF$_6$ compound have been recorded, and the vibrational analysis is presented.

## 2. Experimental Section

PEO, $M_w = 4 \times 10^6$, was obtained from Aldrich and dried under vacuum at 50 °C for 24 h. Thin films were made by casting a solution of PEO in acetonitrile onto Teflon sheets. The P(EO)$_6$:LiAsF$_6$ compound was obtained from Professor Peter Bruce, St. Andrews University. To prepare the sample, dried PEO and LiAsF$_6$ were ground together in an inert atmosphere glovebox at liquid $N_2$ temperature, sealed in a capillary tube, heated, and annealed. The sample was characterized by powder X-ray diffraction. Details on the preparation method and the experimental instrumentation can be found in ref 28.

After being shipped in a sealed vial, the P(EO)$_6$:LiAsF$_6$ sample was transferred directly to a dry $N_2$ glovebox (VAC Corp., ≤1 ppm moisture). Raman and mid-infrared spectra were recorded on the as-received sample. Infrared spectra were recorded with a Bruker IFS66V FT-IR spectrometer over a range of 4000−400 cm$^{-1}$ with a resolution of 1 cm$^{-1}$. Mid-infrared spectra were taken as KBr pellets. Raman scattering spectra were recorded on an I.S.A. Jobin-Yvon T6400 in the triple subtractive mode with a scan time of 16 s and 10 accumulations using a 180° geometry. The 514 nm line of an argon laser focused through an 80× microscope lens was used for excitation. The laser was operated at 300 mW, and the power at the sample was 50−100 mW. Local heating of the sample by the focused beam was not observed in similar systems.[27]

## 3. Results and Discussion

**A. Symmetry-Based Vibrational Analysis.** The isolated AsF$_6^-$ anion has octahedral symmetry, and the symmetries of the six normal vibrational modes are described by the irreducible representations of the $O_h$

* To whom correspondence should be addressed.

10.1021/ma0008387 CCC: $20.00 
Published on Web 01/23/2001

**Table 1. Factor Group Correlation of Intramolecular $AsF_6^-$ Vibrations in a $C_{2h}^5$ Crystal**

| Mode | Point Group ($O_h$) | Site Group ($C_1$) | Factor Group ($C_{2h}^5$) |
|---|---|---|---|
| $\nu_1$ | $A_{1g}$ | A | $A_g$ |
| | | | $B_g$ |
| $\nu_2$ | $E_g$ | | $A_u$ |
| | | | $B_u$ |
| $\nu_3, \nu_4, \nu_5$ | $F_{1u}$, $F_{2g}$ | | |

point group according to

$$\Gamma(AsF_6^-) = A_{1g} + E_g + 2F_{1u} + F_{2g} + F_{2u} \quad (1)$$

The fundamental vibrations, mode labels, and spectral activities of the $AsF_6^-$ ion based on an octahedral geometry have been reported.[29] The crystalline compound $P(EO)_6$:$LiAsF_6$ belongs to the $P2_1/a$ space group,[28] with four $AsF_6^-$ anions in the unit cell. Within the crystal the vibrations of the $AsF_6^-$ anions are not isolated from each other but are correlated through intermolecular forces. The factor group method provides a description of the correlated molecular vibrations as they transform according to the irreducible representations of the factor group.[30] We have previously applied this method to interpret the triflate anion modes in the crystalline compounds $P(EO)_3$:$LiCF_3SO_3$ and P(EO):$NaCF_3SO_3$.[27] In the $P(EO)_6$:$LiAsF_6$ compound the As atoms occupy general 4e positions,[31] and accordingly the site symmetry of the $AsF_6^-$ anions is $C_1$. The relations between the irreducible representations of the isolated anion, its site group, and the correlated vibrations of the full unit cell are calculated by standard methods[30] and are summarized in Table 1. In this paper we will consider only modes originating in the isolated ion $A_{1g}$ and $F_{1u}$ modes. Table 1 shows that these isolated ion vibrations result in the following factor group modes:

$$\Gamma(A_{1g}) = A_g + B_g + A_u + B_u \quad (2)$$

$$\Gamma(F_{1u}) = 3A_g + 3B_g + 3A_u + 3B_u \quad (3)$$

**B. Vibrational Modes of the $AsF_6^-$ Anion.** The Raman-active $\nu_1(A_{1g})$ mode has been used to determine the presence of ionic association of the $AsF_6^-$ anion in a number of solvents. In solutions of $LiAsF_6$ in 1,2-dimethoxyethane,[32,33] methyl acetate,[34] acetone,[35] water,[34] and tetrahydrofuran,[36] a band occurs in the range of 676–682 $cm^{-1}$ and is assigned to a "spectroscopically free" anion. A "spectroscopically free" anion is indistinguishable from a solvent-separated ion pair by vibrational spectroscopic measurements. In crystalline $CsAsF_6$ the $\nu_1$ mode is observed at 685 $cm^{-1}$.[29] Systems of $LiAsF_6$–acetone and $LiAsF_6$–methyl acetate display an additional band at 694 $cm^{-1}$ which is assigned to a contact ion pair.[34,35] The intensity of the 694 $cm^{-1}$ band relative to the 676 $cm^{-1}$ band increases with increasing salt concentration. Further support for the contact ion pair assignment is provided by the decrease of the relative intensity of the 694 $cm^{-1}$ band with the addition of 18-crown-6.[34] The crown ether is assumed to coordinate with the $Li^+$ ion, thereby decreasing the $AsF_6^-$ - -$Li^+$ contact ion pair formation.

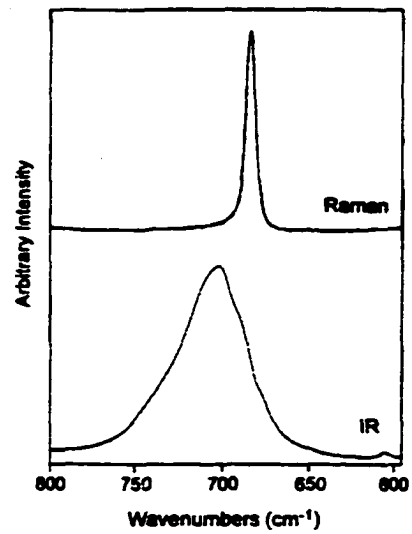


**Figure 1.** Raman and infrared spectra of the $P(EO)_6$:$LiAsF_6$ compound in the 600–800 $cm^{-1}$ region.

The Raman spectrum of the crystalline complex $P(EO)_6$:$LiAsF_6$ is presented in Figure 1. A single, reasonably symmetrical band is observed at 684 $cm^{-1}$ and assigned to the $\nu_1(A_{1g})$ mode. The absence of a 694 $cm^{-1}$ (or higher frequency) band indicates that no contact ion pairs are present, and the anion exists as a "free" $AsF_6^-$ ion in the crystal. The slightly higher frequency compared to the solvent systems may be a result of crystal packing effects. The symmetry-based vibrational analysis predicts Raman-active bands of $A_g$ and $B_g$ symmetry for this mode in the crystal (eq 2). The degree of factor group splitting of the two components is negligibly small, based on the observation of only a single band.

The infrared-active $\nu_3(F_{1u})$ band has also been used to determine ionic association in $AsF_6^-$ systems. Solutions of $LiAsF_6$ in 2-methyltetrahydrofuan,[37] 1,3-dioxolane,[38] and methyl acetate[39] displayed bands which were assigned to free ions and contact ion pairs at ~702 and ~717 $cm^{-1}$, respectively. In the IR spectra of the $LiAsF_6$ solutions the intensity of the contact ion pair band is comparable to that of the free ion band, and the area of each band can be resolved by curve fitting. We note that in the $LiAsF_6$–methyl acetate system, where both the Raman and IR spectra were recorded at similar salt concentrations, the contact ion pair band intensity in the IR (717 $cm^{-1}$) is comparable to the free ion band intensity (702 $cm^{-1}$).[39] However, in the Raman spectrum the contact ion pair band intensity (696 $cm^{-1}$) is very weak compared to the free ion band intensity (676 $cm^{-1}$).[34] Therefore, the bands in the IR are more sensitive to ionic association. In this region an additional band at ~676 $cm^{-1}$ is observed in the solvent systems which has been assigned to a $(\nu_5 + \nu_6)$ combination band ($F_{2g} \times F_{2u} = A_{1u} + E_u + F_{1u} + F_{2u}$).[37] Because this band occurs at the same frequency as the Raman-

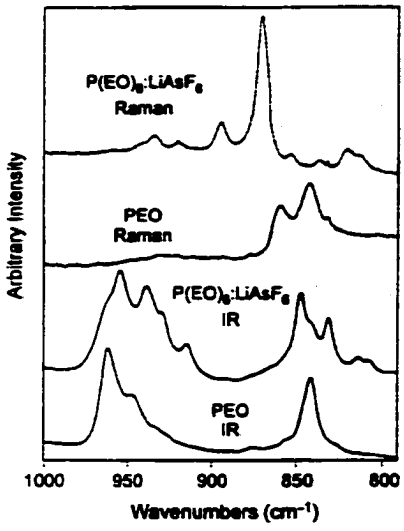


Figure 2. Raman spectra of the P(EO)$_6$:LiAsF$_6$ compound, Raman spectra of the pure PEO, infrared spectra of the P(EO)$_6$:LiAsF$_6$ compound, and infrared spectra of pure PEO in the 800−1000 cm$^{-1}$ region.

active $\nu_1$ mode, it is also possible that the 676 cm$^{-1}$ IR band is due to the $\nu_1$ mode becoming weakly IR-active upon relaxation of the isolated anion $O_h$ symmetry due to solvent−anion interactions.

The infrared spectrum in the region from 640 to 760 cm$^{-1}$, presented in Figure 1, shows a broad band centered at approximately 702 cm$^{-1}$ with shoulders on the low-frequency side. The analysis of this region is complicated by the fact that both the $\nu_1$ and the $\nu_3$ vibrations have infrared-active components in this area. For the $\nu_3$ vibrations of four coupled $AsF_6^-$ anions in the unit cell, the symmetry-based analysis predicts six IR-active modes, $3A_u + 3B_u$ (eq 3). Additionally, the $\nu_1$ vibrations are formally predicted to be infrared-active with an $A_u$ and a $B_u$ mode. The major component of the band is at 702 cm$^{-1}$ and is attributed to the $\nu_3$ mode of a free $AsF_6^-$ anion. The broad band shape is attributed to factor group splitting of the $\nu_3$ mode, as stated above. Further evidence for splitting is present in the $\nu_4$ mode (not shown), where multiple band components are observed. Similar splitting patterns are observed in the $\nu_3$ and $\nu_4$ modes in rhombohedral $KAsF_6$.[40] Additional contributions to the low-frequency band structure are the $(\nu_5 + \nu_6)$ combination band and weakly IR-active components of the $\nu_1$ mode. Because of the broad, complex nature of the band, we cannot completely neglect the possibility that a small contribution from contact ion pairs exists. Such a contribution would presumably originate in the presence of a minor amorphous phase. There is no evidence in the Raman spectrum for such a phase, although the Raman spectrum is less sensitive to the presence of a $Li^+$--$AsF_6^-$ ion pair than is the IR spectrum.

**C. Chain Conformation and $CH_2$ Rocking Modes.** In Figure 2 the infrared and Raman spectra of the P(EO)$_6$:LiAsF$_6$ compound are compared with the spectra of pure PEO for the region from 800 to 1000 cm$^{-1}$. Modes in this spectral region have been assigned to a mixture of predominantly $CH_2$ rocking and C−O stretching motions.[41] The frequencies and intensities of these modes are sensitive to the values of the backbone torsional angles;[15,42,43] thus, the frequency shifts that occur upon complexation with a cation provide insight into the local conformational changes accompanying the polymer−cation interaction.

The conformation of the polymer backbone in P(EO)$_6$:LiAsF$_6$ is significantly different than in crystalline PEO. The conformation of crystalline PEO is $(tgt)_7$ for the dihedral angles C−O−C−C, O−C−C−O, and C−C−O−C, where t is trans and g is gauche.[44] In comparison, the conformation for the same bond sequence in the P(EO)$_6$:LiAsF$_6$ compound is tct-gg't-gcg'-tct-tgt-g'cg where c refers to cis and g' refers to gauche-minus.[28]

Both the infrared and Raman spectra of P(EO)$_6$LiAsF$_6$ in this region are more complex than the analogous PEO spectra, with at least five distinct, noncoincident bands visible in each spectrum. In the absence of either a detailed normal coordinate analysis or polarized spectroscopic measurements of an oriented single crystal, it is difficult to make precise vibrational assignments. However, the lack of coincidence in mode frequencies between the Raman and the infrared spectra is clearly due to the presence of a center of symmetry in the unit cell. More specifically, the two polymer chains that comprise a cylindrical structure enclosing the lithium ions also enclose the center of symmetry. Thus, the vibrations of a pair of such chains are correlated through the center of symmetry.

General correlations between torsional angle sequences and frequencies have been previously described. Ethylene oxide units with gauche O−C−C−O torsional angles are reported to have bands in the range 825−890 cm$^{-1}$, while units with trans O−C−C−O torsional angles exhibit bands in the range 810−825 cm$^{-1}$.[42,45] The spectra of the P(EO)$_6$:LiAsF$_6$ compound (Figure 2) show a dominant Raman-active band at 871 cm$^{-1}$ and IR-active bands at 848 and 832 cm$^{-1}$. The crystal structure has two ethylene oxide units with gauche O−C−C−O torsional angles, so the presence of these bands is consistent with the reported structure. In the 810−825 cm$^{-1}$ range, bands are present in both the Raman and infrared spectra of the compound. According to the crystal structure, there are four cis O−C−C−O torsional angles and no trans O−C−C−O torsional angles. Therefore, the bands in the spectral region previously attributed to ethylene oxide units with trans O−C−C−O torsional angles may actually arise from torsional angle sequences rather than a particular value of a torsional angle present in the crystal. Conformation-frequency correlations for the range 900−1000 cm$^{-1}$ are limited because specific torsional angle sequences have overlapping frequency ranges.[42]

## 4. Conclusions

The vibrational correlation analysis establishes the number and spectral activities of the Brillouin zone center modes originating in the intermolecular vibrations of the $AsF_6^-$ ion. The single band observed in the Raman spectral region of the As−F symmetric stretching mode at 684 cm$^{-1}$ is assigned to the $\nu_1(A_{1g})$ mode. The frequency of this band shows that there is no contact ion pairing of the $AsF_6^-$ with the $Li^+$ ion, a result that is consistent with the reported crystal structure. We attribute the broad-band structure of the infrared feature centered at 702 cm$^{-1}$ to the factor group splitting of the $\nu_3$ mode.

Our study of the polymer modes in $P(EO)_6$:$LiAsF_6$ provides insight into the correlation between vibrational frequencies and specific conformational sequences. The $CH_2$ rocking region has a complicated multiplet structure in both the infrared and Raman spectrum. Bands were observed at relatively low frequencies in this region; similar band frequencies in related ethylene oxide-based systems have been previously assigned to ethylene oxide units with trans O−C−C−O torsional angles. However, the clear absence of trans O−C−C−O torsional angles in the crystal structure suggests that these modes may instead originate in the complex torsional angle sequences observed in this compound.

The $P(EO)_6$:$LiAsF_6$ compound represents an interesting structure in polymer electrolytes in that the cation is completely coordinated by the polymer ether oxygens with no coordination by the anion. It has been reported that for $LiAsF_6$ in cross-linked PEO (MW 2000) the $AsF_6^-$ anions exist predominately as free ions even at high salt concentrations.[46] This suggests that the local structure in the low molecular weight, cross-linked PEO may be similar to that in the high molecular weight $P(EO)_6$:$LiAsF_6$ compound.

**Acknowledgment.** We thank Professor Peter Bruce and co-workers for generously making available to us samples of crystalline $(PEO)_6$:$LiAsF_6$. This work was partially supported by funds from the Oklahoma Center of Advancement of Science and Technology under Grant 5548.

## References and Notes

(1) Armand, M. B.; Chabagno, J. M.; Duclot, M. J. Polyethers as solid electrolytes. In *Fast Ion Transport in Solids*; Vashista, P., Mundy, J. M., Shenoy, G. K., Eds.; Elsevier: Amsterdam, 1979; pp 131−136.
(2) Gray, F. M. *Solid Polymer Electrolytes: Fundamentals and Technological Applications*; VCH Publishers: New York, 1991.
(3) Bruce, P. G.; Vincent, C. A. *J. Chem. Soc., Faraday Trans.* **1993**, *89*, 3187−3203.
(4) Lightfoot, P.; Mehta, M. A.; Bruce, P. G. *Science* **1993**, *262*, 883−885.
(5) Andreev, Y. G.; Lightfoot, P.; Bruce, P. G. *Chem. Commun.* **1996**, 2169−2170.
(6) Frech, R.; Chintapalli, S.; Bruce, P. G.; Vincent, C. A. *Macromolecules* **1999**, *32*, 808−813.
(7) Andreev, Y. G.; Bruce, P. G. *Electrochim. Acta* **2000**, *45*, 1417−1423.
(8) Berthier, C.; Gorecki, W.; Minier, M. *Solid State Ionics* **1983**, *11*, 91−95.
(9) Stainer, M.; Hardy, L. C.; Whitmore, D. H.; Shriver, D. F. *J. Electrochem. Soc.* **1984**, *131*, 784−790.
(10) Ratner, M. A.; Nitzan, A. *Faraday Discuss. Chem. Soc.* **1989**, *88*, 19−42.
(11) Ratner, M. A.; Johansson, P.; Shriver, D. F. *MRS Bull.* **2000**, *25*, 31−37.
(12) Papke, B. L.; Ratner, M. A.; Shriver, D. F. *J. Phys. Chem. Solids* **1981**, *42*, 493−500.
(13) Huang, W.; Frech, R.; Johansson, P.; Lindgren, J. *Electrochim. Acta* **1995**, *40*, 2147−2151.
(14) Frech, R.; Huang, W. *Solid State Ionics* **1994**, *72*, 103−107.
(15) Frech, R.; Huang, W. *Macromolecules* **1995**, *28*, 1246−1251.
(16) Gejji, S. P.; Tegenfeldt, J.; Lindgren, J. *Chem. Phys. Lett.* **1994**, *226*, 427−432.
(17) Gejji, S. P.; Johansson, P.; Tegenfeldt, J.; Lindgren, J. *Comput. Polym. Sci.* **1995**, *5*, 99−105.
(18) Johansson, P.; Tegenfeldt, J.; Lindgren, J. *Polymer* **1999**, *40*, 4399−4406.
(19) Johansson, P.; Tegenfedlt, J.; Lindgren, J. *J. Phys. Chem. A* **1998**, *102*, 4660−4665.
(20) Mujica, V.; Malaver, M.; Ruette, F. *J. Phys. Chem. A* **1999**, *103*, 89−94.
(21) Borodin, O.; Smith, G. D. *Macromolecules* **1998**, *31*, 8396−8406.
(22) Borodin, O.; Smith, G. D. *J. Phys. Chem. B* **2000**, *104*, 8017−8022.
(23) Bruce, P. G. *Faraday Discuss. Chem. Soc.* **1989**, *88*, 43−54.
(24) Schantz, S.; Sandahl, J.; Borjesson, L.; Torell, L. M.; Stevens, J. R. *Solid State Ionics* **1988**, *28−30*, 1047−1053.
(25) Huang, W.; Frech, R.; Wheeler, R. A. *J. Phys. Chem.* **1994**, *98*, 100−110.
(26) Frech, R.; Huang, W.; Dissanayake, M. A. K. L. *Mater. Res. Soc. Symp. Proc.* **1995**, *369*, 523−534.
(27) Rhodes, C. P.; Frech, R. *Solid State Ionics* **2000**, *136−137*, 1131−1137.
(28) MacGlashan, G. S.; Andreev, Y. G.; Bruce, P. G. *Nature* **1999**, *398*, 792−794.
(29) Begun, G. M.; Rutenberg, A. C. *Inorg. Chem.* **1967**, *6*, 2212−2216.
(30) Fateley, W. G.; Dollish, F. R.; McDevitt, N. T.; Bentley, F. F. *Infrared and Raman Selection Rules for Molecular and Lattice Vibrations: The Correlation Method*; John Wiley & Sons: New York, 1972.
(31) Andreev, Y., personal communication.
(32) Farber, H.; Irish, D. E.; Petrucli, S. *J. Phys. Chem.* **1983**, *87*, 3515−3520.
(33) Muhuri, P. K.; Das, B.; Hazra, D. K. *J. Phys. Chem. B* **1997**, *101*, 3329−3332.
(34) Deng, Z.; Irish, D. *Can. J. Chem.* **1991**, *69*, 1766−1773.
(35) Deng, Z.; Irish, D. E. *J. Chem. Soc., Faraday Trans.* **1992**, *88*, 2891−2896.
(36) Huang, W. Ph.D. Dissertation, University of Oklahoma, 1994.
(37) Inoue, N.; Xu, M.; Petrucci, S. *J. Phys. Chem.* **1987**, *91*, 4628−4635.
(38) Xu, M.; Inoue, N.; Eyring, E. M.; Petrucci, S. *J. Phys. Chem.* **1988**, *92*, 2781−2789.
(39) Salomon, M.; Uchiyama, M.; Xu, M.; Petrucci, S. *J. Phys. Chem.* **1989**, *93*, 4374−4382.
(40) Heyns, A. M.; Pistorius, C. W. F. T. *Spectrochim. Acta* **1975**, *31A*, 1293−1301.
(41) Matsuura, H.; Miyazawa, T. *Bull. Chem. Soc. Jpn.* **1968**, *41*, 1798−1808.
(42) Matsuura, H.; Fukuhara, K. *J. Polym. Sci., Part B* **1986**, *24*, 1383−1400.
(43) Murcko, M. A.; DiPaola, R. A. *J. Am. Chem. Soc.* **1992**, *114*, 10010−10018.
(44) Takahashi, Y.; Tadokoro, H. *Macromolecules* **1973**, *6*, 672−675.
(45) Maxfield, J.; Shepherd, I. W. *Polymer* **1975**, *16*, 505−509.
(46) Laik, B.; Legrand, L.; Chausse, A.; Messina, R. *Electrochim. Acta* **1998**, *44*, 773−780.

MA0008387

# IV

# Local Structures in Crystalline and Amorphous Phases of Diglyme–$LiCF_3SO_3$ and Poly(ethylene oxide)–$LiCF_3SO_3$ Systems: Implications for the Mechanism of Ionic Transport

**Christopher P. Rhodes and Roger Frech***

*Department of Chemistry and Biochemistry, University of Oklahoma, Norman, Oklahoma 73019*

*Received October 10, 2000; Revised Manuscript Received January 31, 2001*

ABSTRACT: The ability of ethylene oxide-based materials to dissolve salts and form ionically conducting systems has attracted widespread interest. Our molecular level understanding of ionic conductivity in these systems critically depends on our understanding of local structures. The crystal structure of *diethylene glycol dimethyl ether*:$LiCF_3SO_3$ or *diglyme*:$LiCF_3SO_3$ consists of diglyme–salt dimers with the lithium ion in a 5-fold coordination strikingly similar to that in crystalline poly(ethylene oxide)$_3$:$LiCF_3SO_3$. However, spectroscopic studies of diglyme–$LiCF_3SO_3$ solutions indicate that lithium ion is coordinated by only three oxygen atoms from a diglyme molecule and one oxygen atom from a $CF_3SO_3^-$ anion as part of a contact ion pair. A parallel spectroscopic study of high molecular weight PEO–$LiCF_3SO_3$ suggests that the ionically conducting amorphous phase also contains four-coordinate lithium ions in a local structure similar to that in the diglyme solution. Analysis of Raman and X-ray data of PEO–$LiCF_3SO_3$ films suggests that the amorphous phase contains local structures which resemble the structure present in crystalline P(EO)$_3$:$LiCF_3SO_3$. The significance of local structures for the mechanism of ion transport is discussed.

## 1. Introduction

Polymer electrolytes based on poly(ethylene oxide) with dissolved salts are of considerable interest for rechargeable lithium batteries and fundamental research of ionic transport in disordered phases. The mechanism of ionic transport in high molecular weight PEO–salt systems is poorly understood at the molecular level, although it is recognized that cation–anion interactions,[1] cation–polymer interactions,[2] and polymer segmental motion[3] play a critical role. The ionic conductivity of high molecular weight poly(ethylene oxide), PEO, with dissolved lithium trifluoromethanesulfonate, $LiCF_3SO_3$, has been found to occur primarily in an amorphous phase.[4,5] Determining the local structure of the ionically conducting phase serves to further our understanding of the microscopic mechanism of ionic conductivity within these systems. Vibrational spectroscopy has provided considerable information on the local structures in polymer electrolytes and is a particularly useful probe of local structure in the amorphous phase. To gain insight into the amorphous phase, two general strategies have been used: investigation of the crystalline phase(s) of the system[6–8] and use of low molecular weight analogues containing the ethylene oxide monomer as models.[9–11] Here both strategies are combined to advance our insight into the local structures present in the ionically conducting phase of PEO–$LiCF_3SO_3$. In turn this insight leads to a deeper understanding of the ionic transport mechanism in the system.

## 2. Experimental Section

Diethylene glycol dimethyl ether (diglyme), PEO ($M_v = 4 \times 10^6$), and $LiCF_3SO_3$ were obtained from Aldrich. Diglyme was used as received. $LiCF_3SO_3$ was heated under vacuum at 120 °C for 48 h, and PEO was dried under vacuum at 50 °C for 24 h. The reagents were stored and manipulated in a dry nitrogen glovebox (VAC, ≤1 ppm of $H_2O$). To prepare the diglyme:$LiCF_3SO_3$ crystals, a solution of $LiCF_3SO_3$ dissolved in diglyme at an ether oxygen:cation ratio of 5:1 was stirred for ~48 h and left inside the glovebox at room temperature. An intermediate gellike phase appeared which then became crystalline after a number of months. Crystalline P(EO)$_3$:$LiCF_3SO_3$ was prepared by a method previously published.[12] The 10:1 diglyme–$LiCF_3SO_3$ solution was prepared by dissolving the salt directly in diglyme. To prepare the PEO–$LiCF_3SO_3$ films, stoichiometric amounts of PEO and $LiCF_3SO_3$ were combined with acetonitrile. For the pure PEO film, PEO was combined with acetonitrile. The solutions were stirred for 24 h, and then films were cast onto either Teflon (for Raman and differential scanning calorimetry (DSC) measurements) or glass slides (for X-ray diffraction measurements). The cast films were left in the glovebox for 24 h to evaporate solvent and then heated at 50 °C for 24 h under vacuum. The heating temperature was chosen to avoid heating the film above the melting point of PEO. The same sample preparation, heating temperature, and time were used for the Raman, X-ray, and DSC specimens to enable direct comparison of the data. Data on the films were taken within 1–2 h after removing the films from the vacuum oven.

A single-crystal specimen was isolated from the 5:1 diglyme–$LiCF_3SO_3$ solution for X-ray analysis. X-ray diffraction data were collected at 173(2) K on a Siemans P4 diffractometer using Mo Kα radiation ($\lambda$ = 0.718 73 Å). The data were corrected for Lorentz and polarization effects; an absorption correction was not applied since it was judged to be insignificant. The structure was solved by the direct method using the SHELXTL system and refined by a full matrix least squares on $F^2$ using all reflections. All non-hydrogen atoms were refined anisotropically, and all hydrogen atoms were included in the refinement with idealized parameters. The final $R1$ = 0.037 is based on 3852 "observed reflections" ($I > 2\sigma(I)$), and the $wR2$ = 0.099 is based on all reflections (4566 unique data). For the PEO–$LiCF_3SO_3$ films, powder X-ray diffractograms were recorded at ambient conditions from $5 \le 2\theta \le 70$ in $2\theta$ steps of 0.05° on a Rigaku D/4MAX automated diffractometer using Cu Kα radiation.

Raman scattering spectra were recorded on an I.S.A. Jobin-Yvon T64000 in the triple subtractive mode with a scan time

* Corresponding author.

10.1021/ma001749x CCC: $20.00 
Published on Web 03/16/2001

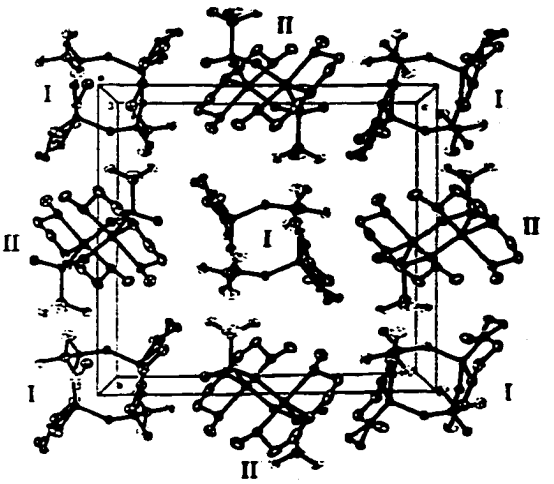


**Figure 1.** Packing diagram of crystalline diglyme:$LiCF_3SO_3$ showing type I and type II dimers. Hydrogen atoms are not shown in the diagram.

of 16 s and 10 accumulations using a 90° scattering geometry (for the diglyme–$LiCF_3SO_3$ system) and a 180° geometry (for the PEO–$LiCF_3SO_3$ system). The 514 nm line of an argon laser operating at 300 mW was used for excitation. Bands were curve-fit by the Levenberg–Marquardt method using Galactic Grams software. DSC thermograms were collected on a Mettler DSC 820 calorimeter under nitrogen purge in sealed aluminum crucibles. Data for the diglyme:$LiCF_3SO_3$ crystal were collected from 25 to −100 to 80 °C with a heating/cooling rate of 10 °C/min. Data for the PEO–$LiCF_3SO_3$ films and the $P(EO)_3$:$LiCF_3SO_3$ compound were collected from 25 to 220 °C with a heating rate of 10 °C/min. Ab initio calculations were performed using the B3LVP hybrid Hartree–Fock density functional method using the 6-31G(d) basis.

## 3. Results and Discussion

**3.1. Diglyme–$LiCF_3SO_3$.** We begin by reporting the discovery of the 1:1 compound of diglyme, $CH_3(OCH_2CH_2)_2OCH_3$, with $LiCF_3SO_3$, hereafter labeled diglyme:$LiCF_3SO_3$. A single crystal of the 1:1 compound was isolated, and its structure was determined by X-ray diffraction techniques. The compound provides an excellent opportunity to markedly extend our insight into local structures and their corresponding vibrational spectroscopic signatures in ethylene oxide-based systems containing dissolved salts. DSC measurements showed that the phase was stable to −100 °C and had an onset of melting at ~27 °C. The compound crystallizes with $Z = 4$ in the monoclinic $P2_1/c$ space group with $a = 9.6117(10)$ Å, $b = 16.2782(13)$ Å, $c = 16.6202(15)$ Å, and $\beta = 93.549(8)°$. The asymmetric unit contains two independent halves of two dimers. Therefore, the unit cell consists of four dimers, two of which are identical and slightly different in structure from the other identical pair. An extended unit cell showing the two types of dimers is presented in Figure 1. Each dimer has a crystallographically imposed center of symmetry, with the inversion center lying at the midpoint between the two sulfur atoms of the triflate anions. Figure 2 shows the details of a single dimer. Every monomeric unit of the dimer contains a single lithium ion coordinated with the three oxygen atoms of a diglyme molecule. Two triflate anions then join the two diglyme molecules into a dimer through the coordination of two oxygen atoms of each triflate anion to the lithium ion associated with each diglyme molecule.

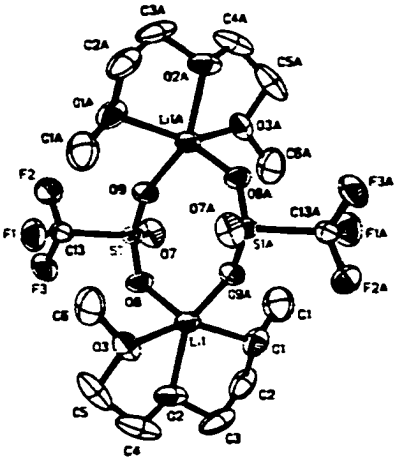


**Figure 2.** Crystal structure of diglyme:$LiCF_3SO_3$ showing the geometry of one dimer. Hydrogen atoms are not shown in the diagram.

**Table 1. Lithium–Oxygen Bond Distances in Diglyme–$LiCF_3SO_3$ and $P(EO)_3$:$LiCF_3SO_3$ Crystals[a]**

| | diglyme:$LiCF_3SO_3$ | | |
|---|---|---|---|
| Li–O distance (Å) | dimer I | dimer II | $P(EO)_3$:$LiCF_3SO_3$ |
| Li1–O1(ether oxy) | 2.166 | 2.105 | 2.38(9) |
| Li1–O2(ether oxy) | 2.044 | 2.075 | 1.72(7) |
| Li1–O3(ether oxy) | 2.113 | 2.105 | 2.01(8) |
| Li1–O8 (trif oxy) | 1.965 | 1.959 | 2.21(8) |
| Li1–O9A(trif oxy) | 1.949 | 1.944 | 2.14(8) |

[a] The data for the $P(EO)_3$:$LiCF_3SO_3$ compound were obtained from the published crystal structure parameters.[8] For the diglyme:$LiCF_3SO_3$ crystal, uncertainties are 0.003–0.004 Å for the bond distances. The specific distances and angles are defined based on the type I dimer (Figure 2), and the parameters for the type II dimer and $P(EO)_3$:$LiCF_3SO_3$ are for an analogous geometry as in the type I dimer.

**Table 2. Oxygen–Lithium–Oxygen Bond Angles in Diglyme–$LiCF_3SO_3$ and $P(EO)_3$:$LiCF_3SO_3$ Crystals[a]**

| | diglyme:$LiCF_3SO_3$ | | |
|---|---|---|---|
| O–Li–O angle (deg) | dimer I | dimer II | $P(EO)_3LiCF_3SO_3$ |
| O1–Li1–O2 | 77.0 | 78.0 | 85(3) |
| O2–Li1–O3 | 78.1 | 77.6 | 94(4) |
| O1–Li1–O3 | 146.2 | 141.9 | 174(5) |
| O8–Li1–O9A | 108.8 | 109.1 | 112(4) |
| O2–Li1–O8 | 103.6 | 100.0 | 107(4) |
| O2–Li1–O9A | 147.6 | 150.8 | 134(5) |

[a] For the diglyme:$LiCF_3SO_3$ crystal, uncertainties are 0.2–0.4° for the bond angles. Further information on the parameters and labels are provided in the Table 1 footnote.

The crystal structure of the diglyme:$LiCF_3SO_3$ compound is remarkably similar to the crystal structure of the high molecular weight $P(EO)_3$:$LiCF_3SO_3$ compound. Selected lithium–oxygen bond lengths, oxygen–lithium–oxygen angles, and torsional angles in the two compounds are presented in Table 1, Table 2, and Table 3, respectively. From the comparison of distances and angles, it can be seen that the 5-fold coordination of the lithium ion in diglyme:$LiCF_3SO_3$ is remarkably similar to that observed in the crystal structure $P(EO)_3$:$LiCF_3$-

**Table 3. Torsional Angles for the Ethylene Oxide Units in the Diglyme–$LiCF_3SO_3$ and $P(EO)_3$:$LiCF_3SO_3$ Crystals[a]**

| bond sequence | diglyme:$LiCF_3SO_3$ dimer I | diglyme:$LiCF_3SO_3$ dimer II | $P(EO)_3LiCF_3SO_3$ | label |
|---|---|---|---|---|
| C1–O1–C2–C3 | −177.4 | 159.0 | −166.9 | t |
| O1–C2–C3–O2 | 56.2 | 50.1 | 70.3 | g |
| C2–C3–O2–C4 | −175.9 | −163.3 | 176.5 | t |
| C3–O2–C4–C5 | 171.6 | 171.5 | 158.8 | t |
| O2–C4–C5–O3 | −55.3 | −54.3 | −44.1 | g′ |
| C4–C5–O3–C6 | 179.6 | −175.5 | −177.7 | t |
| C–O–C–C | | | 166.5 | t |
| O–C–C–O | | | 64.3 | g |
| C–C–O–C | | | −162.4 | t |

[a] For the diglyme:$LiCF_3SO_3$ crystal, uncertainties are estimated to be 0.4–0.8° for the torsional angles. Further information on the parameters and labels is provided in the Table 1 footnote.

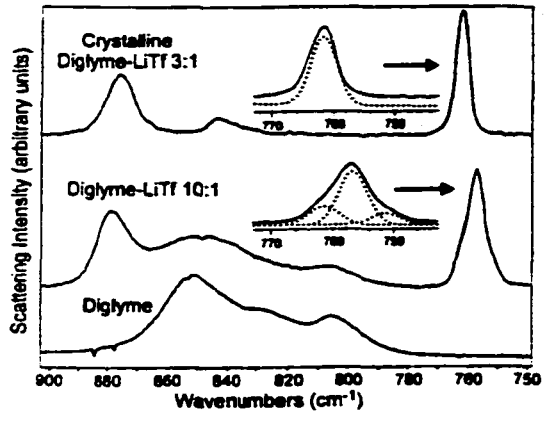


Figure 3. Raman spectra of crystalline diglyme:$LiCF_3SO_3$, diglyme–$LiCF_3SO_3$ solution with an ether oxygen:lithium ratio of 10:1, and pure diglyme in the region 700–900 $cm^{-1}$. The expanded views are curve-fitting analysis of the $\delta_s(CF_3)$ region.

$SO_3$. In both crystalline compounds, the lithium ion is coordinated by three oxygen atoms from the ethylene oxide chain and two oxygen atoms from different triflate anions. In the diglyme:$LiCF_3SO_3$ compound, the torsional angle sequence which coordinates the lithium ion is tgt-tg′t. In the $P(EO)_3$:$LiCF_3SO_3$ compound the torsional angle sequence is tgt-tg′t-tgt, and a closer inspection reveals that the unit coordinating the lithium contains three oxygen atoms and consists of the same torsional angle sequence tgt-tg′t with the additional tgt unit "linking" coordinating units.

Vibrational spectroscopy has proven to be a powerful technique to examine cation–anion interactions[13,14] and changes of the ethylene oxide backbone conformation[9,15] accompanying the interaction of the ether oxygen atoms with the cations. The spectroscopic data described here initially focuses on those intramolecular modes of the triflate ion whose frequencies are especially sensitive to interactions with the cations: the $CF_3$ symmetric deformation mode, $\delta_s(CF_3)$, and the $SO_3$ symmetric stretching vibration, $\nu_s(SO_3)$. The Raman spectrum of the crystalline diglyme:$LiCF_3SO_3$ compound in the $\delta_s(CF_3)$ region is shown in Figure 3. The single band at 763 $cm^{-1}$ is due to the triflate ion $\delta_s(CF_3)$ mode. Similarly, a single $\nu_s(SO_3)$ band is observed in the crystal at 1053 $cm^{-1}$ (data not shown). The observation of a single Raman-active triflate anion mode in these two spectral regions rather than the four modes predicted by a factor group vibrational analysis[12] can be explained by assuming that the triflate intramolecular vibrations are vibrationally coupled within each dimer but highly decoupled between the dimers in the unit cell. An isolated dimer with the formula $[CH_3O(CH_2CH_2O)_2CH_3LiCF_3SO_3]_2$ belongs to the $C_i$ point group and accordingly yields a Raman-active mode of $A_g$ symmetry and an infrared-active mode of $A_u$ symmetry in both the $\delta_s(CF_3)$ region and the $\nu_s(SO_3)$ region. Although the two pairs of dimers in the unit cell have slightly different structures, the observation of just one band in each region demonstrates that the structural difference between the two kinds of dimers is not sufficient to allow a spectroscopic distinction between the two.

**Table 4. Band Frequencies, Relative Percent Area, and Assignments of Triflate Anion Species from Curve-Fitting Analysis of Raman Spectra of the $\delta_s(CF_3)$ Region[a]**

| system | band ($cm^{-1}$) | relative percent (%) | assignment |
|---|---|---|---|
| diglyme–LiTf (10:1) | 762 | 23 | aggregate |
| | 757 | 63 | ion pairs |
| | 753 | 14 | free ions |
| PEO–LiTf (10:1) | 761 | 73 | aggregate |
| | 757 | 22 | ion pairs |
| | 753 | 5 | free ions |
| PEO–LiTf (20:1) | 761 | 29 | aggregate |
| | 757 | 65 | ion pairs |
| | 753 | 6 | free ions |

[a] Relative percent area is obtained by dividing the percent area for a specific band from the total area of all three bands. The error in percent area is estimated to be ±3%.

The $\delta_s(CF_3)$ and $\nu_s(SO_3)$ modes have been well-studied in a variety of ethylene oxide–lithium triflate systems. Both the $\delta_s(CF_3)$ band at 763 $cm^{-1}$ and the $\nu_s(SO_3)$ mode at 1053 $cm^{-1}$ have been assigned to the vibration of a triflate anion in which two of the three oxygen atoms of the anion are coordinated by lithium ions; i.e., the triflate anion essentially vibrates as a $[Li_2CF_3SO_3]^+$ entity.[16] As noted earlier, two oxygen atoms of a triflate ion are each coordinated with the lithium ion uniquely associated with a diglyme monomeric unit. Consequently, each triflate ion in the crystal vibrates as an $[Li_2CF_3SO_3]^+$ entity, and the observed frequencies of $\delta_s(CF_3)$ and $\nu_s(SO_3)$ can be easily understood in terms of the crystal structure.

It is revealing to compare the spectrum of the crystal in this region with the spectrum of a diglyme solution at a 10:1 (ether oxygen:cation) composition also shown in Figure 3. That spectrum consists of a broad asymmetric band which can be deconvolved into a major component at 757 $cm^{-1}$, assigned to contact ion pairs, and minor components at 753 and 761 $cm^{-1}$, attributed to "free" ions and $[Li_2CF_3SO_3]^+$ entities, respectively.[16] The curve-fitted bands are shown in Figure 3, and the contribution of each component band to the total integrated intensity is presented in Table 4. A comparison of the experimental splitting of the $\nu_{as}(SO_3)$ mode (not shown) with the calculated values[16] suggests that the Li···$SO_3CF_3$ ion pair is a monodentate structure rather than a bidentate structure. The major component of the $\nu_s(SO_3)$ band is observed at 1043 $cm^{-1}$, a frequency which has also been assigned to contact ion pairs.[17] It follows that the ionic species present in the 10:1 diglyme solution are predominantly ion pairs. The presence of a minor component at 762 $cm^{-1}$ coincident (within error) with the frequency of the $\delta_s(CF_3)$ mode in the crystal suggests the presence of isolated dimers in the solution.

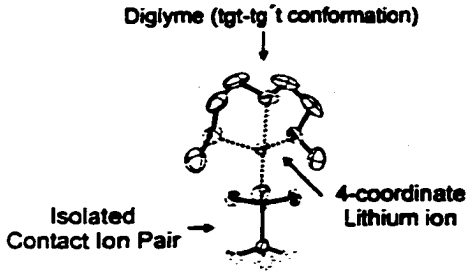


**Figure 4.** Pictoral representation of proposed local structure occurring in 10:1 solution of diglyme–$LiCF_3SO_3$ contianing a four-coordinate lithium ion, a diglyme molecule in a tgt-tg't conformation, and an isolated triflate anion. Hydrogen atoms are not shown in the diagram.

The spectral region from 800 to 900 $cm^{-1}$ (also shown in Figure 3) contains modes that are a mixture of $CH_2$ rocking and CO stretching motions.[18,19] These mode frequencies[19,20] and intensities[9] depend on the O–C–C–O torsional angle(s) and hence the backbone conformation. When a salt is dissolved in an ethylene oxide-based system, the interaction of the cation with the ether oxygen atoms changes the torsional angle(s).[9] The frequency shifts accompanying these interactions provide important insight into the change of local backbone structure occurring upon complexation with a cation. Computational and experimental studies suggest that the frequency of at least one band in this region increases with decreasing values of the O–C–C–O torsional angle.[20] In the spectrum of the diglyme:$LiCF_3SO_3$ crystal, the most intense band in this region is at 877 $cm^{-1}$, and an additional feature is present at 842 $cm^{-1}$. Since the structure of the crystal is known, these bands can be attributed to a mixture of $CH_2$ rocking and CO stretching vibrations resulting from the local structure of the diglyme molecule in diglyme:$LiCF_3SO_3$ which consists of the torsional angle sequence tgt-tg't. The relatively high frequency of the 877 $cm^{-1}$ band compared with the bands in pure diglyme (see Figure 3) reflects the smaller O–C–C–O torsional angles present in the crystal; torsional angles of 77.0° and −77.0° have been calculated by ab initio methods for the pure diglyme in a tgt-tg't conformation.

The Raman spectrum of the 10:1 diglyme–$LiCF_3SO_3$ solution is presented in Figure 3. The observation of a band in the 10:1 solution at 877 $cm^{-1}$, the same frequency as in the crystal, is especially significant because it establishes that the diglyme molecule in solution is in a conformation with a O–C–C–O torsional angle sequence very similar to those in the diglyme:$LiCF_3SO_3$ crystal, almost certainly through the interaction of the lithium cation with all three oxygen atoms of the diglyme molecule. However, the dominant ionic species in the solution is a contact ion pair, as described earlier. Therefore, we conclude that the lithium ion is 4-fold coordinated in solution, interacting with three oxygen atoms from a diglyme molecule and one oxygen atom from a triflate anion as represented in Figure 4. The formation of the dimer units occurs in concentrated salt solutions and upon crystallization is accompanied by 5-fold coordination of the lithium ion. This analysis is supported by the correlation between the decrease in the relative amount of the ion pair species and the increase in the relative amount of the aggregate species as the salt concentration is increased.[21]

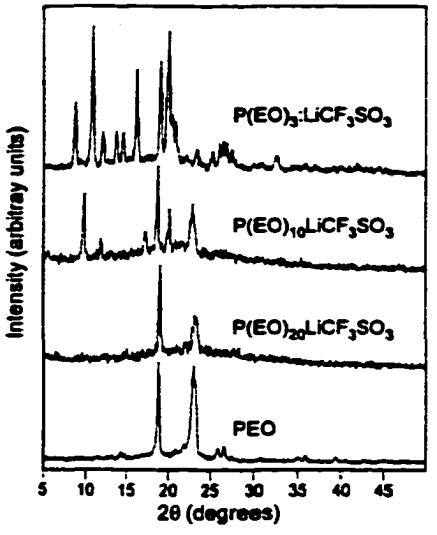


**Figure 5.** X-ray diffraction patterns for $P(EO)_3$:$LiCF_3SO_3$, $P(EO)_{10}LiCF_3SO_3$, $P(EO)_{20}LiCF_3SO_3$, and pure PEO.

**3.2. Poly(ethylene oxide)–$LiCF_3SO_3$.** The phase diagram of PEO–$LiCF_3SO_3$ has been previously reported.[7,22] At room temperature for salt concentrations up to 3:1, two phases are reported to be present, crystalline PEO and crystalline polymer–salt compound $P(EO)_3$:$LiCF_3SO_3$. Subsequent studies of the system have shown that in addition to these two phases an amorphous phase is present, and this amorphous phase is primarily where the ionic conductivity occurs.[4,5] Differences in the structures and properties of the PEO–$LiCF_3SO_3$ system have been observed and are attributed to differences in the molecular weight of the polymer,[23] the sample preparation method,[24] the thermal history,[25] and time.[26] Studies of pure PEO demonstrate the importance of molecular weight on the morphology and the degree of crystallinity.[27,28] For PEO–salt systems with different molecular weights of PEO, different relative amounts of ionic species were observed,[23] and the relative amounts of ionic species are dependent on temperature and time.[26] For samples with same salt concentration, various thermal histories were found to give different ionic conductivities.[25] These observed differences highlight the overall importance of kinetics, particularly crystallization kinetics, for both crystalline PEO and crystalline $P(EO)_3$:$LiCF_3SO_3$, in determining the state of the system.

To examine the local structure of the room-temperature amorphous phase of high molecular weight PEO–$LiCF_3SO_3$, films with a 10:1 and 20:1 composition were compared to crystalline $P(EO)_3$:$LiCF_3SO_3$ and crystalline PEO. The X-ray data are presented in Figure 5. We note that the X-ray data for this study are different than reported in a previous study,[7] and we attribute the difference to the different molecular weight of PEO used and different heating temperature and time used. The comparison of the 10:1 and 20:1 samples to pure PEO shows that both samples contain domains of crystalline PEO. Comparison of the 20:1 sample to crystalline $P(EO)_3$:$LiCF_3SO_3$ shows that the sample contains no

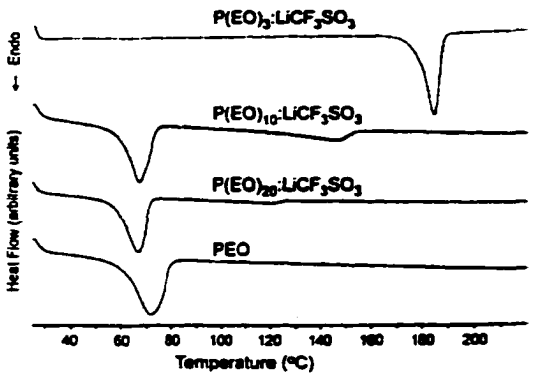


Figure 6. DSC thermograms of the crystalline $P(EO)_3:LiCF_3SO_3$ compound and films of $P(EO)_{10}LiCF_3SO_3$, $P(EO)_{20}LiCF_3SO_3$, and pure PEO.

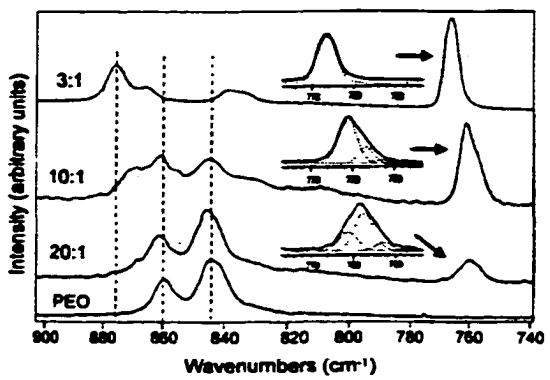


Figure 7. Raman spectra of crystalline $P(EO)_3:LiCF_3SO_3$, PEO–$LiCF_3SO_3$ complex with an ether oxygen:lithium ratio of 10:1, and pure PEO in the region 700–900 $cm^{-1}$. The expanded views are curve-fitting analysis of the $\delta_s(CF_3)$ region.

diffraction peaks that can be identified with the 3:1 crystalline compound. It is possible that this sample contains domains of crystalline $P(EO)_3:LiCF_3SO_3$ whose sizes are sufficiently small so that distinct peaks are not observed. In the 10:1 sample a few diffraction peaks are observed which coincide with peaks of the 3:1 compound. However, there are at least two peaks that are not present in the 3:1 crystal, suggesting that there is ordering present in the 10:1 sample that is different than the ordering present in the crystal. This ordering may be due to regions or domains with a structure similar to but not identical with structure in the crystalline $P(EO)_3:LiCF_3SO_3$. Possible structures will be discussed further below. As in the case for the 20:1 sample, the 10:1 sample may also contain domains of crystalline $P(EO)_3:LiCF_3SO_3$ whose sizes are sufficiently small so that distinct peaks are not observed.

DSC thermograms of the 10:1 and 20:1 samples are compared to thermograms of pure PEO and $P(EO)_3:LiCF_3SO_3$ in Figure 6. Both the 10:1 and 20:1 films clearly show the presence of an endotherm peak at 66 °C corresponding to the melting of crystalline PEO. The higher temperature of the melting endotherm in pure PEO compared to the melting endotherm in the PEO–LiTf films may be explained by the large crystallite sizes in pure PEO and the relatively fast heating rate. The 10:1 sample has a weak endotherm peak at 145 °C, and the 20:1 sample has a very weak endotherm peak at 120 °C. According to the phase diagram, these peaks indicate the presence of very small amounts of the crystalline $P(EO)_3:LiCF_3SO_3$ compound. A comparison of the data for the 10:1 and 20:1 films to previous DSC studies of the system[4,5,29] shows that the specific sample preparation used for this study, most notably heating below the melting point of PEO, produces very small amounts of the $P(EO)_3:LiCF_3SO_3$ phase.

Raman spectra of the 10:1 and 20:1 samples are shown in Figure 7. The $\delta_s(CF_3)$ region can be deconvolved into a minor "free" ion component at 753 $cm^{-1}$, a contribution from contact ion pairs at 757 $cm^{-1}$, and a dominant band at 761 $cm^{-1}$ originating in the $[Li_2CF_3SO_3]^+$ entity. The relative percent of these species is summarized in Table 4. The 10:1 sample has more of the $[Li_2CF_3SO_3]^+$ aggregate and less of the ion pair species compared to the 20:1 sample. We again note that the relative amounts of the three components may depend on the sample preparation, thermal history, and aging. The crystalline $P(EO)_3:LiCF_3SO_3$ compound has only a single band at 766 $cm^{-1}$,[12] also shown in Figure 7. The frequency of this band, 766 $cm^{-1}$, is higher than the frequency observed for the $[Li_2CF_3SO_3]^+$ aggregate in the diglyme:$LiCF_3SO_3$ crystal and for similar species in solution, 763 $cm^{-1}$,[18] and we attribute the higher frequency to crystal packing effects present in the $P(EO)_3:LiCF_3SO_3$ compound. Support for the well-ordered potential energy environment of the triflate anion in the $P(EO)_3:LiCF_3SO_3$ crystal is the frequency difference between the Raman and infrared bands which indicates a modest amount of dynamical coupling.[12] The observed frequency of the $[Li_2CF_3SO_3]^+$ species, 761 $cm^{-1}$, in both the 10:1 and 20:1 sample argues that the local potential energy environment of the triflate anion is different than that present in the crystal. This analysis is supported by the X-ray data for the 10:1 sample which shows different $d$ spacings than are present in the crystal.

Also shown in Figure 7 are the mixed $CH_2$ rocking and CO stretching modes. Bands in the 10:1 sample at 861 and 845 $cm^{-1}$ (second and third dashed lines) are easily identified as contributions from the crystalline PEO fraction, whose spectrum in this region is also shown. Of particular interest in the 10:1 sample is the band at 870 $cm^{-1}$ and a broad feature at approximately 830 $cm^{-1}$; these features can be identified with bands at 875 (first dashed line) and 836 $cm^{-1}$ in the 3:1 crystalline compound. Therefore, the local conformational structure of the polymer backbone in the 10:1 material is similar to, but not identical with, the analogous structure in the crystalline compound. This difference again reflects, in part, the disordered nature of the system. The broad band between 800 and 820 $cm^{-1}$, which appears in the Raman spectra of PEO above its melting point,[30] shows that the amorphous phase contains a distribution of backbone conformational sequences similar to PEO in the melt. The spectra of the 20:1 sample in this region show bands at 861 and 845 $cm^{-1}$ due to PEO and show a slight shoulder on the high-frequency side of the 860 $cm^{-1}$ band. The 20:1 sample has no observable bands which can be clearly identified with the $P(EO)_3:LiCF_3SO_3$ compound.

We consider the nature of the local structures present in the 10:1 and 20:1 samples. Within the PEO–$LiCF_3SO_3$ films there exists crystalline PEO, small domains

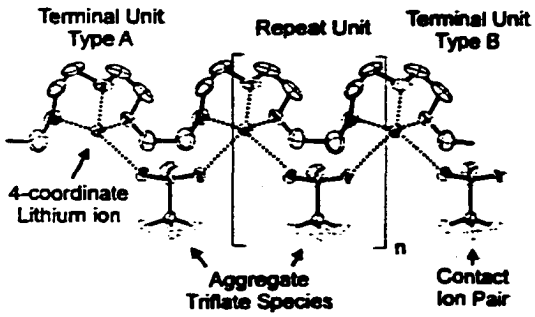


**Figure 8.** Pictorial representation of proposed localized complex occurring in 10:1 PEO–$LiCF_3SO_3$. For ease of graphic representation, the adjoining segments of the PEO chain are represented in an unfavored conformation. A more accurate pictorial representation would have the PEO chain in a tgt-tg't-tgt conformation with the $CF_3$ end of the triflate anions on opposite sides of the chain. Hydrogen atoms are not shown in the diagram.

of crystalline $P(EO)_3$:$LiCF_3SO_3$, and a disordered phase. We earlier noted the two additional peaks seen in the X-ray data of the 10:1 sample and suggested that these result from a small amount of ordering present in the (primarily) disordered phase. It is not impossible that these reflections originate in a second ordered phase, although no such phase has ever been reported, especially at this salt concentration. Comparison of the 10:1 and 20:1 PEO–$LiCF_3SO_3$ films to the crystalline $P(EO)_3$:$LiCF_3SO_3$ compound shows that clear differences are present: the X-ray data show different diffraction peaks, the frequency of the $[Li_2CF_3SO_3]^+$ aggregate is different, and the frequencies of $CH_2$ rocking and CO stretching bands do not directly coincide with those present in the crystal. However, the frequency of aggregate species observed in the $\delta_s(CF_3)$ mode and the 10:1 X-ray data suggest that a local structure is present which is similar to the local structure present in the crystalline $P(EO)_3$:$LiCF_3SO_3$ phase. Therefore, we propose that within the disordered phase there exist numerous small regions (we will refer to such a region as a localized complex) where a few lithium ions and triflate ions form local structures with the polymer backbone that resemble the crystalline $P(EO)_3$:$LiCF_3SO_3$ phase. This perspective is supported by comparison of $^{13}C$ chemical shifts in amorphous PEO and crystalline $P(EO)_3$:$LiCF_3SO_3$ which suggest that a similar coordination of lithium to the ether oxygens is present in the amorphous phase as is present in $P(EO)_3$:$LiCF_3SO_3$.[31] Details of the proposed local structure are described below. Specifically, each lithium ion is 3-fold coordinated by adjacent polymer oxygen atoms. Further, as in the crystal, triflate ions link adjacent lithium ions, leading to 5-fold coordinate lithium ions and triflate ions vibrating as $[Li_2CF_3SO_3]^+$ entities. A representation of a localized complex is presented in Figure 8. The complex consists of $n$ repetitions of a repeat unit bounded with terminal groups on each end. The repeat unit is essentially the local structure found in crystalline $P(EO)_3$:$LiCF_3SO_3$. The localized complex may be quite small ($n = 0$) or may be an extended structure ($n$ = large). The terminal unit of the localized complex contains either a four-coordinate lithium ion and a terminal $[Li_2CF_3SO_3]^+$ entity (type A) or a five-coordinate lithium ion and a terminal Li–$CF_3SO_3$ contact ion pair (type B). As a sidenote, we envision a critical, early step in the growth of the crystalline $P(EO)_3$:$LiCF_3SO_3$ compound to occur through the extension and coalescence of these localized regions to form long chain lengths of the line compound. The formation of microcrystalline domains then results when several of these extended regions are brought into translational registry through attractive interchain forces, although the domain size may be so small as to yield only weak, extremely broad features in an X-ray diffraction measurement.

We also assume the existence of isolated species such as $[Li_2CF_3SO_3]^+$ units, Li–$CF_3SO_3$ contact ion pairs, and solvent-separated ion pairs (spectroscopically "free" ions) along the chain. We propose a local structure of the isolated contact ion pair to be analogous to the structure proposed for the diglyme–LiTf solution (Figure 4) with the ethylene oxide repeat units replacing the terminal methyl groups present in diglyme.

**3.3. Implications for Ionic Transport in High MW PEO–$LiCF_3SO_3$.** We consider the role of these local structures in ionic transport. The terminal unit of a localized complex, an isolated $[Li_2CF_3SO_3]^+$ species, and an isolated contact ion pair each contains 4-fold coordinate lithium ions. A "free" lithium ion may have an even lower effective coordination number. These lithium ions are coordinated by a potential energy environment that is dynamically disordered through polymer segmental motion and presumably less deep than 5-fold coordinated lithium in crystalline domains of $P(EO)_3$:$LiCF_3SO_3$. In the spirit of the dynamic bond percolation (DBP) model,[3,32] it follows that polymer segmental motion is more likely to open transient conduction pathways for lithium ions with relative low coordination numbers. Therefore, we argue that 4-fold coordinate lithium ions as part of a terminal unit of a localized complex, an isolated $[Li_2CF_3SO_3]^+$ species, and a contact ion pair species contribute to the ionic conductivity in the amorphous phase. We wish to emphasize that it is not the contact ion pair itself that contributes to the conductivity, because the diffusion of a neutral, discrete contact ion species would not contribute to the ionic conductivity as is well-known. Instead, the contribution comes from the lithium ion (and triflate ion) resulting from a dissociative process that underscores the dynamical nature of the equilibrium between the various ionic species present. We note that the time scale of the dissociative process of contact ion pairs, whether isolated or part of a localized complex, is a critical factor in their contribution to the ionic conductivity.

The involvement of the anion in ionic transport in these systems is supported by transference number measurements[33–35] and recent neutron scattering experiments.[36] From spectroscopic studies it is known that the anion exists as a "free" ion, a Li–$CF_3SO_3$ contact ion pair, and a $[Li_2CF_3SO_3]^+$ entity on a time scale of at least several vibrational periods (femtoseconds). It is also important to recognize the important role played by the terminal units of a localized complex in the transport of anions. Consider a localized complex with a terminal Li–$CF_3SO_3$ contact ion pair such as a type B structure shown in Figure 4. The potential energy environment of the triflate anion is defined primarily by the interaction with the cation of the contact ion pair; there is only a very weak interaction with the polymer itself. This is a marked contrast to the much stronger interaction of the cation with its coordinative environment of oxygen atoms. As a consequence, we expect the

transport mechanism of the triflate ion to be significantly different than that of the cation. A similar conclusion follows from considering an isolated contact ion pair. In both instances the arguments presented here would result in a highly labile anion. This perspective supported by measurements of the cation and anion diffusion coefficients in PEO–$LiCF_3SO_3$ which show that the anion is more mobile than the cation.[37,38] The actual contribution to the ionic conductivity might be mediated by other factors such as the steric interaction of the anion with the host matrix.

## 4. Conclusions

We have isolated and characterized a crystalline phase of diglyme–$LiCF_3SO_3$. In the diglyme:$LiCF_3SO_3$ crystal, the local environment of the Li ion and the torsional angle sequence of the bonds in the ethylene oxide units are remarkably similar to those present in the high molecular weight $P(EO)_3$:$LiCF_3SO_3$ compound. A comparison of the Raman bands in a 10:1 diglyme–$LiCF_3SO_3$ solution to the Raman bands in the diglyme:$LiCF_3SO_3$ crystal suggests that in the solution Li may be four-coordinate.

Raman, X-ray data, and DSC data of PEO–$LiCF_3SO_3$ films prepared at several compositions show that local structures are present which are similar but not identical with local structures present in the $P(EO)_3$:$LiCF_3SO_3$ crystal. Further work to determine the specific ordering which is observed in the 10:1 sample is currently in progress. We propose that in the "amorphous" phase of the polymer–salt system there exist microscopic domains of salt-rich regions whose local structures may resemble the crystalline compound phase. These microscopic domains may be localized regions of a single polymer chain as described above or even several adjacent localized regions in translational registry. In any case the cations and anions at the boundaries of these salt-rich regions are relatively mobile because of two factors: their potential energy environments are less attractive than in the interior of the microscopic domains, and those environments are dynamically disordered through the increased motion of the polymer chains in the interface. Therefore, we suggest that the ions at the domain boundaries make a significant contribution to the ionic conductivity, although we emphasize that this model does not necessarily describe the sole mechanism of ionic transport in polymer salt systems. Finally, we note that although this model has been developed for the PEO–$LiCF_3SO_3$ system, its general features can be extended to describe ionic transport in other polymer–salt electrolytes.

**Acknowledgment.** We acknowledge Masood Kahn for his assistance with the single X-ray diffraction analysis. This work was partially supported by funds from the Oklahoma Center for the Advancement of Science and Technology, Contract No. 5377. We appreciate the assistance of Scott Boesch in the ab initio calculations.

**Supporting Information Available:** Single X-ray diffraction data file (.cif file) containing fractional coordinates and additional structural information. This material is available free of charge via the Internet at http://pubs.acs.org.

## References and Notes

(1) Papke, B. L.; Ratner, M. A.; Shriver, D. F. *J. Electrochem. Soc.* **1982**, *129*, 1434–1438.
(2) Armand, M. B.; Chabagno, J. M.; Duclot, M. J. Polyethers as solid electrolytes. In *Fast Ion Transport in Solids*; Vashista, P., Mundy, J. M., Shenoy, G. K., Eds.; Elsevier: Amsterdam, 1979; pp 131–136.
(3) Ratner, M. A.; Nitzan, A. *Faraday Discuss. Chem. Soc.* **1989**, *88*, 19–42.
(4) Berthier, C.; Gorecki, W.; Minier, M. *Solid State Ionics* **1983**, *11*, 91–95.
(5) Minier, M.; Berthier, C.; Gorecki, W. *J. Phys. (Paris)* **1984**, *45*, 739–744.
(6) Stainer, M.; Hardy, L. C.; Whitmore, D. H.; Shriver, D. F. *J. Electrochem. Soc.* **1984**, *131*, 784–790.
(7) Robitaille, C. D.; Fauteux, D. *J. Electrochem. Soc.* **1986**, *133*, 315–325.
(8) Lightfoot, P.; Mehta, M. A.; Bruce, P. G. *Science* **1993**, *262*, 883–885.
(9) Frech, R.; Huang, W. *Macromolecules* **1995**, *28*, 1246–1251.
(10) Sutjianto, A.; Curtiss, L. A. *J. Phys. Chem. A* **1998**, *102*, 968–974.
(11) Johansson, P.; Tegenfedlt, J.; Lindgren, J. *J. Phys. Chem. A* **1998**, *102*, 4660–4665.
(12) Rhodes, C. P.; Frech, R. *Solid State Ionics* **2000**, *136–137*, 1131–1137.
(13) Papke, B. L.; Ratner, M. A.; Shriver, D. F. *J. Phys. Chem. Solids* **1981**, *42*, 493–500.
(14) Schantz, S.; Sandahl, J.; Borjesson, L.; Torell, L. M.; Stevens, J. R. *Solid State Ionics* **1988**, *28–30*, 1047–1053.
(15) Frech, R.; Huang, W. *Solid State Ionics* **1994**, *72*, 103–107.
(16) Huang, W.; Frech, R.; Wheeler, R. A. *J. Phys. Chem.* **1994**, *98*, 100–110.
(17) Peterson, G.; Jacobsson, P.; Torell, L. M. *Electrochim. Acta* **1992**, *37*, 1495–1497.
(18) Yoshida, H.; Matsuura, H. *J. Phys. Chem. A* **1998**, *102*, 2691–2699.
(19) Matsuura, H.; Fukuhara, K. *J. Polym. Sci., Part B* **1986**, *24*, 1383–1400.
(20) Murcko, M. A.; DiPaola, R. A. *J. Am. Chem. Soc.* **1992**, *114*, 10010–10018.
(21) Petrowsky, M.; Rhodes, C. P.; Frech, R. *J. Solution Chem.*, submitted.
(22) Vallée, A.; Besner, S.; Prudhomme, J. *Electrochim. Acta* **1992**, *37*, 1579–1583.
(23) Brodin, A.; Mattsson, B.; Nilsson, K.; Torell, L. M.; Hamara, J. *Solid State Ionics* **1996**, *85*, 111–120.
(24) Weston, J. E.; Steele, B. C. H. *Solid State Ionics* **1982**, *7*, 81–88.
(25) Yang, L.; Zhang, A.; Qiu, B.; Yin, J.; Liu, Q. *Solid State Ionics* **1988**, *28–30*, 1029–1031.
(26) Chintapalli, S.; Frech, R. *Electrochim. Acta* **1998**, *43*, 1395–1400.
(27) Godovsky, Y. K.; Slonimsky, G. L.; Garbar, N. M. *J. Polym. Sci., Part C* **1972**, *38*, 1–21.
(28) Maclaine, J. Q. G.; Booth, C. *Polymer* **1975**, *16*, 680–684.
(29) Frech, R.; Chintapalli, S.; Bruce, P. G.; Vincent, C. A. *Macromolecules* **1999**, *32*, 808–813.
(30) Maxfield, J.; Shepherd, I. W. *Polymer* **1975**, *16*, 505–509.
(31) Spevacek, J.; Dybal, J. *Macromol. Rapid Commun.* **1999**, *20*, 435–439.
(32) Druger, S. D.; Ratner, M. A.; Nitzan, A. *Solid State Ionics* **1983**, *9 & 10*, 1115–1120.
(33) Bouridah, A.; Dalard, F.; Deroo, D.; Armand, M. B. *J. Appl. Electrochem.* **1987**, *17*, 625–634.
(34) Munshi, M. Z. A.; Owens, B. B.; Nguyen, S. *Polym. J.* **1988**, *20*, 597–602.
(35) Walls, H. J.; Zawodzinski, T. A. J. *Electrochem. Solid-State Lett.* **2000**, *3*, 321–324.
(36) Mao, G.; Perea, R. F.; Howells, W. S.; Price, D. L.; Saboungi, M.-L. *Nature* **2000**, *405*, 163–165.
(37) Bhattacharja, S.; Smoot, S. W.; Whitmore, D. H. *Solid State Ionics* **1986**, *18 & 19*, 306–314.
(38) Boden, N.; Leng, S. A.; Ward, I. M. *Solid State Ionics* **1991**, *45*, 261–270.

MA001749X

# V

*Submitted to the Journal of Physical Chemistry, November 2001*
*Reproduced with permission*


# Structural investigation of crystalline and solution phases of monoglyme:lithium triflate systems

Christopher P. Rhodes, Masood A. Khan and Roger Frech*
*Department of Chemistry and Biochemistry*
*University of Oklahoma, Norman, OK 73072*

Michael Ruf
*Bruker AXS, Inc.*
*Madison, WI 53711-5373*

ABSTRACT: Two crystalline phases of monoglyme and lithium triflate have been isolated and characterized. DSC thermograms reveal the transition temperatures of the crystalline phases. The crystal structure was determined at room temperature and at 153 K and confirmed the phase transition. However, the structure at both temperatures is similar with only differences in conformation and packing of the monoglyme and triflate anion. The stoichiometry for both temperatures is monoglyme:$(LiCF_3SO_3)_2$. The conformation of monoglyme in both phases is trans-trans-trans, which represents a different monoglyme conformation interacting with $Li^+$ in a condensed phase than previously reported. The spectral comparison of the two crystals shows the $\delta_s(CF_3)$ and $\nu_s(SO_3)$ modes provide complementary information about the local environment of the triflate anion. The spectroscopic comparison of the monoglyme:$(LiCF_3SO_3)_2$ crystalline phase at 295 K to solutions of monoglyme-$LiCF_3SO_3$ shows that the structure present in the crystalline phase is distinctly different from the structure in solution.

## 1. Introduction

Polymer electrolytes have been widely studied for use in electrochemical devices, especially rechargeable lithium batteries.[1-5] For battery applications, the technological challenge is to develop a polymer electrolyte system that has a high room temperature ionic conductivity, a high cation transference number, desirable mechanical properties, and interfacial and electrochemical stability. To meet these requirements, new systems such as composite polymer electrolytes,[6,7] single ion conductors,[8] and new polymer electrolyte systems[9] continue to be developed. Systems based on poly(ethylene oxide), PEO, with dissolved inorganic salts continue to be of significant interest since PEO shows a particular propensity to solvate and transport ions. In addition to systems based on pure PEO, various polymer architectures containing ethylene oxide units have been investigated.[10-14] Ionic transport in a number of PEO-salt systems has been shown to occur primarily in the amorphous phase[15,16] and is strongly coupled to the segmental motion of the polymer backbone.[17,18]

The mechanism of ionic transport in polymer electrolytes is still not well understood, and a fundamental understanding of ion-ion and ion-polymer interactions is needed. The importance of ion-ion interactions is apparent from transference number measurements,[19] diffusion coefficients,[20,21] and the failure of the Nernst-Einstein relationship to describe the experimental ionic conductivity.[22-25] Negative cation transference number measurements which result from cations being transported by anionic clusters have been reported.[26-28] In some polymer-salt systems, at high salt concentrations a transport mechanism which is different than the mechanism at low salt concentrations is suggested by measurements of the temperature-dependent cation diffusion coefficients.[23] It has been suggested that ionic transport in these systems may occur via cation hopping between ionic clusters [23] and/or correlated motion of cations and anions.[29,30] Determining the local structure of the amorphous phase provides a basis for understanding of the mechanism of ionic transport and contributes to the rational synthesis of new materials.

One approach used to understand the local structure in polymer electrolytes is to study polymer-salt crystalline phases.[31,32] The study of crystalline polymer-salt compounds has yielded considerable insight into the coordination environment of the cation and anion as well as the conformation of the polymer backbone.[33] The structure of polymer-salt crystalline phases has been used to suggest local structures in the amorphous phase of these systems.[34-37] In addition, studies of crystalline phases[38] and recent results showing enhanced conductivity in stretched polymer electrolyte films[39,40] suggest that ionic transport may be enhanced along certain ordered pathways.

Another useful approach is to study low molecular weight analogs of PEO, namely glycol dimethoxy ethers (abbreviated as glymes) with the general formula $CH_3(OCH_2CH_2)_nOCH_3$ where usually $n \leq 6$. Glyme-salt systems are useful structural models of PEO-salt systems,[41-46] and have also been used to model dynamical behavior and transport properties.[47-50] Monoglyme is a useful conformational model for PEO,[51-58] and the conformational properties of monoglyme have been studied in all phases.[59-65] Monoglyme-salt systems have also been used to model structure and dynamics of PEO-salt systems.[66-70]

To gain insight into the local structure of polymer electrolytes, we have combined the strategies of studying crystalline phases and glymes to study glyme-salt crystalline phases. Crystalline glyme-salt complexes serve to further our understanding of local structure in polymer electrolytes and specifically the changes in coordination and conformation due to different chain lengths. We have previously reported the crystalline phase of diglyme:lithium triflate and used the structure to provide insight into the ionically conducting phase of PEO-lithium triflate systems.[37] Crystalline phases of tetraethylene glycol dimethyl ether with cadmium chloride[71] and with mercuric chloride[72] have also been reported. Here we report x-ray structures and vibrational spectra of crystalline phases of monoglyme:lithium triflate and a spectroscopic comparison of the crystalline phase with monoglyme-lithium triflate solutions.

## 2. Experimental

Monoglyme (ethylene glycol dimethyl ether, 99.9%) was obtained from Aldrich and used as received. Lithium trifluoromethanesulfonate, $LiCF_3SO_3$, (99.995%), also called lithium triflate and abbreviated here as LiTf, was obtained from Aldrich and heated under vacuum at 120°C for 48 h prior to use. The reagents were stored and manipulated in a dry nitrogen glovebox (VAC, ≤ 1ppm $H_2O$). The salt was combined with the solvent in stoichiometric amounts to yield

**Table 1.** Data for crystalline phases of monoglyme:$(LiTf)_2$

| | G1:$(LiTf)_2$ "room temp" | G1:$(LiTf)_2$ "low temp" |
|---|---|---|
| Empirical formula | $C_6H_{10}F_6Li_2O_8S_2$ | $C_6H_{10}F_6Li_2O_8S_2$ |
| Temperature | 295(2) K | 153(2) K |
| Space group | P-1 | P-1 |
| Crystal system | Triclinic | Triclinic |
| a | 5.025(8) Å | 5.040(13) Å |
| b | 7.616(11) Å | 7.523(19) Å |
| c | 10.063(15) Å | 10.20(3) Å |
| α | 106.762(10)° | 105.427(17)° |
| β | 100.845(12)° | 98.596(19)° |
| γ | 93.514(12)° | 95.346(19)° |
| Volume | 359.4(9) $Å^3$ | 365.1(16) $Å^3$ |
| Density (calculated) | 1.858 $Mg/m^3$ | 1.828 $Mg/m^3$ |
| RI | 0.123 | 0.100 |

solutions of the desired ether oxygen to metal cation ratio (O:M). The solutions were stirred in the glovebox for at least 48 h prior to measurement. To prepare the monoglyme:LiTf crystals, LiTf was dissolved in monoglyme with a solution concentration of 7.7 M which represents an ether oxygen to metal cation ratio of 2.5:1. The solution was stirred for ~48 h and left inside the glovebox at room temperature. After a number of weeks, an intermediate gel-like phase appeared which then produced a crystalline phase after a number of months. Single crystals specimens were isolated from the concentrated solution.

For the x-ray diffraction (XRD) measurements, a colorless crystal with the dimensions of 1.05 mm × 0.734 mm × 0.730 mm mounted in a glass capillary was aligned on a Bruker SMART APEX CCD diffractometer (Platform with full three circle goniometer). Intensity measurements were performed using graphite monochromated Mo-$K_\alpha$-radiation. Data were collected at 295 K and 153 K. SMART was used for preliminary determination of the cell constants and data collection control. RLATT was used to separate reflections from different domains of a multiple twinned crystal. The intensities of reflections of a sphere were collected by a combination of 4 sets of exposures (frames). Each set had a different $\phi$ angle for the crystal and each exposure covered a range of 1° in $\omega$. A total of 720 frames were collected with an exposure time per frame of 30s. Determination of integral intensities and global cell refinement were performed with the Bruker SAINT (V6.02) software package using a narrow-frame integration algorithm. Two data

**Table 2.** Selected bond lengths (Å), bond angles (°) and torsional angles (°) for room temperature and low temperature crystalline phases of G1:$(LiTf)_2$.

| | G1:$(LiTf)_2$ "room temp" | G1:$(LiTf)_2$ "low temp" |
|---|---|---|
| *Bond distances* | | |
| Li-O1 | 1.894(16) | 1.931(18) |
| Li-O2 | 1.874(17) | 1.932(19) |
| Li-O3 | 1.872(16) | 1.94(2) |
| Li-O4 | 1.873(15) | 1.917(18) |
| C2-O4 | 1.355(14) | 1.415(14) |
| O4-C3 | 1.40(2) | 1.433(12) |
| C3-C3 | 1.51(4) | 1.51(2) |
| S1-O1 | 1.384(6) | 1.407(8) |
| S1-O2 | 1.399(7) | 1.420(8) |
| S1-O3 | 1.381(6) | 1.444(8) |
| C1-F1 | 1.266(13) | 1.315(15) |
| C1-F2 | 1.265(13) | 1.304(14) |
| C1-F3 | 1.268(12) | 1.312(13) |
| C1-S1 | 1.769(10) | 1.816(12) |
| *Bond angles* | | |
| O1-Li1-O2 | 109.0(8) | 106.2(9) |
| O1-Li1-O3 | 106.6(8) | 110.1(9) |
| O1-Li1-O4 | 107.8(8) | 108.6(9) |
| O2-Li1-O4 | 113.1(8) | 106.6(9) |
| O2-Li1-O3 | 110.8(8) | 106.6(9) |
| O3-Li1-O4 | 109.3(8) | 118.0(9) |
| C2-O4-C3 | 100.0(1) | 108.6(3) |
| O4-C3-C3 | 106(2) | 106.6(10) |
| C2-O4-Li1 | 116.3(9) | 115.2(8) |
| C3-O4-Li1 | 135.8(11) | 130.8(8) |
| Li1-O1-S1 | 141.4(6) | 127.3(7) |
| Li1-O2-S1 | 130.0(6) | 137.8(7) |
| Li1-O3-S1 | 130.4(6) | 126.7(7) |
| O1-S1-O2 | 115.4(4) | 114.6(5) |
| O1-S1-O3 | 115.0(4) | 114.4(4) |
| O2-S1-O3 | 113.7(4) | 115.2(4) |
| *Tors. angles* | | |
| C2-O4-C3-C3 | 175.2(2) | 176.1(8) |
| O4-C3-C3-O4 | 180.0(1) | 180.0(1) |
| O4-Li1-O2-S1 | -130.1(7) | -39.5(10) |
| O1-S1-C1-F1 | -178.3(8) | -179.5(5) |
| O3-S1-C1-F3 | -179.0(8) | -178.1(5) |
| S1-O2-Li1-O1 | -10.2(11) | -154.9(5) |
| O2-Li1-O4-C2 | -172.8(10) | -72.9(8) |

sets from the strongest diffracting domains of a multiple twinned crystal were obtained. GEMINI was used to remove reflections from one of the datasets, which were affected by overlap from the other dataset. A semi-empirical absorption correction was applied, based on the intensities of symmetry-related reflections measured at different angular settings using SADABS. The program suite SHELXTL (V5.1) was used for space group determination (XPREP), structure solution (XS) and refinement (XL). The structures were solved using direct methods and subsequent difference Fourier synthesis, and

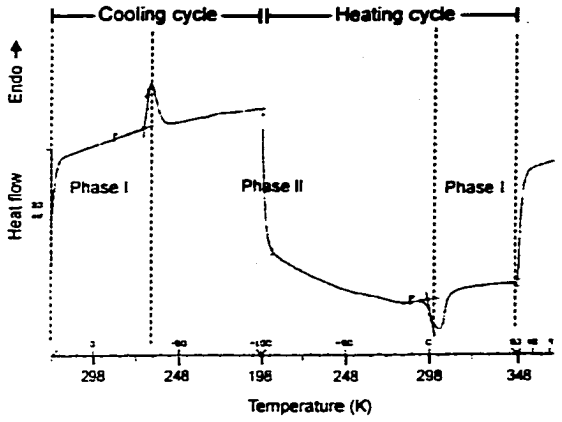


**Figure 1.** Differential scanning calorimetry thermogram of single crystal specimen of crystalline G1:$(LiTf)_2$ showing the presence of two crystalline phases and their phase transition temperatures for the cooling and heating cycles.

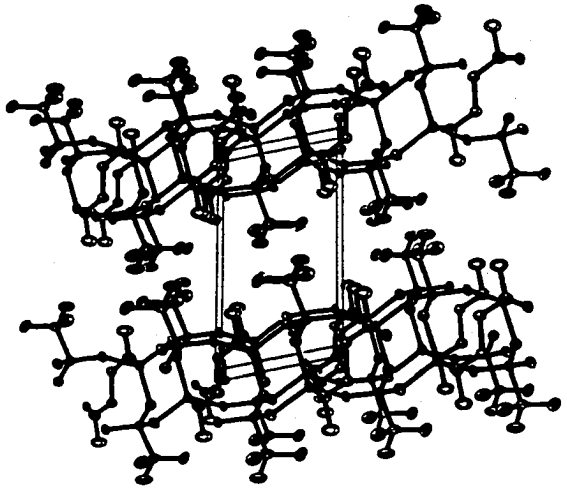

**Figure 2.** Packing diagram (projected parallel to the b-axis for crystalline phase of G1:$(LiTf)_2$ at 295 K. Hydrogen atoms are not shown in the diagram. The structure is networked by the triflate anion.

refined by full-matrix least squares on $F^2$. For the hydrogen atoms a riding model was employed under restriction of ideal geometry at the corresponding non-hydrogen atom attached. All non-hydrogen atoms were refined anisotropically. For the room temperature structure, the C3 atom of the monoglyme ligand was disordered and refined with 50% occupancy of the two disordered components. Further details of the structural refinement are presented in the supplemental information, Table VS.

Differential scanning calorimetry (DSC) thermograms were collected on a Mettler DSC 820 calorimeter under nitrogen purge in sealed aluminum crucibles. Specimens of the monoglyme:LiTf crystals were first cooled from 298 K to 198 K and then heated from 198 K to 348 K with a heating/cooling rate of 10 K/min. Raman scattering spectra were recorded on an I.S.A. Jobin-Yvon T64000 in the triple subtractive mode with a scan time of 16 s and 10 accumulations using a 180° geometry. The 514 nm line of an Argon laser focused through an 80x microscope lens was used for excitation. The laser was operated at 300 mW, measured at the laser head. Local heating of the sample by the focused beam was not observed in similar systems.[73] Since the specimens were single crystals, spectra were taken using different orientations of the crystal relative to the incoming beam. Only minor differences in relative intensities were observed for the different orientations. Raman spectra were collected at 298 K and198 K. The crystal was cooled from room temperature to -100 °C using a MMR Technologies K-20 Temperature Controller. Infrared spectra were recorded with a Bruker IFS66V FT-IR spectrometer over a range of 4000 $cm^{-1}$ to 400 $cm^{-1}$ with a resolution of 1 $cm^{-1}$. Mid-infrared spectra of the crystalline material were taken as KBr pellets in an evacuated sample chamber, and IR spectra of the monoglyme-LiTf solutions were obtained using ZnSe plates and a dry-air purged sample chamber. Bands were curve-fit by the Levenberg-Marquardt method using Galactic Grams software (ver. 5.2).

## 3. Results and Discussion

*3.1 Crystalline phases of monoglyme:$LiCF_3SO_3$*

A differential scanning calorimetry thermogram of a single crystal specimen is shown in Fig. 1. Data taken for the cooling cycle from 298 K to 198 K shows the presence of an endothermic peak with an onset temperature of 244 K. This endotherm is due to the enthalpy change due to the transformation from one crystalline phase (defined as Phase I) to another crystalline phase (defined as Phase II). Data for the heating cycle from 198 K to 348 K shows the presence of an exothermic peak with an onset temperature of 271 K. The exothermic peak is due to the enthalpy change associated with the transformation from the crystalline phase stable at low temperatures (Phase II) to the crystalline phase stable at room temperature (Phase I). The difference between the phase transformation temperature for the cooling cycle and the phase

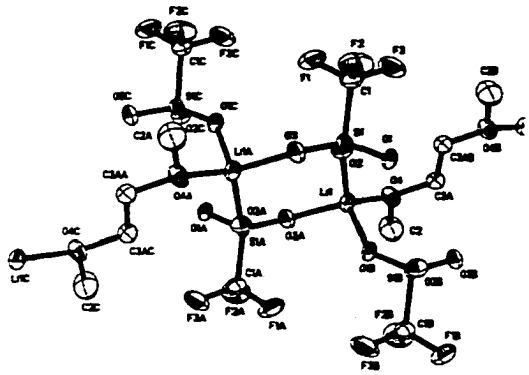

**Figure 3.** Crystal structure of G1:$(LiTf)_2$ at 295 K showing the trans-trans-trans conformation of the monoglyme and the four-fold coordination of lithium.

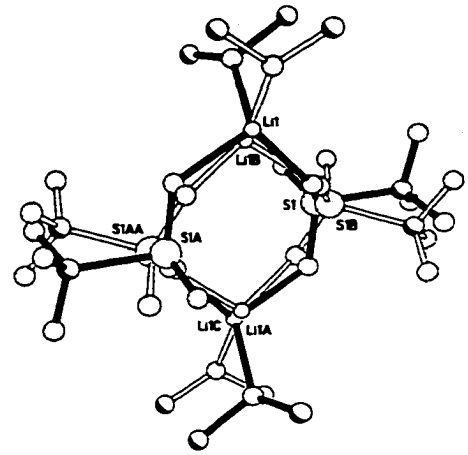

**Figure 4.** Visual comparison of the structures of the room temperature (white bonds) and low temperature (black bonds) crystalline phases of G1:$(LiTf)_2$ showing the different orientations of the triflate anion in the two compounds.

transformation temperature for the heating cycle can be attributed to the relatively fast heating rate and the kinetics of crystallization for the compounds.

The crystal structure was determined at 295 K and at 153 K and confirmed the phase change. Crystal data for the two temperatures are presented in Table 1. For both temperatures, the occupancy of the unit cell is one monoglyme and two lithium triflate ions, with the monoglyme situated at the inversion center. The stoichiometry for both temperatures is monoglyme:$(LiCF_3SO_3)_2$, abbreviated here as G1:$(LiTf)_2$, and the ether oxygen to cation ratio is 1:1. The unit cell parameters for the two temperatures shows an interesting feature of an increase in the volume of the unit cell at the lower temperature of 153 K, thus a decrease in the calculated density indicating a slightly more open structure at the lower temperature. Selected bond lengths, bond angles, and torsional angles for both structures are listed in Table 2. Figure 2 shows the packing diagrams indicating polymeric chain formation which runs along the crystallographic a-axis. Figure 3 shows the selected portion of the polymeric chain with the atomic labeling scheme. Both the room temperature and low temperature structures are similar in overall packing. Figures 2 and 3 show the room temperature structure; this is similar to the low temperature structure which also forms polymeric chains along the a-axis. However, there are small differences in the two structures in the conformation of the monoglyme ligand and the triflate anion as noted in Table 2 and shown in Figure 4.

In both the room temperature (RT) and the low temperature (LT) crystalline structures. lithium is coordinated to four oxygens, one oxygen from monoglyme and three oxygens from different triflate anions. In both of the crystals, the coordination geometry of the lithium can be described as a distorted tetrahedron as observed by the values of the O-Li-O angles. The conformation of monoglyme can be described by the values of the torsional angles for the bond sequences, C-O-C-C, O-C-C-O, C-C-O-C, where trans (180° ± 60°) is abbreviated by t and gauche (60° ± 60°) is abbreviated by g. In the RT and LT crystalline compounds the monoglyme molecule has a conformation of trans-trans-trans, ttt. The O-C-C-O angle in both crystals is 180.0(1)°, and the C-O-C-C angles are 175.2(2)° in the RT crystal and 176.1(8)° in the LT crystal. In both crystals, the monoglyme molecule sits on an inversion center within the unit cell, and each of the oxygen atoms of monoglyme is coordinated to a different lithium ion.

Monoglyme in a ttt conformation that coordinates $Li^+$ ions is interesting since quantum chemical calculations and spectroscopic studies of monoglyme complexed with cations have reported that the tgt conformation is favored to interact with cations. Quantum chemical calculations of tgt-$Li^+$ and ttt-$Li^+$ complexes shows the ttt-$Li^+$ complex is ~26 kcal/mol higher in energy than the tgt-$Li^+$ complex.[74,70] The

lower energy of the tgt-$Li^+$ complex can be attributed to coordination of both ether oxygens to the $Li^+$ by the monoglyme in a tgt conformation. The ttt conformation allows only one oxygen to coordinate to the lithium ion. Computational and experimental studies of pure monoglyme have shown that the ttt conformer is the most stable conformer in the gas phase,[75,52,53] and the energy difference between the ttt and tgt conformers is around 0.2 kcal/mol. However, in the liquid phase the preferred conformation is tgt rather than ttt,[65,58] and in the crystalline phase of pure monoglyme the conformation of the molecule is tgt.[64] A critical factor in stabilizing the ttt conformer within the G1:$(LiTf)_2$ RT and LT crystals is the contribution of the triflate anions and solid state packing effects.

*3.2 Vibrational spectra of crystalline phases*

Since the x-ray structures of the G1:$(LiTf)_2$ room temperature and low temperature crystals have been determined, the vibrational spectra provide mode frequencies of these specific structures. In turn, these frequency-structure correlations can be used to analyze systems where the structure is not known. In particular, the analysis of the frequencies of the anion and monoglyme modes provides insight into local structure. Previous experimental and computational studies have established that modes of the triflate anion are sensitive to the interaction of the triflate anion with one or more cations.[76,77] In particular, the symmetric $SO_3$ stretching mode, $\nu_s(SO_3)$, and the symmetric $CF_3$ deformation mode, $\delta_s(CF_3)$, have been used to probe the local potential energy environment of the triflate anion in polymer electrolyte systems.

In both the room temperature and low temperature G1:$(LiTf)_2$ crystal structures, there are two triflate anions in a unit cell and their vibrational modes are not isolated, but rather correlated through intermolecular forces. The factor group correlation method provides a description of the symmetries and selection rules of the correlated modes. We have previously applied the factor group correlation method to describe the symmetries of anion modes in crystalline polymer electrolytes and glyme:salt compounds.[73,78] The presence of multiple bands in the $\nu_s(SO_3)$ and $\delta_s(CF_3)$ regions in crystalline $P(EO)_3$:LiTf and P(EO):NaTf has been previously observed by us and has been interpreted as arising from dynamical coupling of the multiple triflate anions in the unit cell.[73] Using this method, modes of the isolated triflate

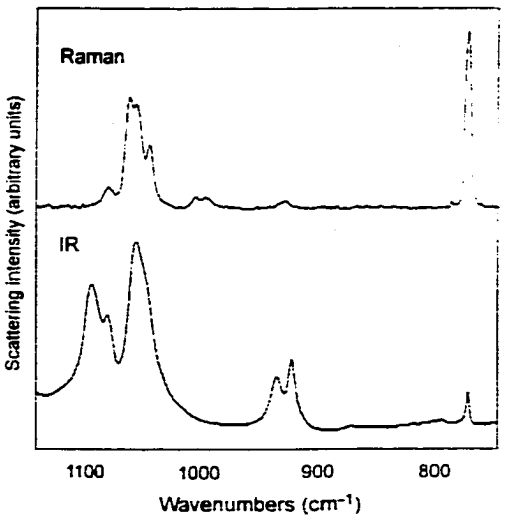


**Figure 5.** Raman and IR spectra in the 750-1150 $cm^{-1}$ region of crystalline G1:$(LiTf)_2$ at 295 K

anion, belonging to point group $C_{3v}$, are correlated to the site group, which is the symmetry of the center of mass of the anion and is of trivial symmetry in this instance. These modes are then correlated to the factor group, which is isomorphous to the space group of the crystal, $P\bar{1}$ in this case. Here we consider the $\delta_s(CF_3)$ and $\nu_s(SO_3)$ modes which are of $A_{1g}$ symmetry in the isolated triflate anion. A single mode with $A_{1g}$ symmetry in the isolated triflate anion under $C_{3v}$ point group symmetry results in two modes with symmetries given by

$$\Gamma_{FG} = A_g + A_u . \qquad (1)$$

The $A_g$ mode is Raman active and the $A_u$ mode is IR active.

Raman and IR spectra of the room temperature crystalline phase in the 700-1200 $cm^{-1}$ region are presented in Fig. 5. Bands observed at 770 $cm^{-1}$ in the Raman and 769 $cm^{-1}$ in the IR correspond to the $\delta_s(CF_3)$ mode of the triflate anion in the crystalline phase. The experimental spectra show the presence of a single Raman-active mode and a single IR-active mode, as predicted by the symmetry analysis. The x-ray structure of the room temperature crystalline phase reveals that within the crystal the triflate anion is coordinated to three lithium ions with one lithium coordinated to each of the three triflate oxygens. Spectral evidence for a triflate species with similar coordination environment was observed in a solution of LiTf

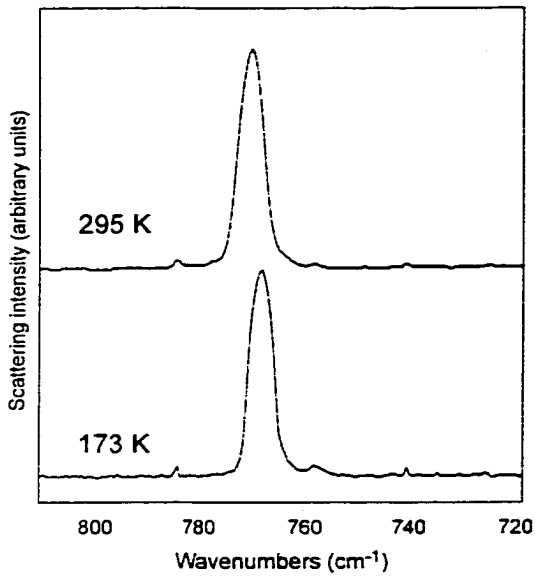


**Figure 6.** Comparison of the Raman spectra of room temperature (300 K) and low temperature (173 K) G1:$(LiTf)_2$ crystals in the $\delta_s(CF_3)$ regions.

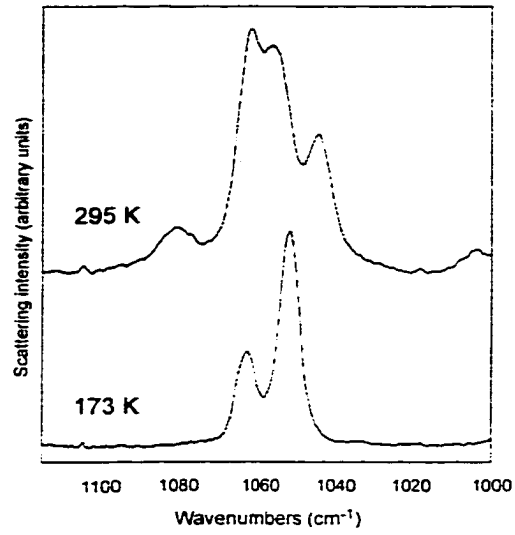


**Figure 7.** Comparison of the Raman spectra of room temperature (295 K) and low temperature (173 K) G1:$(LiTf)_2$ crystals in the $\nu_s(SO_3)$ regions which shows different bands and frequencies due to the different structures of the crystals.

in 2-methyltetrahydrofuran, where this species had a frequency of the 767 $cm^{-1}$.[79] The structure and frequency of $\delta_s(CF_3)$ mode within the RT crystal provides evidence for the existence of a $[Li_3Tf]^{2+}$ species and supports the earlier frequency assignment. The higher frequency of the triflate anion species in the RT crystal, 770 $cm^{-1}$, compared to its frequency in solution, 767 $cm^{-1}$, can be attributed to crystal packing effects.

The frequency of the $\nu_s(SO_3)$ mode has also been used as a probe of the local environment of the triflate anion. In the $\nu_s(SO_3)$ region, spectra of the RT crystal presented in Fig 5 shows Raman-active bands at 1062, 1056, and 1044 $cm^{-1}$ and IR-active bands at 1095 $cm^{-1}$, 1081 $cm^{-1}$ and 1056 $cm^{-1}$ with a low frequency shoulder. The Raman-active band at 1062 $cm^{-1}$ is attributed to the C-O and C-C stretching of monoglyme in a ttt conformation.[59,56] The band at 1044 $cm^{-1}$ is also assigned to a monoglyme mode. Support for this assignment is provided by calculations of vibrational modes of a ttt-$Li^+$ complex, which shows a monoglyme band in this frequency region.[70] The 1056 $cm^{-1}$ band in the Raman and 1056 $cm^{-1}$ band in the IR are assigned to the $\nu_s(SO_3)$ modes of the triflate anions in the unit cell. The presence of a single Raman-active band and a single IR-active band is consistent with the symmetry analysis describe by eq. 1.

Monoglyme modes in the 800-1000 $cm^{-1}$ region, which are sensitive to the conformational sequences, have been used to examine the presence of various conformers[59,80,56] and determine preferred conformations that interact with cations.[41,70] The IR spectra of the room temperature crystal presented in Fig. 5 shows the presence of two bands in this region with frequencies of 933 and 920 $cm^{-1}$. The bands are absent in the Raman spectra which can be attributed to the fact that monoglyme occupies an inversion center in the crystal. The frequencies of these bands have reasonable agreement to the calculated frequencies for ttt[59,56] and ttt-$Li^+$,[70] bearing in mind that that these calculated frequencies are for an isolated monoglyme molecule and an isolated monoglyme-$Li^+$ complex, respectively. Hence, neither of the aforementioned complexes represents the actual potential energy environment of monoglyme in the room temperature crystal.

The structural differences between the room temperature and low temperature crystals have been described above. It is of interest to determine how the vibrational spectra differ between the two crystalline phases. Fig. 6 shows Raman spectra in the $\delta_s(CF_3)$ region of the room temperature crystal (295 K) and the low

temperature crystal (173 K). The frequency of the $\delta_s(CF_3)$ mode in the RT crystal, 770 $cm^{-1}$, is almost identical to the frequency of the $\delta_s(CF_3)$ mode in the LT crystal, 768 $cm^{-1}$. However as presented in Fig. 7, differences in the $\nu_s(SO_3)$ region are observed between the two crystalline phases. The RT crystal has bands at 1062, 1056, and 1044 $cm^{-1}$, and the LT crystal has bands at 1063 and 1052 $cm^{-1}$. The 1063 $cm^{-1}$ and 1052 $cm^{-1}$ bands in the LT crystal correspond to the 1062 and 1056 $cm^{-1}$ bands, respectively, in the RT crystal. Comparing the RT and LT spectra, the frequency change of 1056 to 1052 $cm^{-1}$ is attributed to differences in the local potential energy environment of the triflate anion in the two structures. The absence of the 1044 $cm^{-1}$ band may result from the different potential energy environment of the monoglyme in the LT structure. In particular, the coordination geometry of monoglyme to $Li^+$ is different between the two structures. However, the complete absence of this band in the LT spectrum is a little surprising given the degree of similarity of the two crystal structures.

*3.3 Comparison of crystalline phase to solution*

The spectral comparison of the crystalline phase to monoglyme-LiTf solutions allows a determination of whether local structures present in the crystalline phase persist in solution. In Fig. 8, the IR spectrum of the RT crystal is compared to IR spectra of monoglyme-LiTf solutions in the $\delta_s(CF_3)$ region. The crystalline phase has a single IR-active band at 769 $cm^{-1}$. This frequency results from the potential energy environment of the triflate anion within the RT crystal, where the triflate is coordinated to three lithium ions. Spectra of the monoglyme-LiTf solutions in the $\delta_s(CF_3)$ region can be curve-fit to bands at 766, 762 $cm^{-1}$, 757 and 753 $cm^{-1}$. These band frequencies correspond to triflate anions that are coordinated to three, two, one and no lithium ions, respectively.[79] The relative intensities of the curve-fit bands depend on the salt concentration. The 766 $cm^{-1}$ band is a very minor component in the 5:1 and 10:1 solutions and this band is nearly absent in the 20:1 and 40:1 solutions. The 766 $cm^{-1}$ band identifies the presence of a triflate species in solution with a local structure that is similar to the local structure in the room temperature crystalline phase. The weak intensity of the 766 $cm^{-1}$ band indicates that this species is not the predominant local structure in solution. The predominant band in the monoglyme-LiTf solutions occurs at 757 $cm^{-1}$,

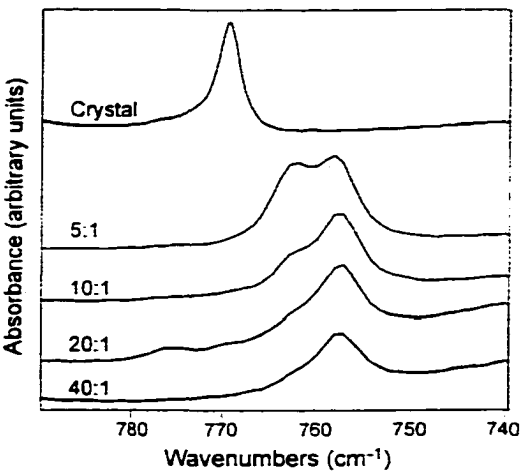


**Figure 8.** IR spectra of crystalline G1:$(LiTf)_2$ at 295 K and monoglyme-LiTf solutions in the $\delta_s(CF_3)$ region. The concentrations of the solutions are represented by the ether oxygen to metal cation ratio (O:M).

which corresponds to a contact ion pair species. The band at 762 $cm^{-1}$, corresponding to a local structure of a triflate anion coordinated to two lithium ions, is also present, and the relative intensity of this band increases with increasing salt concentration. The 753 $cm^{-1}$ "free" ion band has a weak intensity, and its relative intensity decreases with increasing salt concentration. The $\nu_s(SO_3)$ region (not shown) shows similar behavior, however the analysis in this frequency region is complicated by overlapping monoglyme bands .

The spectral comparison of the G1:$(LiTf)_2$ RT crystal and monoglyme-LiTf solutions in the 800-1000 $cm^{-1}$ region is presented in Fig. 9. This spectral region also shows the clear difference between the structure in solution and in the crystal. The bands at 920 and 933 $cm^{-1}$ in the crystalline monoglyme:LiTf RT crystal are assigned to mixed C-O stretching and $CH_2$ rocking modes of monoglyme in a ttt conformation, as described previously. In the monoglyme-LiTf solutions, bands from both monoglyme uncoordinated to $Li^+$ and monoglyme coordinated to $Li^+$ are present. Monoglyme uncoordinated to $Li^+$ exists in a number of conformations and therefore a number of bands are present due to the uncoordinated monoglyme. The bands at 938 and 923 $cm^{-1}$ present in the monoglyme-LiTf solutions are due to monoglyme in ttt and ttg conformations

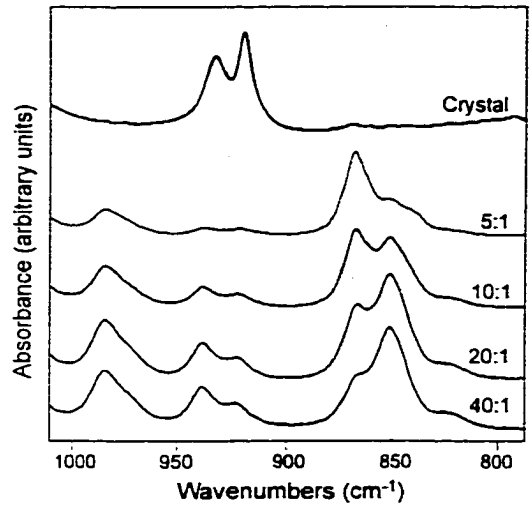


**Figure 9.** IR spectra of crystalline G1:$(LiTf)_2$ at 295 K and monoglyme-LiTf solutions in the 800-1000 $cm^{-1}$ region. The concentrations of the solutions are represented by the ether oxygen to metal cation ratio (O:M).

respectively, and the 852 $cm^{-1}$ band is due to monoglyme in tgt and tgg conformations.[59,56] The band which results from the interaction of monoglyme with LiTf occurs at 869 $cm^{-1}$ and increases in intensity with increasing salt concentration. This band has been identified with monoglyme in a tgt conformation interacting with $Li^+$ and possibly with one or more triflate anions.[41,70] From the analysis of this spectral region, it is clear that in solution monoglyme in a tgt conformation interacts with $Li^+$, and in the crystal monoglyme in a ttt conformation interacts with $Li^+$.

## 4. Conclusions

Two crystalline phases of G1:$(LiTf)_2$ have been identified and characterized. In both phases, lithium is coordinated to one ether oxygen and three triflate oxygens, while the triflate anion is coordinated to three lithium ions. The crystal structure supports earlier evidence for a three-coordinate triflate anion in solution, i.e. $[Li_3Tf]^{2+}$. In the crystals the cation is four-fold coordinate; due to the interaction with three triflate oxygen atoms, a lithium ion can only interact with one of the monoglyme oxygen atoms. Crystal packing effects then result in each monoglyme coordinating two lithium ions.

The conformation of the monoglyme in the crystals is trans-trans-trans, and this conformation is different than previously reported conformations of monoglyme coordinated to cations. To our knowledge, this is the only experimental structure that shows a ttt conformation of monoglyme interacting with $Li^+$ in a solid phase. The two structures are different in their relative positions of the monoglyme and triflate anions within the unit cell.

The factor group correlation method is used to describe the dynamical coupling of the vibrations of the triflate anions in the unit cell. The number and symmetry of triflate bands in the $\delta_s(CF_3)$ and $\nu_s(SO_3)$ regions correspond well to those predicted by the symmetry analysis. The structural differences between the two structures result in small frequency shifts in the $\delta_s(CF_3)$ and $\nu_s(SO_3)$ modes. The spectral comparison of the G1:$(LiTf)_2$ crystal phase to monoglyme-LiTf solutions shows that the predominant triflate anion environment and the monoglyme conformation present in solution are very different than the triflate anion environment and the monoglyme conformation present in the crystalline phase. In solution, the conformation of monoglyme is tgt rather than ttt, and the predominant ionic species in solution are the contact ion pair and $[Li_2Tf]^+$ aggregate. However, the $Li^+$ coordination environments and monoglyme conformations present in these crystalline phases and in solution may also exist in PEO-salt systems, particularly in the amorphous phase where a multiplicity of conformations and ionic environments has been measured.


## Acknowledgements

This work was partially supported by the Oklahoma Center for the Advancement of Science and Technology, Contract # 5377.


## References


(1) Armand, M. B.; Chabagno, J. M.; Duclot, M. J. Polyethers as solid electrolytes. In *Fast Ion Transport in Solids*; Vashista, P., Mundy, J. M., Shenoy, G. K., Eds.; Elsevier: Amsterdam, 1979; pp 131.

(2) *Polymer Electrolyte Reviews*; MacCallum, J. R.; Vincent, C. A., Eds.; Elsevier Applied Science: New York, 1987; Vol. 1, pp 351.

(3) *Polymer Electrolyte Reviews*; MacCallum, J. R.; Vincent, C. A., Eds.; Elsevier Applied Science: New York, 1989; Vol. 2, pp 338.

(4) Meyer, W. H. *Adv. Mater.* **1998**, *10*, 439.

(5) Dias, F. B.; Plomb, L.; Veldhuis, J. B. J. *J. Power Sources* **2000**, *88*, 169.

(6) Capuano, F.; Croce, F.; Scrosati, B. *J. Electrochem. Soc.* **1991**, *138*, 1918.

(7) Croce, F.; Appetecchi, G. B.; Persi, L.; Scrosati, B. *Nature* **1998**, *394*, 456.
(8) Onishi, K.; Matsumoto, M.; Shigehara, K. *J. Power Sources* **2001**, *92*, 120.
(9) Wei, X.; Shriver, D. F. *Chem. Mater.* **1998**, *10*, 2307.
(10) Nagaoka, K.; Naruse, H.; Shinohara, I. *J. Polym. Sci., Polym. Lett.* **1984**, *22*, 659.
(11) Nishimoto, A.; Watanabe, M.; Ikeda, Y.; Kohjiya, S. *Electrochim. Acta* **1998**, *43*, 1177.
(12) Qiao, J.; Chen, Y.; Baker, G. L. *Chem. Mater.* **1999**, *11*, 2542.
(13) Allcock, H. R.; Napierala, M. E.; Olmeijer, D. L.; Best, S. A.; Merz, K. M., Jr. *Macromolecules* **1999**, *32*, 732.
(14) Imrie, C. T.; Ingram, M. D.; McHattie, G. S. *Adv. Mater.* **1999**, *11*, 832.
(15) Minier, M.; Berthier, C.; Gorecki, W. *J. Physique* **1984**, *45*, 739.
(16) Berthier, C.; Gorecki, W.; Minier, M. *Solid State Ionics* **1983**, *11*, 91.
(17) Ratner, M. A.; Nitzan, A. *Faraday Discuss. Chem. Soc.* **1989**, *88*, 19.
(18) Nitzan, A.; Ratner, M. A. *J. Phys. Chem.* **1994**, *98*, 1765.
(19) Walls, H. J.; Zawodzinski, T. A. J. *Electrochem. Solid-State Lett.* **2000**, *3*, 321.
(20) Bhattacharja, S.; Smoot, S. W.; Whitmore, D. H. *Solid State Ionics* **1986**, *18&19*, 306.
(21) Lindsey, S. E.; Whitmore, D. H.; Halperin, W. P. *Polym. Prepr. (Am. Chem. Soc., Div. Polym. Chem.)* **1989**, *30*, 442.
(22) Bruce, P. G. *Faraday Discuss. Chem. Soc.* **1989**, *88*, 43.
(23) Arumugam, S.; Shi, J.; Tunstall, D. P.; Vincent, C. A. *J. Phys.: Condens. Matter* **1993**, *5*, 153.
(24) McLin, M. G.; Angell, C. A. *J. Phys. Chem. B* **1996**, *100*, 1181.
(25) Ferry, A.; Orädd, G.; Jacobson, P. *J. Chem. Phys.* **1998**, *108*, 7426.
(26) Ma, Y.; Doyle, M.; Fuller, T. F.; Doeff, M. M.; Jonghe, L. C. D.; Newman, J. *J. Electrochem. Soc.* **1995**, *142*, 1859.
(27) Ferry, A.; Doeff, M. M.; DeJonghe, L. C. *Electrochim. Acta* **1998**, *43*, 1387.
(28) Doeff, M. M.; Georen, P.; Qiao, J.; Kerr, J.; De Jonghe, L. C. *J. Electrochem. Soc.* **1999**, *146*, 2024.
(29) Boden, N.; Leng, S. A.; Ward, I. M. *Solid State Ionics* **1991**, *45*, 261.
(30) Bruce, P. G.; Vincent, C. A. *J. Chem. Soc. Faraday Trans.* **1993**, *89*, 3187.
(31) Papke, B. L.; Ratner, M. A.; Shriver, D. F. *J. Phys. Chem. Solids* **1981**, *42*, 493.
(32) Lightfoot, P.; Mehta, M. A.; Bruce, P. G. *Science* **1993**, *262*, 883.
(33) Bruce, P. G. *Electrochim. Acta* **1995**, *40*, 2077.
(34) Latham, R. J.; Linford, R. G. *Solid State Ionics* **1996**, *85*, 193.
(35) Frech, R.; Chintapalli, S.; Bruce, P. G.; Vincent, C. A. *Chem. Commun.* **1997**, 157.
(36) Frech, R.; Chintapalli, S.; Bruce, P. G.; Vincent, C. A. *Macromolecules* **1999**, *32*, 808.
(37) Rhodes, C. P.; Frech, R. *Macromolecules* **2001**, *34*, 2660.
(38) Andreev, Y. G.; Bruce, P. G. *Electrochim. Acta* **2000**, *45*, 1417.
(39) Chung, S. H.; Wang, Y.; Greenbaum, S. G.; Golodnitsky, D.; Peled, E. *Electrochem. Solid State Lett.* **1999**, *2*, 553.
(40) Golodnitsky, D.; Livshits, E.; Rosenberg, Y.; Peled, E.; Chung, S. H.; Wang, Y.; Bajue, S.; Greenbaum, S. G. *J. Electroanal. Chem.* **2000**, *491*, 203.
(41) Frech, R.; Huang, W. *Solid State Ionics* **1994**, *72*, 103.
(42) Frech, R.; Huang, W. *Macromolecules* **1995**, *28*, 1246.
(43) Huang, W.; Frech, R.; Johansson, P.; Lindgren, J. *Electrochim. Acta* **1995**, *40*, 2147.
(44) Gejji, S. P.; Johansson, P.; Tegenfeldt, J.; Lindgren, J. *Comput. Polym. Sci.* **1995**, *5*, 99.
(45) Johansson, P.; Tegenfeldt, J.; Lindgren, J. *Polymer* **1999**, *40*, 4399.
(46) Johansson, P. *Polymer* **2001**, *42*, 4367.
(47) Johansson, P.; Tegenfedlt, J.; Lindgren, J. *J. Phys. Chem. A* **1998**, *102*, 4660.
(48) Sutjianto, A.; Curtiss, L. A. *J. Phys. Chem. A* **1998**, *102*, 968.
(49) Baboul, A. G.; Redfern, P. C.; Sutjianto, A.; Curtiss, L. A. *J. Am. Chem. Soc.* **1999**, *121*, 7220.
(50) Mujica, V.; Malaver, M.; Ruette, F. *J. Phys. Chem. A* **1999**, *103*, 89.
(51) Murcko, M. A.; DiPaola, R. A. *J. Am. Chem. Soc.* **1992**, *114*, 10010.
(52) Smith, G. D.; Jaffe, R. L.; Yoon, D. Y. *J. Phys. Chem.* **1993**, *97*, 12752.
(53) Jaffe, R. L.; Smith, G. D.; Yoon, D. Y. *J. Phys. Chem.* **1993**, *97*, 12745.
(54) Smith, G. D.; Jaffe, R. L.; Yoon, D. Y. *J. Am. Chem. Soc.* **1995**, *117*, 530.
(55) Liu, H.; Muller-Plathe, F.; van Gunsteren, W. F. *J. Chem. Phys.* **1995**, *102*, 1722.
(56) Yoshida, H.; Matsuura, H. *J. Phys. Chem. A* **1998**, *102*, 2691.
(57) Bedrov, D.; Smith, G. D. *J. Chem. Phys.* **1998**, *109*, 8118.
(58) Goutev, N.; Ohno, K.; Matsuura, H. *J. Phys. Chem. A* **2000**, *104*, 9226.

(59) Ogawa, Y.; Ohta, M.; Sakakibara, M.; Matsuura, H.; Harada, I.; Shimanouchi, T. *Bull. Chem. Soc. Japan* **1977**, *50*, 650.
(60) Astrup, E. E. *Acta. Chem. Scand. , Ser. A* **1979**, *33*, 655.
(61) Abe, A.; Tasaki, K. *J. Mol. Struct.* **1986**, *145*, 309.
(62) Abe, A.; Inomata, K. *J. Mol. Struct.* **1991**, *245*, 399.
(63) Tsuzuki, S.; Uchimaru, T.; Tanabe, K.; Hirano, T. *J. Phys. Chem.* **1993**, *97*, 1346.
(64) Yokoyama, Y.; Uekusa, H.; Ohashi, Y. *Chem. Lett.* **1996**, *6*, 443.
(65) Williams, D. J.; Hall, K. B. *J. Phys. Chem.* **1996**, *100*, 8224.
(66) Payne, V. A.; Xu, J.; Forsyth, M.; Ratner, M. A.; Shriver, D. F.; Leeuw, S. W. D. *Electrochim. Acta* **1995**, *40*, 2087.
(67) Ray, D.; Feller, D.; More, M. B.; Glendening, E. D.; Armentrout, P. B. *J. Phys. Chem.* **1996**, *100*, 16116.
(68) Boinske, P. T.; Curtiss, L.; Halley, J. W.; Lin, B.; Sutjianto, A. *J. Comput.-Aided Mater. Des.* **1996**, *3*, 385.
(69) Hill, S. E.; Feller, D.; Glendening, E. D. *J. Phys. Chem. A* **1998**, *102*, 3813.
(70) Boesch, S. E.; Rhodes, C. P.; Frech, R.; Wheeler, R. A. to be submitted to *Phys. Chem. Comm.*
(71) Iwamoto, R. *Bull. Chem. Soc. Japan* **1973**, *46*, 1114.
(72) Iwamoto, R.; Wakano. H. *J. Am. Chem. Soc.* **1976**, *98*, 3764.
(73) Rhodes, C. P.; Frech, R. *Solid State Ionics* **2000**, *136-137*, 1131.
(74) Smith, G. D.; Jaffe, R. L.; Partridge, H. *J. Phys. Chem. A* **1997**, *101*, 1705.
(75) Yoshida, H.; Kaneko, I.; Matsuura, H.; Ogawa, Y.; Tasumi, M. *Chem. Phys. Lett.* **1992**, *196*, 601.
(76) Schantz, S.; Sandahl, J.; Borjesson, L.; Torell, L. M.; Stevens, J. R. *Solid State Ionics* **1988**, *28-30*, 1047.
(77) Huang, W. Ion-Ion and Ion-Polymer Interactions in Polyether Salt Complexes. Ph.D. Dissertation, University of Oklahoma, 1994.
(78) Rhodes, C. P.; Frech, R. *Macromolecules* **2001**, *34*, 1365.
(79) Huang, W.; Frech, R.; Wheeler, R. A. *J. Phys. Chem.* **1994**, *98*, 100.
(80) Matsuura, H.; Fukuhara, K. *J. Polym. Sci. B* **1986**, *24*, 1383.

# VI

*Submitted to the Journal of Physical Chemistry, November 2001*
*Reproduced with permission*


# Crystalline phases of poly(ethylene oxide) oligomers and sodium triflate: changes in coordination and conformation with chain length

Christopher P. Rhodes, Masood Khan and Roger Frech

*Department of Chemistry and Biochemistry*
*University of Oklahoma, Norman, OK 73072*

ABSTRACT: Crystalline phases of monoglyme:$NaCF_3SO_3$, diglyme:$NaCF_3SO_3$ and tetraglyme:$NaCF_3SO_3$ have been characterized by DSC, x-ray diffraction and vibrational spectroscopy. The comparison of the structures allows the investigation of the effect of the number of ethylene oxide units on local structure in these systems. The cation environments, anion environments and glyme conformations of the three compounds are compared with each other and to the high molecular weight crystalline poly(ethylene oxide):$NaCF_3SO_3$ compound. The cation coordination number varies from 5 to 7 and consists of varying contributions of ether and triflate oxygens. Higher coordination numbers are observed with increasing numbers of ethylene oxide units. Similar conformational sequences are observed in the structures. The comparison of the vibrational spectra of the compounds reveal differences in the $\nu_s(SO_3)$ and $\delta_s(CF_3)$ modes related to the different potential energy environments of the triflate anion in the compounds.

## 1. Introduction

Research on polymer electrolytes continues to be of significant interest due to potential applications in rechargeable batteries and other electrochemical devices.[1-5] Polymer electrolytes offer the possibility of an all solid state battery and provide improved safety over liquid electrolytes. The mechanism of ionic transport in polymer electrolyte systems is not well understood. Studies have shown that in polymer electrolytes with flexible backbones ionic transport is highly coupled to relaxation processes of the polymer backbone.[6,7] A number of results also suggest that in some systems the anion plays a role in the transport of cations, either through correlated motion of cations and anions or via transport of cation-anion clusters.[5,8-10] Understanding the relationship between ionic transport and local structures is essential to improving the transport properties of these materials.

Systems based on poly(ethylene oxide), PEO, with dissolved alkali metal salts have received considerable attention as polymer electrolytes. For a number of PEO-salt systems, multiple phases are present depending on the temperature and salt concentration, and phase diagrams have been previously reported.[11-14] The relative amounts of the phases depend on the molecular weight of the polymer,[15] sample preparation method,[16] thermal history[17] and time.[18] Crystalline polymer-salt compounds exist for numerous different PEO-salt systems.[19] Studies have shown that for a number of PEO-based electrolytes where crystalline and amorphous phases coexist, the ionic conductivity occurs primarily in the amorphous phase.[20-22] However, a recent study reported a higher ionic conductivity for a crystalline phase compared to an amorphous phase of the same system.[23] For polymer-salt systems, the higher conductivity of a crystalline phase compared to an amorphous phase underscores the importance of examining the structure and transport properties of crystalline phases. Crystalline polymer-salt compounds have provided significant insight into the local structure of polymer electrolytes, particularly the nature of cation-polymer and cation-anion interactions.[24,25] Polymer-salt compounds are useful models of the amorphous phase, and a number of studies have shown that local structures occurring in the crystalline phase persist in the amorphous phase.[26-28]

We are interested in the effect of chain length on structure and transport properties and

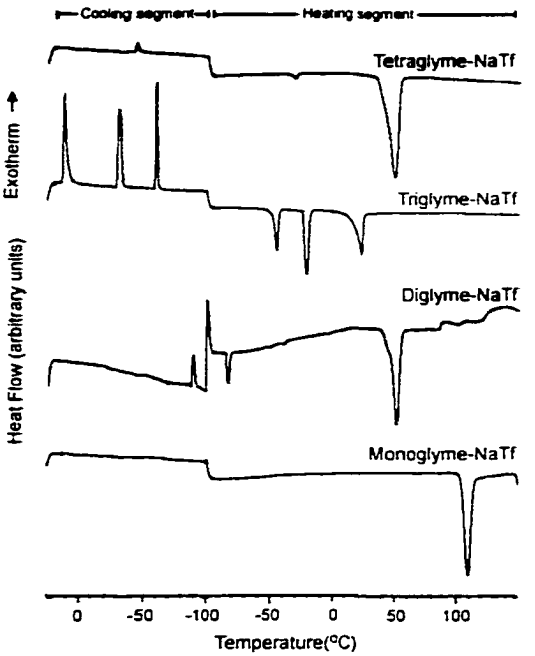


**Figure 1.** Differential scanning calorimetry thermograms of specimens of monoglyme:NaTf, diglyme:NaTf, triglyme:NaTf, and tetraglyme:NaTf showing the presence of crystalline phases and their phase transition temperatures for the cooling and heating segments.

have used systems of salts dissolved in low molecular weight oligomers to examine structure in polymer electrolytes. For PEO, the low molecular weight analogs are glycol dimethoxy ethers (abbreviated as glymes) with the general formula $CH_3(OCH_2CH_2)_nOCH_3$ where generally $n \leq 6$. Here we consider glymes with n=1-4 which are well below the chain entanglement limit of $M_w$=3200 (n=22) reported for pure PEO.[5] Systems of glymes with dissolved salts serve as useful models of structure and dynamics of PEO-salt systems.[29-36] In addition, a number of polymer electrolytes with ethylene oxide units in side chains or present as a copolymer have been developed;[37-39] glyme-salt systems are also useful to model structure and dynamics in these polymer electrolytes. Systems of salts with polyphosphazenes bearing oligoethyleneoxy side groups demonstrate that the number of ethylene oxide units in the side groups has a definite effect of the ionic conductivity[38] and local structure.[40]

We have considered a series of monoglyme, diglyme, triglyme and tetraglyme hosts containing sodium triflate (NaTf) to study

**Table 1.** Data for crystalline phases of monoglyme:NaTf, diglyme:NaTf, and tetraglyme:NaTf

| | Monoglyme:NaTf | Diglyme:NaTf | Tetraglyme |
|---|---|---|---|
| Formula | $C_5H_{10}F_3NaO_5S$ | $C_7H_{14}F_3NaO_6S$ | $C_{11}H_{22}F_3N$ |
| Temperature | 173 K | 173 K | 173 K |
| Crystal system | Monoclinic | Orthorhombic | Monoclinic |
| Space group | $P2_1/c$ | $P2_12_12_1$ | $P2_1/c$ |
| a | 5.8784(6) Å | 8.625(2) Å | 15.3093(12 |
| b | 17.3462(15) Å | 10.560(2) Å | 9.6185(7) Å |
| c | 10.8042(12) Å | 14.637(4) Å | 12.6945(13 |
| α | 90.00° | 90.00° | 90.00° |
| β | 92.891(8) ° | 90.00° | 107.549(7) |
| γ | 90.00° | 90.00° | 90.00° |
| Unit cell volume | 1100.3(2) Å$^3$ | 1333.1(6) Å$^3$ | 1782.3(3) Å |
| Density (calculated) | 1.583 Mg/m$^3$ | 1.526 Mg/m$^3$ | 1.470 Mg/m |
| $T_m$ (peak, DSC) | 109°C | 52°C | 49°C |
| R1 | 0.0514 | 0.0764 | 0.0372 |

the dependence of local structure on the number of ethylene oxide units in the oligomer. Here we report a series of crystalline phases of glyme-NaTf systems. We have previously reported a crystalline phase for diglyme:lithium triflate and used the crystalline and solution phases to provide insight into the amorphous phase of PEO-lithium triflate.[28] We have also reported two crystalline phases of monoglyme:lithium triflate.[41] Crystalline complexes of 1:1 tetraglyme-$HgCl_2$[42] and 1:2 tetraglyme-$CdCl_2$[43] have also been reported. It is of particular interest to compare the structures of glyme-NaTf crystalline phases to the structure of crystalline P(EO):NaTf.

Most of the research efforts on polymer electrolytes have focused on lithium-based systems, however systems based on other cations such as sodium have also received attention.[44-50] The study of a sodium salt with PEO oligomers furthers our efforts for developing sodium-based electrolytes.

## 2. Experimental

Ethylene glycol dimethyl ether (99.9%, monoglyme), di(ethylene glycol) dimethyl ether (99.5%, diglyme), tri(ethylene glycol) dimethyl ether (99%, triglyme) and tetra(ethylene glycol) dimethyl ether (99%, tetraglyme) were obtained from Aldrich and used as received. Sodium trifluoromethanesulfonate (97 %), also called sodium triflate and abbreviated here as NaTf, was obtained from Fluka and heated under vacuum at 120°C for 48 h prior to use. The reagents were stored and manipulated in a dry nitrogen glovebox (VAC, ≤ 1ppm $H_2O$). Solutions of monoglyme-NaTf, diglyme-NaTf, triglyme-NaTf and tetraglyme-NaTf were prepared by dissolving NaTf directly in the

**Table 2.** Selected bond lengths (Å), bond angles (°) and torsional angles (°) for crystalline monoglyme:NaTf.

| *Parameter* | *Value* |
|---|---|
| *Bond lengths* | |
| Na1-O1 | 2.370(2) |
| Na1-O2 | 2.382(2) |
| Na1-O3 | 2.313(3) |
| Na1-O4 | 2.300(3) |
| Na1-O5 | 2.261(3) |
| *Bond angles* | |
| O1-Na1-O2 | 69.16(9) |
| O3-Na1-O2 | 159.70(10) |
| O4A-Na1-O2 | 88.10(10) |
| O5A-Na1-O2 | 91.67(10) |
| O3-Na1-O1 | 91.10(10) |
| O4A-Na1-O1 | 121.05(11) |
| O5A-Na1-O1 | 115.30(11) |
| O4A-Na1-O3 | 98.71(10) |
| O5A-Na1-O3 | 101.44(10) |
| O5A-Na1-O4A | 119.13(11) |
| *Torsional angles* | |
| C1-O1-C2-C3 | 178.16(0.35) |
| O1-C2-C3-O2 | 51.34(0.48) |
| C2-C3-O2-C4 | 175.64(0.33) |

liquids and stirring the solutions for 48 h at room temperature. The concentrations of the solutions, described by the ether oxygen:sodium cation ratios, were 5:1, 5:1, 6:1 and 5:1 for the monoglyme-NaTf, diglyme-NaTf, triglyme-NaTf and tetraglyme-NaTf respectively. The monoglyme-NaTf and tetraglyme-NaTf were stored at room temperature, and the diglyme-NaTf and triglyme-NaTf solutions were stored at 4°C to promote crystal growth. After a number of weeks a gel-like phase appeared in the solutions. Crystalline phases formed from the gel-like phase after several months. Single crystal specimens from these solutions were isolated from the monoglyme-NaTf, diglyme-NaTf, and tetraglyme-NaTf gel phases.

The structures were solved by direct method using the SHELXTL system,[51] and refined by full-matrix least-squares on $F^2$ using all reflections. All the non-hydrogen atom were refined anisotropically and all the hydrogen atoms were included in the refinement with idealized parameters. The final R-factors were $R_1$=0.051 (monoglyme:NaTf), 0.076 (diglyme:NaTf structure), and 0.037 (tetraglyme:NaTf). Further details are provided in the supplemental information, Table VS.

DSC thermograms were collected on a Mettler DSC 820 calorimeter under nitrogen

**Table 3.** Selected bond lengths (Å), bond angles (°) and torsional angles (°) for crystalline diglyme:NaTf.

| *Parameter* | *Value* |
|---|---|
| *Bond lengths* | |
| Na1-O1A | 2.369(6) |
| Na1-O2 | 2.746(6) |
| Na1-O2A | 2.739(6) |
| Na1-O3 | 2.358(6) |
| Na1-O4 | 2.264(7) |
| Na1-O5A | 2.240(7) |
| *Bond angles* | |
| O1A-Na1-O2A | 65.86(18) |
| O1A-Na1-O3 | 85.7(2) |
| O1A-Na1-O4 | 110.4(3) |
| O1A-Na1-O5A | 104.2(3) |
| O2A-Na1-O3 | 147.5(2) |
| O2A-Na1-O4 | 78.1(2) |
| O2A-Na1-O5A | 88.3(2) |
| O3-Na1-O4 | 98.9(2) |
| O3-Na1-O5A | 114.8(3) |
| O4-Na1-O5A | 133.0(4) |
| O5A-Na1-O2 | 77.7(2) |
| O4-Na1-O2 | 88.0(2) |
| O3-Na1-O2 | 66.21(17) |
| O1A-Na1-O2 | 148.9(2) |
| O2A-Na1-O2 | 147.72(12) |
| *Torsional angles* | |
| C1-O1-C2-C3 | -174.5(7) |
| O1-C2-C3-O2 | 62.6(9) |
| C2-C3-O2-C4 | 172.6(6) |
| C3-O2-C4-C5 | 172.9(6) |
| O2-C4-C5-O3 | 67.0(7) |
| C4-C5-O3-C6 | 179.1(7) |

**Table 4.** Selected bond lengths (Å), bond angles (°) and torsional angles (°) for crystalline tetraglyme:NaTf.

| *Parameter* | *Value* |
|---|---|
| *Bond lengths* | |
| Na1-O1 | 2.502(2) |
| Na1-O2 | 2.456(2) |
| Na1-O3 | 2.452(2) |
| Na1-O4 | 2.533(2) |
| Na1-O5 | 2.433(2) |
| Na1-O6A | 2.403(2) |
| Na1-O8 | 2.367(2) |
| *Bond angles* | |
| O8-Na1-O6A | 169.94(6) |
| O8-Na1-O5 | 84.17(5) |
| O6A-Na1-O5 | 87.57(5) |
| O8-Na1-O3 | 98.49(6) |
| O6A-Na1-O3 | 83.19(5) |
| O5-Na1-O3 | 134.26(5) |
| O8-Na1-O2 | 91.33(5) |
| O6A-Na1-O2 | 98.48(6) |
| O5-Na1-O2 | 157.65(6) |
| O3-Na1-O2 | 68.03(5) |
| O8-Na1-O1 | 98.68(6) |
| O6A-Na1-O1 | 87.04(5) |
| O5-Na1-O1 | 90.04(5) |
| O3-Na1-O1 | 133.75(5) |
| O2-Na1-O1 | 68.96(5) |
| O8-Na1-O4 | 83.75(5) |
| O6A-Na1-O4 | 87.81(5) |
| O5-Na1-O4 | 67.84(5) |
| O3-Na1-O4 | 67.13(5) |
| O2-Na1-O4 | 133.53(5) |
| O1-Na1-O4 | 157.48(5) |
| *Torsional angles* | |
| C1-O1-C2-C3 | 90.65(0.23) |
| O1-C2-C3-O2 | 61.70(0.24) |
| C2-C3-O2-C4 | -178.60(0.18) |
| C3-O2-C4-C5 | 173.09(0.18) |
| O2-C4-C5-O3 | -63.66(0.24) |
| C4-C5-O3-C6 | -176.97(0.18) |
| C5-O3-C6-C7 | -175.75(0.17) |
| O3-C6-C7-O4 | 65.66(0.21) |
| C6-C7-O4-C8 | -171.32(0.16) |
| C7-O4-C8-C9 | 178.39(0.16) |
| O4-C8-C9-O5 | -64.43(0.20) |
| C8-C9-O5-C10 | 171.64(0.17) |

purge in sealed aluminum crucibles. Solid specimens were isolated from the monoglyme:NaTf, diglyme:NaTf and tetraglyme:NaTf solutions, and a gel-like specimen was isolated from the triglyme:NaTf solution. Samples were first cooled from 25°C to –100°C and then heated from -100°C to 50°C with a heating/cooling rate of 10 °C/min. Raman scattering spectra were recorded on an I.S.A. Jobin-Yvon T64000 in the triple subtractive mode with a scan time of 16 s and 10 accumulations using a 180° geometry. The 514 nm line of an Argon laser focused through an 80x microscope lens was used for excitation. The laser was operated at 300 mW measured at the laser head. Local heating of the sample by the focused beam was not observed in similar systems.[52]

## 3. Results and Discussion

### *3.1 Thermal analysis*

DSC thermograms of monoglyme-NaTf, diglyme-NaTf, triglyme-NaTf and tetraglyme-NaTf samples are presented in Fig. 1. The thermograms were taken in two segments: (a) a cooling segment from 25°C to -100°C, and (b) a heating segment from -100°C to 150°C. For the monoglyme:NaTf sample, the cooling segment showed no thermal events, and the heating segment showed the presence of an endotherm with an peak temperature of 109°C, which corresponds to the enthalpy of melting of the monoglyme:NaTf crystalline phase. For the diglyme:NaTf sample, the cooling segment shows an exotherm with a peak temperature of –89°C, and the heating segment has two endotherms with peak temperatures of –84°C and 52°C. The endotherm at 52°C is due to the

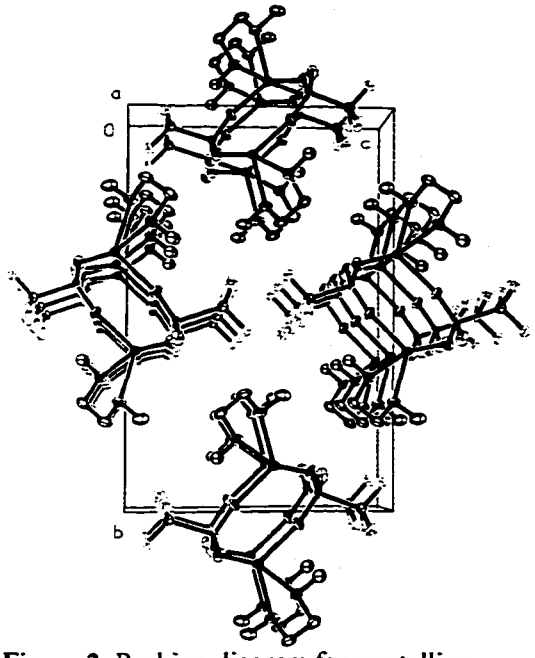


**Figure 2.** Packing diagram for crystalline phase of monoglyme:NaTf. Hydrogen atoms are not shown in the diagram.

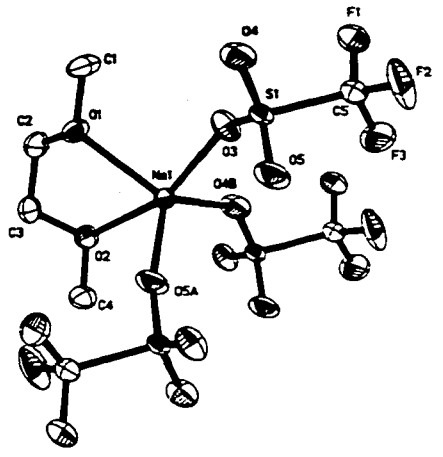


**Figure 3.** Crystal structure of monoglyme:NaTf showing tgt conformation of monoglyme and the five-fold coordination of sodium.

enthalpy of melting of the diglyme:NaTf crystalline phase. The origin of the exotherm at –89°C and the endotherm at –84°C is uncertain. The transition temperature does not coincide with the crystallization temperature for pure diglyme, –68°C.[53] The transition is apparently reversible and may be due to a structural phase transition of diglyme:NaTf. For the triglyme:NaTf sample, the cooling segment shows three exotherms with peak temperatures of 14°C, -30°C, and –59°C, and the heating segment shows three endotherms with peak temperatures of –44°C, -22°C and 23°C. The endotherm at –45°C and the exotherm at -59°C correspond to the melting and crystallization respectively of pure triglyme, -45°C,[53] which indicates that the sample contained uncomplexed triglyme in addition to a complex of triglyme:NaTf. The endotherms at –22°C and 23°C and the corresponding exotherms at -30°C and 14°C indicate the presence of two crystalline phases of triglyme:NaTf. The triglyme:NaTf sample was a gel at room temperature, in contrast to the other glyme-salt samples which were solids at room temperature. The temperature of the exotherm at 23°C explains the gel-like behavior observed at 25°C. We were not able to isolate single crystals of triglyme:NaTf adequate for a x-ray diffraction structure solution. For the tetraglyme:NaTf sample, the cooling segment shows an exotherm with a peak temperature of –46°C, and the heating segment shows the presence of two endotherms with peak temperatures of –30°C and 49°C. The endotherm at –30°C and the exotherm at -46°C correspond to the melting and crystallization respectively of pure tetraglyme, –27°C,[54] and the presence of these features indicates the presence of a small amount of pure tetraglyme in the sample. The endotherm at 49°C is attributed to enthalpy of melting for the crystalline phase of tetraglyme:NaTf. The melting temperatures of the monoglyme:NaTf, diglyme:NaTf and tetraglyme:NaTf compounds are presented in Table 1.

*3.2 X-ray structures*

*Monoglyme:NaTf.* Crystal data for the monoglyme:NaTf crystal is presented in Table 1. The empirical formula consists of one monoglyme and one sodium triflate, which represents an ether oxygen to cation ratio of 2:1. Selected bond length, bond angles and torsional angles are presented in Table 2. A packing diagram for crystalline monoglyme:NaTf showing the formation of chains along the a axis is presented in Fig. 2. A representation of the structure presented in Fig. 3 shows the cation coordination and monoglyme conformation. Each Na atom is bonded to five O atoms consisting of two oxygens from a single monoglyme and three oxygens from different triflate anions. The coordination geometry can be described as distorted trigonal bipyramid with the extent of the distortion judged from bond

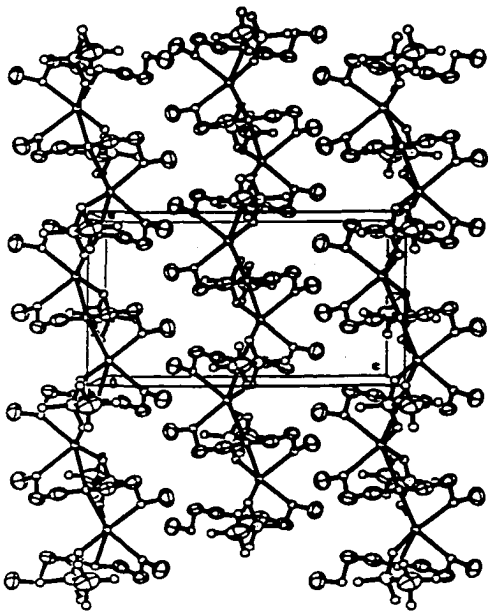

**Figure 4**. Packing diagram for crystalline phase of diglyme:NaTf. Hydrogen atoms are not shown in the diagram.

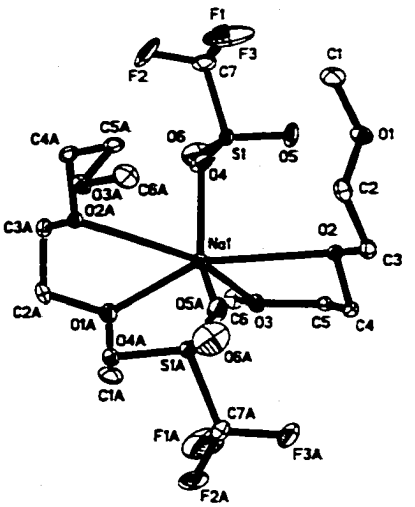


**Figure 5**. Crystal structure of diglyme:NaTf showing the tgttgt conformation of monoglyme and the six-fold coordination of sodium.

angles such as O3-Na1-O2 = 159.7(1)° (ideal value = 180.0°). Within the structure, each triflate anion is coordinated to three Na ions with each oxygen of the triflate coordinated to a Na atom in a monodentate fashion. The conformation of monoglyme can be described by the values of the torsional angles for C-O-C-C, O-C-C-O, C-C-O-C bond sequences where gauche (60° ± 60°) is abbreviated by g, trans (180° ± 60°) is abbreviated by t and gauche minus (270° ± 60°) is abbreviated by g'. In the monoglyme:NaTf structure, the conformation of the monoglyme is trans-gauche-trans (tgt).

*Diglyme:NaTf.* Crystal data for the diglyme:NaTf structure is presented in Table 1. The empirical formula consists of one diglyme and one NaTf which represents an ether oxygen to metal cation ratio of 3:1. Selected bond lengths, bond angles and torsional angles are presented in Table 3. A packing cell diagram of the structure is presented in Fig. 4 which shows that the molecules of diglyme:NaTf form chains along the crystallographic a-axis. Another representation of the structure is presented in Fig. 5 which shows the cation coordination and the diglyme conformation. Each Na atom is 6-coordinate consisting of four ether oxygens, two oxygens from two different diglyme molecules, and two triflate oxygens from different triflate anions. Each triflate anion is coordinated to two Na atoms. There is some local disorder in the triflate ion as indicated by large thermal motion of the F atoms. The conformation of diglyme in the structure is described by the torsional angle sequence tgttgt.

*Tetraglyme:NaTf.* Data for tetraglyme:NaTf is presented in Table 1. The empirical formula consists of one tetraglyme and one NaTf which represents an ether oxygen to metal cation ratio of 5:1. A packing diagram of the structure presented in Fig. 6 shows that the molecules forms chains along the c-axis. Another representation of the structure showing the cation coordination and the tetraglyme conformation is presented in Fig. 7. In the structure, each Na atom is bonded to seven O atoms consisting of five ether oxygens from a single tetraglyme and two oxygens from different triflate anions. The coordination geometry can be described as distorted pentagonal bipyramid with the extent of the distortion judged from bond angles such as O6A-Na1-O8 = 169.9.2(2)° (ideal value = 180.0°) and O5-Na1-O4 = 67.84(5) ° or O2-Na1-O1 = 68.96(2) ° (ideal values = 72.0°). In the crystal structure, each triflate anion is coordinated to two Na atoms. The conformation of tetraglyme in the structure is described by the torsional angle sequence tgttg'ttgttg'g'. This conformation results in the tetraglyme molecule wrapping around the Na atom in a manner similar to crown ethers.

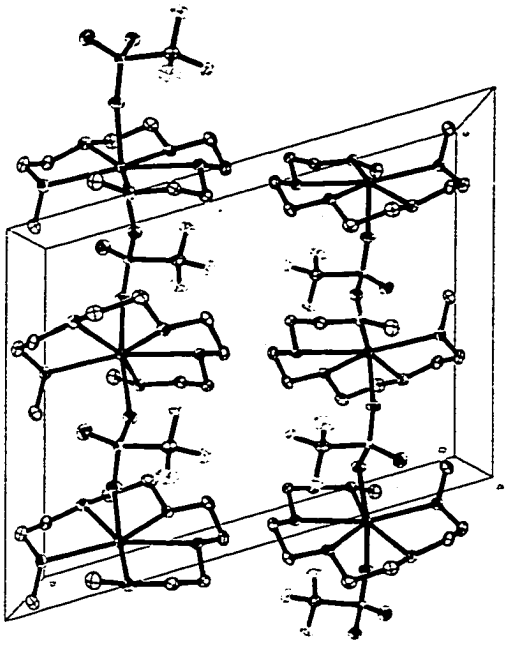

**Figure 6.** Packing diagram for crystalline phase of tetraglyme:NaTf. Hydrogen atoms are not shown in the diagram.

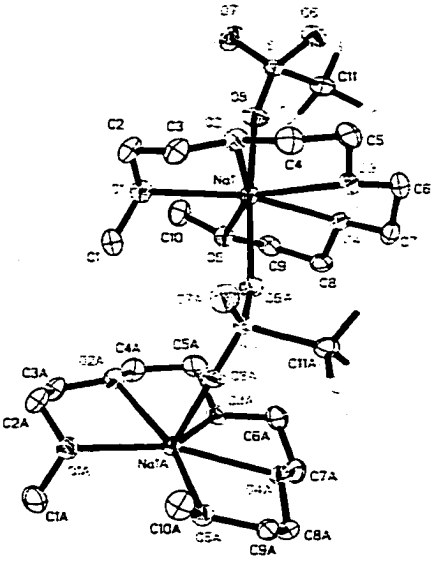


**Figure 7.** Crystal structure of tetraglyme:NaTf showing the tgttg'ttgttg'g' conformation of monoglyme and the seven-fold coordination of sodium.

*3.3 Comparison of the crystal structures*

The cation coordination numbers in the monoglyme:NaTf, diglyme:NaTf, and tetraglyme:NaTf structures are five, six and seven respectively. The trend in this series is an increasing cation coordination number with an increasing number of ethylene oxide units in the glyme. The cation is coordinated by ether oxygens from the glymes and triflate oxygens, and each of the structures have different relative contributions of ether oxygens and triflate oxygens. The number of ether oxygen atoms available for coordination increases from monoglyme to tetraglyme. The Na cation shows preference in coordinating the ether oxygen atoms over the triflate oxygen atoms. As a result, the number of coordinated ether oxygen atoms increases proportionately with the increasing size of the glyme molecule. Results of the three crystal structures along with P(EO):NaTf are summarized in Table 5. The Na coordination number is six in both diglyme:NaTf and P(EO):NaTf. However, in P(EO):NaTf the Na cation coordinates four triflate oxygen atoms compared to two triflate oxygen atoms in the diglyme:NaTf structure. Presumably the difference is due to the fact that the continuous PEO chain can not be wrapped around the Na cation in an energetically favorable mode.

The overall conformation of a glyme can be described by the conformations of the sequence of ethylene oxide units. In turn the conformation of an individual ethylene oxide unit is given by the three dihedral angles C-O-C-C, O-C-C-O, and C-C-O-C. For example, diglyme has two ethylene oxide units, and the conformation is then tgt-tgt where each ethylene oxide unit has a tgt conformation. The four ethylene oxide units in tetraglyme exhibit a more complicated sequence of ethylene oxide conformations, i.e. tgt-tg't-tgt-tg'g'. The conformation of monoglyme is just tgt. The values of the O-C-C-O torsional angles in all of the structures are gauche or gauche-minus, and the angles vary in absolute value from 51.34(0.48)° to 67.0(7)°. We note that ethylene oxide conformation tgt or tg't is present for all the sequences of ethylene oxide units with the exception of one unit in tetraglyme:NaTf where the conformation is tg'g'. In P(EO):NaTf the polymer conformation is tggtg'g' for the portion of PEO chain spanning a unit cell. It would appear that as the chain length increases, packing requirements impose a gauche-minus conformation on the terminal C-O bond in the ethylene oxide sequence of tetraglyme. The packing requirements are more severe in the P(EO):NaTf crystal and two C-C-O-C bonds assume a gauche or gauche-minus conformation.

**Table 5. Comparison of cation environment, anion environment, and conformation for crystalline phases of monoglyme:NaTf, diglyme:NaTf, tetraglyme:NaTf and poly(ethylene oxide):NaTf (abbreviated as P(EO):NaTf). *The parameters for P(EO):NaTf were obtained from the reported crystal structure.[61]**

| | *Cation environment* | | | *Anion environment* | *Conformation* |
|---|---|---|---|---|---|
| | Total $Na^+$ coordination | Ether oxygens | Triflate oxygens | No. of cations | Torsional sequence |
| Monoglyme:NaTf | 5 | 2 | 3 | 3 | tgt |
| Diglyme:NaTf | 6 | 4 | 2 | 2 | tgttgt |
| Tetraglyme: NaTf | 7 | 5 | 2 | 2 | tgttg'ttgttg'g' |
| P(EO):NaTf* | 6 | 2 | 4 | 4 | tggtg'g' |

*3.4 Vibrational spectra*

The comparison of the vibrational spectra of these compounds provides an opportunity to further our understanding of the correlation between band frequencies and local structure in these systems. The frequencies of the $\delta_s(CF_3)$ and $\nu_s(SO_3)$ modes of the triflate anion have been shown to be sensitive to their local potential energy environments and in particular to the number of cations that are coordinated to the anion.[55-57] The frequencies of these modes have been used to infer local structures present in amorphous phases of polymer electrolytes.[55,57,58,26-28] Studying the frequencies of these modes in crystalline phases where the structure is known will facilitate better analysis of local potential energy environments in phases whose structures are not known.

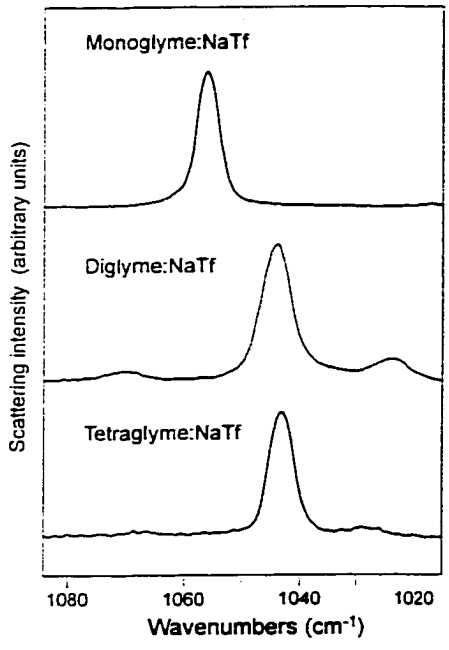


**Figure 8.** Raman spectra of crystalline monoglyme:NaTf, diglyme:NaTf and tetraglyme:NaTf in the $\nu_s(SO_3)$ region.

Raman spectra of monoglyme:NaTf, diglyme:NaTf, and tetraglyme:NaTf in the $\nu_s(SO_3)$ region are presented in Fig. 8, and band frequencies are summarized in Table 6. All the spectra show a single band in this region due to the $\nu_s(SO_3)$ vibration of the triflate anion. The band frequencies are 1056 $cm^{-1}$, 1045 $cm^{-1}$ and 1045 $cm^{-1}$ for monoglyme:NaTf, diglyme:NaTf and tetraglyme:NaTf respectively. The diglyme:NaTf sample has an additional weak band at 1025 $cm^{-1}$ which is attributed to a diglyme mode.[59,60] The frequency of the $\nu_s(SO_3)$ mode in monoglyme:NaTf, 1056 $cm^{-1}$, is the same as the frequency of the $\nu_s(SO_3)$ mode in P(EO):NaTf, 1056 $cm^{-1}$.[52] In these two structures the triflate is highly coordinated to sodium ions relative to the diglyme:NaTf and tetraglyme:NaTf crystals.In monoglyme:NaTf, each triflate is coordinated to three Na atoms, and in P(EO):NaTf each triflate anion is coordinated to four Na atoms. In diglyme:NaTf and tetraglyme:NaTf, each triflate anion is coordinated to two Na atoms. The frequencies follow a general trend established in the PEO-LiTf system: higher degrees of triflate coordination by cations leads to higher triflate ion mode frequencies.

The Raman spectra of monoglyme:NaTf, diglyme:NaTf, and tetraglyme:NaTf compounds in the $\delta_s(CF_3)$ region are presented in Fig. 9, and band frequencies are summarized in Table 6. The frequencies for the bands are 767 $cm^{-1}$, 762 $cm^{-1}$ and 756 $cm^{-1}$ for monoglyme:NaTf, diglyme:NaTf, and tetraglyme:NaTf respectively. The frequency of the $\delta_s(CF_3)$ mode

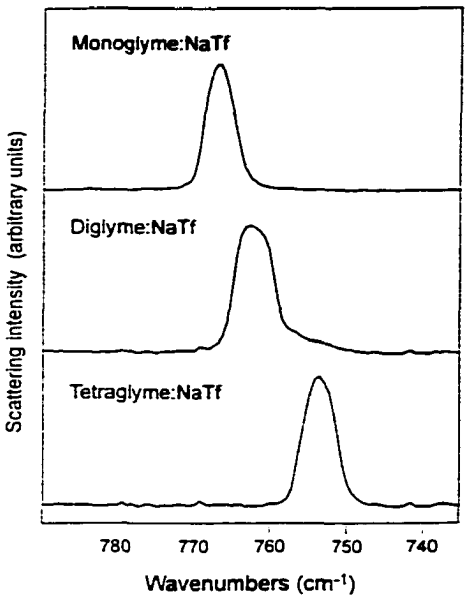


**Figure 9.** Raman spectra of crystalline monoglyme:NaTf, diglyme:NaTf and tetraglyme:NaTf in the $\delta_s(CF_3)$ region.

in monoglyme:NaTf, 767 $cm^{-1}$, is similar to the frequency of $\delta_s(CF_3)$ mode in P(EO):NaTf, 771 $cm^{-1}$.[52] An interesting observation is the relatively low frequency of the $\delta_s(CF_3)$ mode at 756 $cm^{-1}$ in the tetraglyme:NaTf compound. This value is similar to that expected for a triflate anion coordinated to one cation.[57] In the diglyme:NaTf and tetraglyme:NaTf compounds the triflate anions are coordinated to two sodium anions. Although the frequencies of the $\nu_s(SO_3)$ modes in both compounds are the same, 1045 $cm^{-1}$, the frequencies of the $\delta_s(CF_3)$ modes are different: 762 $cm^{-1}$ for diglyme:NaTf and 756 $cm^{-1}$ for tetraglyme:NaTf. The average distance of the triflate oxygen atoms to the sodium cation is 2.25(6) Å and 2.38(3) Å for crystalline diglyme:NaTf and tetraglyme:NaTf respectively. This difference might account for the difference in the $\delta_s(CF_3)$ frequencies, but does not explain the observation that the $\nu_s(SO_3)$ frequencies are the same in the two compounds.

### 4. Conclusions

We have shown crystalline phases of NaTf and PEO oligomers with different numbers of ethylene oxide units exhibit very different cation and anion environments. For example, the coordination number of sodium in these glyme systems ranges from 5 to 7, with an increasing number of ether oxygens participating in the first

**Table 6.** Frequencies of bands in th $\delta_s(CF_3)$ and $\nu_s(SO_3)$ regions from Raman spectra of monoglyme:NaTf, diglyme:NaTf, tetraglyme:NaTf and P(EO):NaTf. *The band frequencies of P(EO):NaTf were obtained from a previous publication and are presented for comparison.[52]

| | $\delta_s(CF_3)$, $cm^{-1}$ | $\nu_s(SO_3)$, $cm^{-1}$ |
|---|---|---|
| Monoglyme:NaTf | 767 | 1056 |
| Diglyme:NaTf | 762 | 1045 |
| Tetraglyme: NaTf | 756 | 1045 |
| P(EO):NaTf* | 771 | 1056 |

coordination sphere as the oligomer chain length increases. We wish to reiterate that the crystals in these glyme-salt systems are a structural compromise resulting from ion-ion interactions, ion- chain heteroatom interactions, and packing constraints from the organic chains. Although the bond distances and valence bond angles of the chain are somewhat inflexible although not rigid, the low barriers to rotation permit a wide range of dihedral angles, thus allowing the chains to assume a variety of conformations in order to achieve a thermodynamically stable structue. As noted earlier, the tgt sequence(s) of the monoglyme: (and diglyme) NaTf system are modified in the longer chain tetraglyme:NaTf system to include a terminal tg`g` conformation.

The spectral data for the $\nu_s(SO_3)$ and $\delta_s(CF_3)$ modes provides some insight into the factors governing the frequency values of the triflate ion in the various structures. It has been long recognized that these frequencies increase with increasing numbers of cations coordinated to the triflate oxygen atoms. This trend is also generally observed in this study. However there are some very interesting deviations which are especially apparent in a comparison of frequency data between the diglyme:NaTf and tetraglyme:NaTf crystals. Because the triflate anion interacts with two sodium cations in both structures, the relatively low frequency of the $\delta_s(CF_3)$ mode in tetraglyme:NaTf suggests that other factors are important. As noted earlier, the distance between the cation and the triflate oxygen atoms may also play a role. However this can be only a partial explanation, given the observation that the frequencies of the $\nu_s(SO_3)$ modes in these two structures are identical within experimental error. These data argue that

the degree of intermolecular mode coupling can also play an important role, given that the degree of mode coupling differs for different vibrations of the triflate anion.

This family of glyme-salt crystals opens a number of exciting opportunities to address fundamental issues of ionic transport. In particular, it would be especially intriguing to measure the ionic conductivity along particular crystallographic axes, correlating the presumed differences with the precise structural data available from the solved crystal structures. Further, we expect that the formation of crystalline phases is general behavior for these systems, and therefore it is worthwhile to search for crystalline phases in pentaglyme, hexaglyme and higher chain lengths complexed with sodium triflate. In addition, there may be multiple crystalline phases for a single glyme:salt composition as is the case in monoglyme:$(LiTf)_2$,[41] and there may exist different crystalline phases for different glyme:salt compositions.

The crystalline phases of this study suggest local structures which may be present in glyme-salt solutions and additionally provide insight into coordination environments present in PEO-based polymer electrolytes. These structures provide insight into cation coordination environments which include both ether oxygens and triflate oxygens and may further our understanding of the role of the anion in the ionic transport. These types of coordination environments may exist as part of an ionic transport mechanism.

**Acknowledgements**

This work was partially supported by funds from the Oklahoma Center for the Advancement of Science and Technology, Contract # 5377.

**References**

(1) Armand, M. B.; Chabagno, J. M.; Duclot, M. J. Polyethers as solid electrolytes. In *Fast Ion Transport in Solids*; Vashista, P., Mundy, J. M., Shenoy, G. K., Eds.; Elsevier: Amsterdam, 1979; pp 131.

(2) *Polymer Electrolyte Reviews*; MacCallum, J. R.; Vincent, C. A., Eds.; Elsevier Applied Science: New York, 1987; Vol. 1, pp 351.

(3) *Polymer Electrolyte Reviews*; MacCallum, J. R.; Vincent, C. A., Eds.; Elsevier Applied Science: New York, 1989; Vol. 2, pp 338.

(4) Gray, F. M. *Solid Polymer Electrolytes: Fundamentals and Technological Applications*; VCH Publishers, Inc.: New York, 1991.

(5) Bruce, P. G.; Vincent, C. A. *J. Chem. Soc. Faraday Trans.* **1993**, *89*, 3187.

(6) Ratner, M. A.; Nitzan, A. *Faraday Discuss. Chem. Soc.* **1989**, *88*, 19.

(7) Ratner, M. A. Aspects of the Theoretical Treatment of Polymer Solid Electrolytes: Transport Theory and Models. In *Polymer Electrolyte Reviews*; MacCallum, J. R., Vincent, C. A., Eds.; Elsevier Applied Science: New York, 1987; Vol. 1; pp 173.

(8) Bhattacharja, S.; Smoot, S. W.; Whitmore, D. H. *Solid State Ionics* **1986**, *18&19*, 306.

(9) Arumugam, S.; Shi, J.; Tunstall, D. P.; Vincent, C. A. *J. Phys.: Condens. Matter* **1993**, *5*, 153.

(10) Boden, N.; Leng, S. A.; Ward, I. M. *Solid State Ionics* **1991**, *45*, 261.

(11) Robitaille, C. D.; Fauteux, D. *J. Electrochem. Soc.* **1986**, *133*, 315.

(12) Vallée, A.; Besner, S.; Prud'homme, J. *Electrochim. Acta* **1992**, *37*, 1579.

(13) Besner, S.; Vallée, A.; Bouchard, G.; Prud'homme, J. *Macromolecules* **1992**, *25*, 6480.

(14) Lascaud, S.; Perrier, M.; Vallée, A.; Besner, S.; Prud'homme, J. *Macromolecules* **1994**, *27*, 7469.

(15) Brodin, A.; Mattsson, B.; Nilsson, K.; Torell, L. M.; Hamara, J. *Solid State Ionics* **1996**, *85*, 111.

(16) Weston, J. E.; Steele, B. C. H. *Solid State Ionics* **1982**, *7*, 81.

(17) Yang, L.; Zhang, A.; Qiu, B.; Yin, J.; Liu, Q. *Solid State Ionics* **1988**, *28-30*, 1029.

(18) Chintapalli, S.; Frech, R. *Electrochimica Acta* **1998**, *43*, 1395.

(19) Armand, M.; Gauthier, M. Polymeric Solid Ion Conductors: the Immobile Solvent Concept. In *High Conductivity Solid Ionic Conductors*; Takahashi, T., Ed.; World Scientific Press: New Jersey, 1989; pp 114.

(20) Berthier, C.; Gorecki, W.; Minier, M. *Solid State Ionics* **1983**, *11*, 91.

(21) Minier, M.; Berthier, C.; Gorecki, W. *J. Physique* **1984**, *45*, 739.

(22) Stainer, M.; Hardy, L. C.; Whitmore, D. H.; Shriver, D. F. *J. Electrochem. Soc.* **1984**, *131*, 784.

(23) Gadjourova, Z.; Andreev, Y. G.; Tunstall, D. P.; Bruce, P. G. *Nature* **2001**, *412*, 520.

(24) Bruce, P. G. *Electrochim. Acta* **1995**, *40*, 2077.

(25) Andreev, Y. G.; Bruce, P. G. *Electrochim. Acta* **2000**, *45*, 1417.

(26) Frech, R.; Chintapalli, S.; Bruce, P. G.; Vincent, C. A. *Macromolecules* **1999**, *32*, 808.

(27) Frech, R.; Chintapalli, S.; Bruce, P. G.;

Vincent, C. A. *Chem. Commun.* **1997**, 157.
(28) Rhodes, C. P.; Frech, R. *Macromolecules* **2001**, *34*, 2660.
(29) Borodin, O.; Smith, G. D. *Macromolecules* **1998**, *31*, 8396.
(30) Sutjianto, A.; Curtiss, L. A. *J. Phys. Chem. A* **1998**, *102*, 968.
(31) Johansson, P.; Tegenfedlt, J.; Lindgren, J. *J. Phys. Chem. A* **1998**, *102*, 4660.
(32) Johansson, P.; Tegenfeldt, J.; Lindgren, J. *Polymer* **1999**, *40*, 4399.
(33) Baboul, A. G.; Redfern, P. C.; Sutjianto, A.; Curtiss, L. A. *J. Am. Chem. Soc.* **1999**, *121*, 7220.
(34) Mujica, V.; Malaver, M.; Ruette, F. *J. Phys. Chem. A* **1999**, *103*, 89.
(35) Borodin, O.; Smith, G. D. *J. Phys. Chem. B* **2000**, *104*, 8017.
(36) Hyun, J.; Dong, H.; Rhodes, C. P.; Frech, R.; Wheeler, R. A. *J. Phys. Chem. B* **2001**, *105*, 3329.
(37) Nagaoka, K.; Naruse, H.; Shinohara, I. *J. Polym. Sci., Polym. Lett.* **1984**, *22*, 659.
(38) Allcock, H. R.; O'Connor, S. J. M.; Olmeijer, D. L.; Napierala, M. E.; Cameron, C. G. *Macromolecules* **1996**, *29*, 7544.
(39) Imrie, C. T.; Ingram, M. D.; McHattie, G. S. *Adv. Mater.* **1999**, *11*, 832.
(40) York, S.; Kellam, E. C.; Allcock, H. R.; Frech, R. *Electrochim. Acta* **2001**, *46*, 1553.
(41) Rhodes, C. P.; Khan, M.; Frech, R. ***to be published.***
(42) Iwamoto, R. *Bull. Chem. Soc. Japan* **1973**, *46*, 1114.
(43) Iwamoto, R.; Wakano, H. *J. Am. Chem. Soc.* **1976**, *98*, 3764.
(44) Abraham, K. M. *Solid State Ionics* **1982**, *7*, 199.
(45) Munshi, M. Z. A.; Gilmour, A.; Smyrl, W. H.; Owens, B. B. *J. Electrochem. Soc.* **1989**, *136*, 1847.
(46) Munshi, M. Z. A.; Smyrl, W. H.; Schmidtke, C. *Chem. Mater.* **1990**, *2*, 530.
(47) Munshi, M. Z. A.; Smyrl, W. H. *Solid State Ionics* **1991**, *45*, 183.
(48) Doeff, M. M.; Peng, M. Y.; Ma, Y.; De Jonghe, L. C. *J. Electrochem. Soc.* **1994**, *141*, L145.
(49) Ma, Y.; Doeff, M. M.; Visco, S. J.; De Jonghe, L. C. *J. Electrochemical Soc.* **1993**, *140*, 2726.
(50) Doeff, M. M.; Visco, S. J.; Ma, Y.; Peng, M.; Ding, L.; De Jonghe, L. C. *Electrochimica Acta* **1995**, *40*, 2205.
(51) Siemens. SHELXTL; 5.03 ed.; Siemens Analytical X-ray Instruments Inc.: Madison, Wisconsin, USA, 1994.
(52) Rhodes, C. P.; Frech, R. *Solid State Ionics* **2000**, *136-137*, 1131.
(53) *CRC Handbook of Chemistry and Physics. 81st Edition*; Lide, D. R., Ed.; CRC Press LLC: New York, 2000.
(54) *The Merck Index. 12th Edition*; Budavari, S., Ed.; Merck and Co., Inc.: Whitehouse Station, 1996.
(55) Schantz, S.; Sandahl, J.; Borjesson, L.; Torell, L. M.; Stevens, J. R. *Solid State Ionics* **1988**, *28-30*, 1047.
(56) Huang, W.; Wheeler, R. A.; Frech, R. *Spectrochimica Acta* **1994**, *50A*, 985.
(57) Huang, W.; Frech, R.; Wheeler, R. A. *J. Phys. Chem.* **1994**, *98*, 100.
(58) Frech, R.; Huang, W.; Dissanayake, M. A. K. L. *Mat. Res. Soc. Symp. Proc.* **1995**, *369*, 523.
(59) Matsuura, H.; Fukuhara, K. *J. Polym. Sci. B* **1986**, *24*, 1383.
(60) Yoshida, H.; Matsuura, H. *J. Phys. Chem. A* **1998**, *102*, 2691.
(61) Andreev, Y. G.; MacGlashan, G. S.; Bruce, P. G. *Phys. Rev. B* **1997**, *55*, 12011.

## Appendix B: Papers not included

I. Studies of cation-anion and cation-polymer association in poly(ethylene oxide): $Pb(CF_3SO_3)_2$ complexes. C. P. Rhodes, B. Klassen, R. Frech, Y. Dai and S. G. Greenbaum. *Solid State Ionics* **126**, 251 (1999).

II. A Comparative Study of Ionic Association in Poly(ethylene oxide)-$MCF_3SO_3$ Systems (M=Lithium and Sodium). R. Frech, C. P. Rhodes and S. S. York. *Mat. Res. Soc. Symp. Proc.* **548**, 335 (1999).

III. Vibrational Spectroscopic Study of 2-Methoxyethyl Ether Complexed with Lithium and Sodium Trifluoromethane Sulfonate. M. Petrowsky, C. P. Rhodes and R. Frech. *J. Solution Chem.* **30**, 171 (2001)

IV. Molecular Dynamics Simulations and Spectroscopic Studies of Amorphous Tetraglyme ($CH_3O(CH_2CH_2O)_4CH_3$) and Tetraglyme:$LiCF_3SO_3$ Structures. J. Hyun, H. Dong, C. P. Rhodes, R. Frech and R. A. Wheeler. *J. Phys.Chem. B* **105**, 3329 (2001).

V. Effect of Temperature on Local Structure in Poly(ethylene oxide)-Zinc Bromide Salt Complexes. B. P. Grady, C. P. Rhodes, S. York, R. Frech, *Macromolecules* **34**, 8523 (2001).

VI. Role of the anion in the structure and vibrations of 1,2-dimethoxyethane complexed with lithium triflate, S. Boesch, C. P. Rhodes, R. Frech and R. A. Wheeler, *to be submitted to PhysChemComm.*

VII. Molecular dynamics simulations and vibrational spectroscopic studies of local structure in tetraglyme:sodium triflate solution. H. Dong, C. P. Rhodes, R. Frech and R. A. Wheeler, *submitted to J. Phys. Chem.*

VIII. A Symmetry-based Study of Vibrational Decoupling in the Crystalline Phases of $CH_3(OCH_2CH_2)_2OCH_3LiCF_3SO_3$ and $P(EO)_3LiCF_3SO_3$. R. Frech and C. P. Rhodes, *Solid State Ionics*, in press.

IX. A Comparison of Local Structures in Crystalline $P(EO)_3LiCF_3SO_3$ and Glyme-$LiCF_3SO_3$ Systems. R. Frech, C. P. Rhodes, M. Khan, *submitted to Polymer Preprints.*